Testing Electroweak Theory and Short Baseline Anomalies with Neutrinos

Blanca Cecilia Cañas Orduz
Víctor Saúl Basto Gonzalez

Testing electroweak theory and short baseline anomalies with neutrinos

Testing Electroweak Theory and Short
Baseline Anomalies with Neutrinos

Blanca Cecilia Cañas Orduz and
Víctor Saúl Basto Gonzalez

Department of Physics, Universidad de Pamplona

Ivaldo Torres Chávez
Rector

Aldo Pardo García
Vicerrector de Investigaciones

To our parents and siblings

TABLE OF CONTENTS

LIST OF TABLES

LIST OF FIGURES

PREFACE

Reading through this book, the reader will learn the extraordinary history of one of the fundamental particles that make up our universe: the neutrino. The readers will understand how the theoretical and experimental study of the interactions of neutrinos with the matter has been of great importance in establishing the electroweak theory, which describes the electromagnetic force and the weak force, and understand the properties of neutrinos. Once we have established the foundations of the Electroweak Standard Model, we will continue studying neutrino-electron scattering at low energies. This inquiry will allow us to investigate one of the fundamental parameters of the Electroweak Standard Model, the weak mixing angle.

Historically, the analysis of neutrinos' interactions with matter from a quantitative perspective (by making a total count of neutrino interactions and/or a partial count by energy interval) has led to the discovery of the phenomenon of neutrino oscillations. This phenomenon constitutes the first direct evidence of a new physics beyond the Standard Model of elementary particles, at least in its minimal version. We will see that the phenomenon of neutrino oscillations - the change of the state of the interaction of neutrinos with matter during its propagation - can be explained because neutrinos are massive particles, and interaction states are a superposition of states with a defined mass.

Parallel to the consolidation of the oscillation model of three active neutrinos, today, there is a number of anomalies in neutrino oscillation experiments that are possible indications of oscillatory phenomena involving a new particle that must be a new massive neutrino with the pages of this book, we will present these anomalies and

approach them, taking into account experimentally obser-
ved Gallium anomaly and the reactor anomaly.

Experimental data analysis in search of parameters
related to weak interactions or parameters related to new
physics are performed using statistical tools. Therefore,
through the pages of this book, the reader will learn the
necessary tools to carry out statistical analysis that will
allow us to carry out precision tests within the Standard
Model and delve into the study of the properties of the
neutrino. For example, we will learn to carry out statistical
analysis that will allow us to obtain limits to the weak
mixing angle with the help of the experimental results of
electron-neutrino scattering, and we will learn how to
perform the statistical analysis of the Gallium anomaly and
the reactor anomaly to put limits on the possible new mass
splitting $\Delta m2$ and the new mixing angles.

INTRODUCTION

The history of neutrino physics began in 1930 when Pauli hypothesized the existence of the neutrino in a famous letter directed to attendees of the 1930 Gauverein meeting in Tübingen. An English version of this letter is on page 27 of the following reference (Brown, 1978) and the original German version at the following web addresses: https://cds.cern.ch/record/83282/files/meitner_0393.pdf. Using the idea of this new particle, he tried to resolve the puzzle of the continuous electron spectrum accompanying nuclear beta decay discovered by J. Chadwick in 1914 (Chadwick, 1914). Pauli suggested that his speculative particle be neutral and spin one-half to guarantee the conservation of electric charge and angular momentum. Besides, the new particle would also carry a fraction of the energy released to conserve energy. Following Pauli's idea, in 1934, Fermi formulated his theory of beta decay (Fermi, 1934), using the proton, electron, neutrino, and the newly discovered neutron by Chadwick in 1932 (Chadwick, 1932).

The success of his theory provided strong credibility to the neutrino hypothesis. Based on Fermi's theory, in 1934, Bethe and Peierls roughly calculated the neutrino interaction cross-section with nuclei. They concluded: "...there is no practically possible way of observing the neutrino" (Bethe & Peierls, 1934). Nevertheless, in 1956, Cowan and Reines reported the first detection of neutrinos at the Savannah River reactor experiment (Figure 1) (Cowan, Reines, Harrison, Kruse, & McGuire, 1956;

Reines & Cowan, 1959). For this discovery, Reines was awarded the Nobel Prize in 1995. The study of beta decay allowed establishing the theoretical description of one of particle physics' fundamental interactions: the weak interaction.

By the 1960s, with the advent of accelerator experiments, a new type of neutrino, muon neutrino, different from the electron neutrino produced in beta decay, was discovered by Lederman, Schwartz, and Steinberger (Danby et al., 1962). Finally, in 2001, the DONUT collaboration at Fermilab announced the first direct evidence of the third neutrino, tau neutrino (Kodama & et al., 2001).

Figure 1
Frederick Reines and Clyde Cowan at the Hanford Reactor (USA)
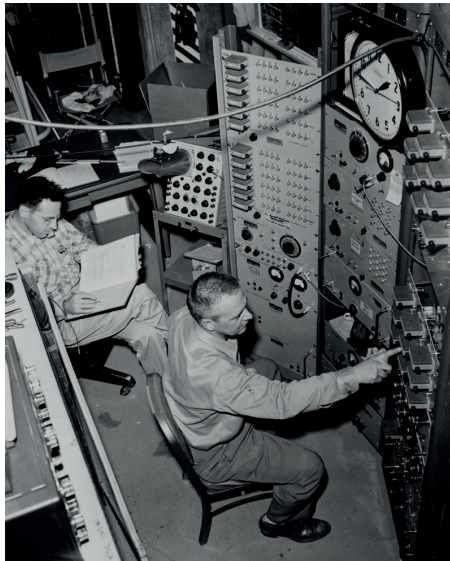
Note. In the Hanford reactor, Frederick Reines (left) and Clyde Cowan (right) observed for the first time the preliminary indications of the existence of the neutrino. Figure from the reference (Lindley, 2007).

Considering that this book is based on a phenomenological study of neutrino physics, we would like to review first, in Chapter 1, the main characteristics of the unified electroweak theory, in which neutrino physics is confined. We will also introduce the historical ideas that guided the development of this successful theory.

Then, in Chapter 2, we will deal with neutrino-electron scattering, emphasizing its primary role in confirming the structure of the electroweak theory. Based on this process and current theoretical and experimental inputs, we will present an improved determination of one of the fundamental parameters in the Standard Model, the weak mixing angle at low energies.

Neutrinos are fermions; they have spin one-half, thence their theoretical description is guided by Dirac's equation. In the electroweak theory, fermions are described by a four-component spinor field (Dirac, 1928) [1] . In the case of neutrinos, they can be characterized by a single chiral field (left-handed neutrino or right-handed antineutrino). Nevertheless, in 1937 Majorana (Majorana, 1937) proposed another description for a fermion field without electric charge. In this description, particles and antiparticles are identical. He found it is possible to describe a neutral fermion with no need for the antineutrino concept or negative energy states advocated by Dirac (Dirac, 1928). When Majorana formulated his theory, he asked if the neutrinos might be truly neutral fermions, but at that time, the neutrino was a hypothetical particle with unknown properties. In fact, after its discovery (Reines & Cowan, 1959), the observed properties seemed to favor Dirac's idea.

---

[1] left- and right-handed particles, and left- and right-handed antiparticles.

Motivated by experimental results that point out the distinction between particles and antiparticles related to the law of lepton number conservation in the electroweak theory. The law of lepton number conservation is the underlying concept whereby different flavors of neutrino are connected with the corresponding charged lepton. If neutrinos are different from antineutrinos, then they are Dirac fermions. Nevertheless, in the late 1990s, the pioneer experiment Super-Kamiokande (Fukuda & et al., 1998a) found evidence favoring neutrino oscillations and opened a new particle physics era. This quantum mechanical phenomenon is intimately connected with neutrino masses and mixing.

In the late 1990s, the pioneer experiment Super-Kamiokande (Fukuda & et al., 1998a) found evidence favoring neutrino oscillations and opened a new particle physics era. This quantum mechanical phenomenon is intimately connected with neutrino masses and mixing. Considering these results, we aim to present in Chapter 3 a brief overview of massive neutrinos beyond the electroweak theory and the current picture of neutrino oscillations, showing the mathematical formulation together with the experimental indications that support it.

Finally, Chapter 4 focuses on the evidence for sterile neutrino, motivated by several anomalies that might be explained if the square mass splitting is around 1 eV². Driven by these observations, we will reanalyze short baseline neutrino oscillation data, considering the deficit of electron neutrinos reported by the GALLEX and SAGE solar neutrino detectors and the reactor antineutrino detectors at distances below 100 *m* from the source.

1. The Electroweak Standard Model
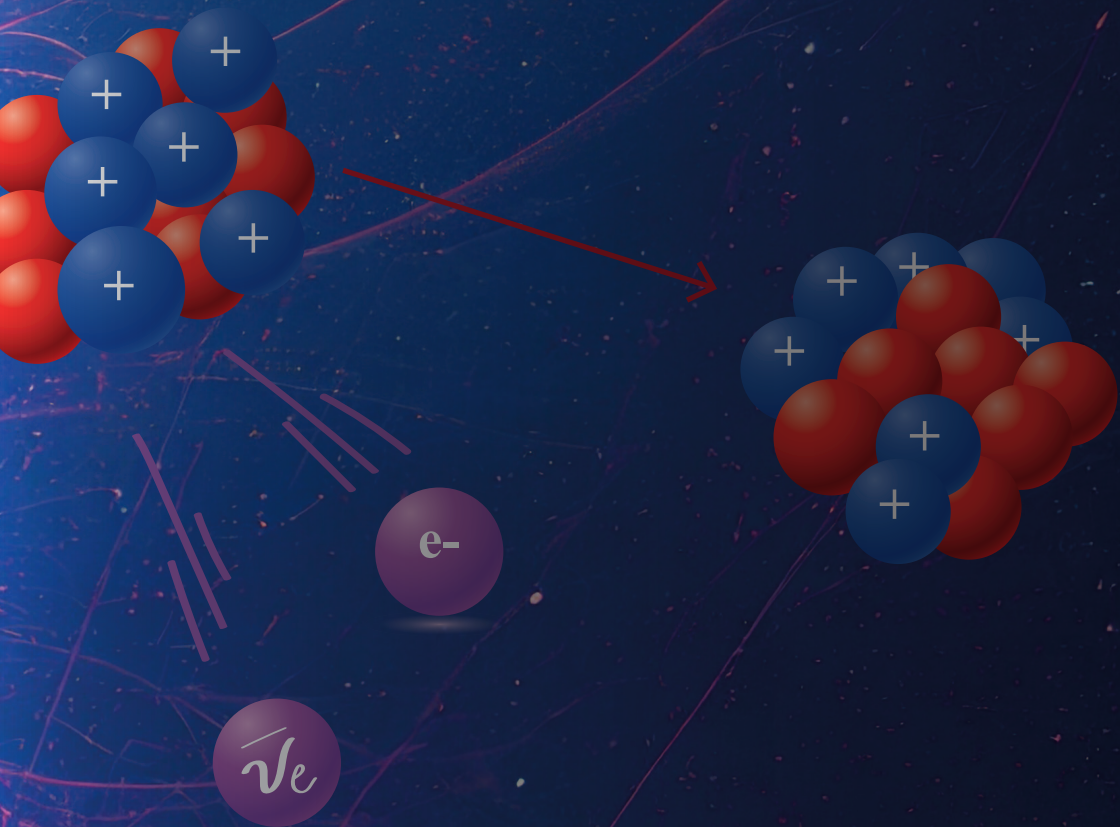
1 The Electroweak Standard Model

The first successful gauge theory (Yang & Mills, 1954) was quantum electrodynamics, QED, which describes the interaction of light with matter. In 1930 it was completed, and later, by the early 1950s, was proved its renormalizability by Feynman, Schwinger, Tomonaga, Dyson, and others (Schwinger, 1957). The enormous success of this theory provided a strong motivation to search for a similar description of strong and weak interactions. In particular, in 1961, Glashow (Glashow, 1961) proposed a model to describe the weak and electromagnetic interactions. The gauge sector was composed by four massless gauge bosons W^+, W^-, Z, and the photon to have local gauge invariance and hence renormalizability. However, there was a big problem; there had to be a mechanism to break the symmetry so that the photon remained massless while leaving large masses in the other gauge bosons. By 1964, Higgs, Brout, Englert, and others studied gauge theories' spontaneous symmetry breaking, giving rise to massive gauge bosons, such as W, Z, and the Higgs. The procedure for this spontaneous breakdown of gauge symmetries is now known as the Higgs Mechanism (Englert & Brout, 1964; Higgs, 1964).

In 1967, Weinberg (Weinberg, 1967) and Salam (Salam, 1968) formulated the unified electroweak theory, incorporating the Glashow's model (Glashow, 1961) and the Higgs mechanism (Englert & Brout, 1964; Higgs,

1964). Later on, in 1971 't Hooft and Veltman ('t Hooft, 1971b; 't Hooft & Veltman, 1972) proved its renormalizability. This theory has been successfully tested by an enormous number of experiments to date. The only undiscovered piece was the Higgs boson; however, on 4 July 2012, the ATLAS and CMS collaborations at CERN reported the discovery of a new particle, consistent with the Higgs boson, with a mass around 126 GeV (Aad & et al., 2012; Chatrchyan & et al., 2012). Up to now, all the measurements for the properties of this new particle are consistent with the Higgs boson of the electroweak theory (Aad & et al., 2015). One may think that the picture has been completed with this final piece. However, despite its great success, the electroweak theory has been shown to be incomplete. In particular, the substantial evidence supportive of neutrino oscillations found by the pioneering experiments of Davies (Reines & Cowan, 1959) together with Kamiokande (Fukuda & et al., 1994) and confirmed by Super-Kamiokande (Fukuda & et al., 1998a), SNO (Ahmad & et al., 2002), KamLAND (Eguchi & et al., 2003), and many others, have proven that neutrinos have a non-zero mass as opposed to the electroweak theory.

As we will see through this book, neutrino physics has played a significant role in confirming the theoretical predictions of the electroweak theory (Hasert & et al., 1973b) and in searchings for new physics (Kumar, Mantry, Marciano, & Souder, 2013). For this reason, we will first discuss the role of neutrino physics within the Glashow-Weinberg-Salam theory.

This chapter is organized as follows: In Section 1.1, we will present the major characteristics of the electroweak theory, as well as some theoretical aspects of the SM Lagrangian. In Section 1.2, we will calculate the interactions between leptons and boson fields, obtaining the

charged-current (CC) and neutral-current (NC) Lagrangian. In Section 1.3, we will survey the spontaneous breaking of the SU(2)×U(1) symmetry and the Higgs mechanism. Moreover, finally, in Section 1.4, we will focus on discussing lepton masses and mixing after spontaneous symmetry breaking. For more detailed treatments, see, e.g., (Giunti & Kim, 2007; Langacker, 2017; Valle & Romao, 2015).

1.1 The Electroweak Standard Model Lagrangian

As we mentioned, the Glashow-Weinberg-Salam theory (Glashow, 1961; Salam, 1968; Weinberg, 1967) of electroweak interactions is based on the symmetry group $SU(2)_L \times U(1)_Y$. This group fixes the interactions and the number of gauge bosons that appear in theory. The model incorporates three families of spin-$\frac{1}{2}$ fermions with their interactions mediated by spin-1 gauge bosons. Besides, it includes a scalar field, the Higgs boson, which is needed to generate gauge boson masses and fermion masses. It must be stressed that those masses are free parameters and must be obtained from experimental measurements. The number of fermions and Higgs fields are unrestricted, and, again, they must be obtained from experimental measurements. As we will see later, each fermion has two chiral states, left and right, which transform differently under the $SU(2)_L \times U(1)_Y$ group. The subscript L emphasizes that only the left-chiral (L) fermions enter into the weak interactions. On the other hand, Y refers to the weak hypercharge quantum number.

The Lagrangian density is given by

$$\mathscr{L} = \mathscr{L}_{gauge} + \mathscr{L}_f + \mathscr{L}_{Higgs} + \mathscr{L}_{Yukawa}. \tag{1.1}$$

The first term in Equation (1.1) describes the gauge sector, which is composed of four boson fields; three W_μ^i, i = 1,2,3 and one $B\mu$. The three first are associated with the three generators of SU(2)$_L$, $I_i = \tau_i/2$ with τ_i being the three Pauli matrices, and the fourth associated with the generator of U(1)$_Y$, Y. Hence, the gauge density Lagrangian is given by

$$\mathscr{L}_{gauge} = -\frac{1}{4} W_{\mu v}^i W^{\mu v i} - \frac{1}{4} B_{\mu v} B^{\mu v} \tag{1.2}$$

where the field strength tensors for SU(2) and U(1) are respectively

$$W_{\mu v}^i = \partial\mu W_v^i - \partial v W_\mu^i - g\varepsilon i jk W_\mu^j W_v^k, \tag{1.3}$$

$$B\mu v = \partial\mu Bv - \partial v B\mu, \tag{1.4}$$

with i, j, k = 1,2,3 and g in Equation (1.3) is the SU(2) coupling constant. Besides, the U(1) factor has a gauge coupling g′. Note that Equation (1.2) includes the gauge boson kinetic energy terms as well as self-interactions for the gauge bosons W_μ^i. The abelian gauge boson, $B\mu$, has no self-interactions. However, mass terms for the gauge boson are forbidden because they would break the gauge invariance and spoil the renormalizability of the theory. Therefore, the SU(2)$_L$ ×U(1)$_Y$ symmetry must be broken to generate gauge boson masses, as we will see in Section 1.3.

The second term in Equation (1.1) describes the interactions between the fermions and the gauge bosons. The fermion fields are classified into three generations of quarks and leptons in the following way:

* 1st generation: $\underbrace{u,d}_{\text{quarks}}$ and $\underbrace{\nu_e,e}_{\text{leptons}}$,

* 2nd generation: $\underbrace{c,s}_{\text{quarks}}$ and $\underbrace{\nu_\mu,\mu}_{\text{leptons}}$,

* 3rd generation: $\underbrace{t,\nu}_{\text{quarks}}$ and $\underbrace{\nu_\tau,\tau}_{\text{leptons}}$.

Each fermion has two chiral states, left and right [1], which transform differently under the $SU(2)_L \times U(1)_Y$ group. Since neutrinos are massless within the electroweak theory, only the left-chiral state can be non-zero. The left-handed fermion fields are SU(2) doublets, while the right-handed fields are SU(2) singlets, i.e.,

$$\text{left-handed fermions:} \quad L'_{\alpha L} = \begin{pmatrix} \nu'_\alpha \\ l'_\alpha \end{pmatrix}_L, \quad Q'_{aL} \begin{pmatrix} u'_\alpha \\ d'_\alpha \end{pmatrix}_L, \quad \text{(1.5)}$$

$$\text{right-handed fermions:} \quad \ell'_{\alpha R}, \quad q'^{U}_{aR}, \quad q'^{D}_{aR}, \quad \text{(1.6)}$$

where $\alpha = e, \mu, \tau$, and $a = 1, 2, 3$. L and Q denote the lepton and quark fields, respectively. The primes on the fermion fields refer to the fact that they are weak eigenstates. It means that, in general, they do not have specific masses. As we will see in Section 1.4, these fields will become mixtures of mass eigenstates fields after spontaneous symmetry breaking.

In addition, to know the quantum number assignment of fermion field generations into electroweak theory, we use the so-called Gell-Mann-Nishijima relation

---

[1] Let ψ be a fermion field so that $\psi = \psi_L + \psi_R$, where $\psi_L \equiv P_L \psi = \frac{1-\gamma^5}{2}\psi$, $\psi_R \equiv P_R \psi = \frac{1-\gamma^5}{2}\psi$ are defined as left (L) and right (R) chiral projections, respectively.

$$Q = I3 + \frac{Y}{2},\qquad\qquad\text{(1.7)}$$

where the hypercharge operator, Y, is calculated from the electric charge operator, Q, and the third generator of SU(2)$_L$, I$_3$. Hence, the action of the hypercharge operator on the left-handed fermion fields is given by

$$Y\,L'_{\alpha L} = 2(Q-I3)L'_{\alpha L} = -L'_{\alpha L}\,,\;\Longrightarrow YL'_{\alpha L} = -L'_{\alpha L},\qquad\text{(1.8)}$$

$$Y\,Q'_{\alpha L} = 2(Q-I3)Q'_{\alpha L} = \tfrac{1}{3}\,Q'_{\alpha L},\;\Longrightarrow YQ'_{\alpha L} = \tfrac{1}{3}Q'_{\alpha L}.\qquad\text{(1.9)}$$

On the other hand, as we have already mentioned, the right-handed fermion fields are assumed to be singlets under the SU(2)$_L$ group, that is, I$if_R = 0$ and therefore,

$$Y\ell'_{\alpha R} = 2Q\ell'_{\alpha R} = -2\ell'_{\alpha R},\;\Longrightarrow\; Y\ell'_{\alpha R} = -2\ell'_{\alpha R},\qquad\text{(1.10)}$$

$$Yq'^{U}_{aR} = 2Qq'^{U}_{aR} = \tfrac{4}{3}q'^{U}_{aR},\;\Longrightarrow\; Y\,q'^{U}_{aR} = \tfrac{4}{3}\,q'^{U}_{aR},\qquad\text{(1.11)}$$

$$Yq'^{D}_{aR} = 2Qq'^{D}_{aR} = -\tfrac{2}{3}\,q'^{D}_{aR},\Longrightarrow Y\,q'^{D}_{aR} = -\tfrac{2}{3}\,q'^{D}_{aR}.\qquad\text{(1.12)}$$

The quantum numbers with respect to the SU(2)$_L$ ×U(1)$_Y$ gauge group are summarized in the Table 1.1. Notice that the SU(2)$_L$ and U(1)$_Y$ representations are chiral. Hence, to preserve the theory's gauge invariance, fermion mass terms are not allowed in the Lagrangian density. Thus, the second term in Equation (1.1) only has gauge-covariant kinetic energy terms, which can be split into lepton and quark sectors, as follows

$$\boxed{\mathscr{L}_f = \mathscr{L}_f^{\,leptons} + \mathscr{L}^{\,quarks}}\qquad\text{(1.13)}$$

with

$$\mathscr{L}_f^{\text{leptons}} = i \sum_\alpha \overline{L'\alpha L}\gamma^\mu D\mu L'\alpha L + i \sum_\alpha \overline{\ell'\alpha R}\,\gamma^\mu D\mu \ell'\alpha R \tag{1.14}$$

$$\mathscr{L}_f^{\text{quarks}} = i \sum_a \overline{Q'\alpha L}\gamma^\mu D\mu Q'\alpha L + i \sum_a \overline{q'\alpha R}^\mu \gamma D\mu q'^\mu_{\alpha R} + i \sum_a \overline{q'^{\prime D}_{\alpha R}}\gamma^\mu D\mu q'^{\prime D}_{\alpha R,} \tag{1.15}$$

where the gauge covariant derivative is defined as

$$\mathscr{D}\mu = \partial\mu + ig\,\frac{\tau i}{2}\,W^i_\mu + ig'B\mu\,\frac{Y}{2}, \tag{1.16}$$

Table 1.1

Quantum Numbers of the Fermions with Respect to the SU(2)$_L$ ×U(1)$_Y$ Gauge Group

Elementary particles	1st gen.	2nd gen.	3rd gen.	I	I_3	Y	Q
Leptons	$\begin{pmatrix} \nu_e \\ e \end{pmatrix}_L$	$\begin{pmatrix} \nu_\mu \\ \mu \end{pmatrix}_L$	$\begin{pmatrix} \nu_\tau \\ \tau \end{pmatrix}_L$	1/2	1/2 \quad -1/2	-1	0 \quad -1
	e_R	μ_R	τ_R	0	0	-2	-1
Quarks	$\begin{pmatrix} u \\ d \end{pmatrix}_L$	$\begin{pmatrix} c \\ s \end{pmatrix}_L$	$\begin{pmatrix} t \\ b \end{pmatrix}_L$	1/2	1/2 \quad -1/2	1/3	2/3 \quad -1/3
	u_R	c_R	t_R	0	0	4/3	2/3
	d_R	s_R	b_R	0	0	-2/3	-1/3

with the three Pauli matrices given by

$$\tau_1 = \begin{pmatrix} 0 & 1 \\ 1 & 0 \end{pmatrix}, \qquad \tau_2 = \begin{pmatrix} 0 & -i \\ i & 0 \end{pmatrix}, \qquad \tau_3 = \begin{pmatrix} 1 & 0 \\ 0 & -1 \end{pmatrix}. \tag{1.17}$$

In particular, we want to know the neutrino couplings to the gauge bosons. Therefore, in Section 1.2 we will discuss in more detail the leptonic sector.

The third term in Equation (1.1) corresponds to the Higgs sector. To carry out the spontaneous symmetry breaking and generate both the fermion masses and the boson masses, a complex scalar Higgs doublet, $\Phi = \begin{pmatrix} \varphi^+ \\ \varphi^- \end{pmatrix}^2$ is introduced. Therefore, the Higgs density Lagrangian is given by

$$\mathscr{L}_{Higgs} = (\mathscr{D}_\mu \Phi)^\dagger (\mathscr{D}^\mu \Phi) - V(\Phi^\dagger \Phi). \qquad \textbf{(1.18)}$$

In Equation (1.18), V(Φ†Φ) is the Higgs potential, which has the form

$$V(\Phi^\dagger \Phi) = \mu^2 \, \Phi^\dagger \Phi + \lambda \, (\Phi^\dagger \Phi)^2, \qquad \textbf{(1.19)}$$

where $\lambda > 0$ in order that the potential has a lower bound. The cases $\mu^2 > 0$ and $\mu^2 < 0$ will be discussed in Section 1.3. It is worth emphasizing that the choice $\mu^2 < 0$ will be responsible for the spontaneous symmetry breaking, giving rise to the W and Z boson masses.

Finally, the last term in Equation (1.1) takes into account the fermionic couplings with the Higgs field, which are known as Yukawa couplings. It is here where all fermions acquire mass except the neutrinos due to the lack of a right-handed neutrino component, as we will see in Section 1.4,

$$\mathscr{L}_{Yukawa} = \mathscr{L}_{Yukawa}^{leptons} + \mathscr{L}_{Yukawa}^{quarks}, \qquad \textbf{(1.20)}$$

---

[2]φ+ and φ⁰refer to a charged complex scalar field and a neutral complex scalar field, correspondingly.

with

$$\mathcal{L}^{leptons}_{Yukawa} = -\sum_{\alpha\beta}(Y'^{\ell}_{\alpha\beta}\overline{L'_{\alpha L}}\Phi\ell'_{\beta R}+Y'^{\ell*}_{\alpha\beta}\overline{\ell'_{\beta R}}\Phi^{\dagger}L'_{\alpha L}), \qquad \textbf{(1.21)}$$

$$\mathcal{L}^{quarks}_{Yukawa} = \sum_{ab}(Y'^{U}_{ab}\overline{Q'_{aL}}\widetilde{\Phi}q'^{U}_{bR}+Y'^{U*}_{ab}\overline{q'^{U}_{bR}}\widetilde{\Phi}^{\dagger}Q'_{aL})$$
$$- \sum_{ab}(Y'^{D}_{ab}\overline{Q'_{aL}}\Phi q'^{D}_{bR}+Y'^{D*}_{ab}\overline{q'^{D}_{bR}}\Phi^{\dagger}Q'_{aL}), \qquad \textbf{(1.22)}$$

where $\Phi = \begin{pmatrix} \varphi^{+} \\ \varphi^{-} \end{pmatrix}^{2}$ is the Higgs doublet, and its conjugate form is defined as $\Phi e \equiv i\tau 2\Phi\dagger$. Besides, the Yukawa matrices Y'ℓ, Y'U , and Y'D are, in general, complex 3×3 matrices. As we will see in Section 1.4, the diagonalization of these matrices encodes the masses and mixings of the fermionsn resulting from the Higgs mechanism.

1.2 Electroweak Interactions

Let us now focus on the Lagrangian part that describes the leptonic couplings to the physical gauge bosons to obtain the charged and neutral current interactions. From Equation (1.14), one has

$$\mathcal{L}^{leptons}_{f} = i\sum_{\alpha}\overline{L'_{\alpha L}}\gamma^{\mu}\mathscr{D}_{\mu}L'_{\alpha L}+i\sum_{\alpha}\overline{\ell'_{\alpha R}}\gamma^{\mu}\mathscr{D}_{\mu}\ell'_{\alpha R}. \qquad \textbf{(1.23)}$$

Considering the covariant derivative in Equation (1.16) and the hypercharge values of the lepton doublets and singlets listed in Table 1.1, one has

$$\mathscr{D}_{\mu}L'_{\alpha L} = (\partial_{\mu}+ig\frac{\tau_{i}}{2}W^{i}_{\mu}+ig'\frac{Y}{2}B_{\mu})L'_{\alpha L}=(\partial_{\mu}+ig\frac{\tau_{i}}{2}W^{i}_{\mu}-i\frac{g'}{2}B_{\mu})L'_{\alpha L}, \textbf{(1.24)}$$

$$\mathscr{D}_{\mu}\ell'_{\alpha R} = (\partial_{\mu}+ig'\frac{Y}{2}B_{\mu})\ell'_{\alpha R}=(\partial_{\mu}-ig'B_{\mu})\ell'_{\alpha R}. \qquad \textbf{(1.25)}$$

To obtain the charged and neutral current interactions between leptons and gauge bosons, we substitute Equations (1.24) and (1.25) into (1.23), thereby

$$
\begin{aligned}
\mathcal{L}_f^{leptons} = \ & i\sum_\alpha \overline{L'_{\alpha L}}\gamma^\mu \partial_\mu L'_{\alpha L} + i\sum_\alpha \overline{\ell'_{\alpha R}}\gamma^\mu \partial_\mu \ell'_{\alpha R} \\
& - \frac{g}{\sqrt{2}}\left(\overline{v'_{\alpha L}}\gamma^\mu \ell'_{\alpha L}W_\mu^+ + \overline{\ell'_{\alpha L}}\gamma^\mu v'_{\alpha L}W_\mu^-\right) \\
& - \frac{g}{2}\left(\overline{v'_{\alpha L}}\gamma^\mu v'_{\alpha L} - \overline{\ell'_{\alpha L}}\gamma^\mu \ell'_{\alpha L}\right)W_\mu^3 + \frac{g'}{2}\left(\overline{v'_{\alpha L}}\gamma^\mu v'_{\alpha L} + \overline{\ell'_{\alpha L}}\gamma^\mu \ell'_{\alpha L} + 2\overline{\ell'_{\alpha R}}\gamma^\mu \ell'_{\alpha R}\right)B_\mu,
\end{aligned} \tag{1.26}
$$

where we have defined the charged fields as

$$
W_\mu^\pm \equiv \frac{W_\mu^1 \mp iW_\mu^2}{\sqrt{2}}, \tag{1.27}
$$

so that, the field W μ destroys the W+ bosons and creates W− bosons. The first line of Equation (1.26) contains the kinetic terms of the leptonic fields. The second and third lines are the charged and neutral current Lagrangian. On the one hand, the charged sector is given by

$$
\boxed{
\begin{aligned}
\mathcal{L}_{lep}^{CC} &= \frac{-g}{2\sqrt{2}}\overline{v'_\alpha}\gamma^\mu(1-\gamma^5)\ell'_\alpha W_\mu^+ + \text{h.c.} \\
&\equiv -\frac{g}{2\sqrt{2}}j_W^\mu W_\mu^+ + \text{h.c.},
\end{aligned}
} \tag{1.28}
$$

where we have defined the leptonic charged-current j_W^μ as

$$
j_W^\mu = 2\sum_\alpha \overline{v'_{\alpha L}}\gamma^\mu \ell'_{\alpha L} = \sum_\alpha \overline{v'_\alpha}\gamma^\mu(1-\gamma^5)\ell'_\alpha. \tag{1.29}
$$

On the other hand, as we will see in Section 1.3, the neutral gauge bosons W³μ and Bμ are orthogonal linear combinations of fields with well-defined masses, i.e., the physical states; one is the electromagnetic field Aμ, and the other one is the boson field Zμ. The rotation in the plane of the

W³μ and Bμ fields is given by

$$\begin{pmatrix} Z_\mu \\ A_\mu \end{pmatrix} = \begin{pmatrix} \cos\theta_W & -\sin\theta_W \\ \sin\theta_W & \cos\theta_W \end{pmatrix} \begin{pmatrix} W_\mu^3 \\ B_\mu \end{pmatrix}, \tag{1.30}$$

where θW is the so-called weak-mixing angle (Glashow, 1961; Weinberg, 1967). It is one of the main parameters in the electroweak theory, and its value is determined from weak neutral current processes and Z pole observables (ALEPH & et al., 2010; Bennett & Wieman, 1999). This fundamental parameter will be studied in the next chapter, where we will obtain a new value at low energies from (anti)neutrino-electron scattering.

Considering Equation (1.30), we may rewrite the electroweak neutral current interaction as

$$\mathcal{L}_{lep}^{NC} = -\frac{1}{2}\left\{ \overline{v'_{\alpha L}}\left[(g\cos\theta_W + g'\sin\theta_W)\not Z + (g\sin\theta_W - g'\cos\theta_W)\not A \right] v'_{\alpha L} \right.$$
$$- \overline{\ell'_{\alpha L}}\left[(g\cos\theta_W - g'\sin\theta_W)\not Z + (g\sin\theta_W + g'\cos\theta_W)\not A \right] \ell'_{\alpha L}$$
$$\left. - 2g'\overline{\ell'_{\alpha R}}\left[-\sin\theta_W \not Z + \cos\theta_W \not A \right] \ell'_{\alpha R} \right\}, \tag{1.31}$$

where $A/ = \gamma\mu A\mu$ and $Z/ = \gamma\,\mu Z\mu$. Note that the second term on the right hand in Equation (1.31) describes the neutrino coupling to the photon field. However, neutrinos are electrically neutral particles; hence this coupling is non-existent, at least at the tree level.

Therefore, at the tree level, let us equal to zero the coefficient of the corresponding term in Equation (1.31) so that

$$g\sin\theta_W = g'\cos\theta_W \implies \tan\theta_W = g'/g. \tag{1.32}$$

Therefore the weak mixing angle is given by the ratio of the two gauge coupling constants.

Inserting the Equation (1.32) in Equation (1.31), we obtain

$$\mathcal{L}_{lep}^{NC} = \frac{-g}{2\cos\theta_W}\left\{\overline{v'_{\alpha L}}\gamma^\mu v'_{\alpha L} - (1 - 2\sin^2\theta_W)\overline{\ell'_{\alpha L}}\gamma^\mu\ell'_{\alpha L} + 2\sin^2\theta_W\overline{\ell'_{\alpha R}}\gamma^\mu\ell_{\alpha R}\right\}Z_\mu \quad (1.33)$$
$$+ \quad g\sin\theta_W\overline{\ell'}\gamma^\mu\ell'A_\mu.$$

Taking into account that both the electromagnetic and the weak interactions have been unified into a single electroweak interaction, the neutral leptonic current must include the electromagnetic Lagrangian

$$\mathcal{L}_{lep}^{em} = -e\overline{\ell}\gamma^\mu Q\ell A_\mu, \qquad (1.34)$$

where Q is the charge operator or generator of U(1)em symmetry group of electromagnetic interactions. On the last term in Equation (1.33), we can identify the electrical charge $e = g\sin\theta_W$. Therefore, the electroweak neutral current interaction can be rewritten as

$$\boxed{\begin{aligned}\mathcal{L}_{lep}^{NC} &= \mathcal{L}_{lep}^{Z} + \mathcal{L}_{lep}^{em}, \\ &\equiv -\frac{g}{2\cos\theta_W}j_Z^\mu Z_\mu - e j_{em}^\mu A_\mu,\end{aligned}} \qquad (1.35)$$

with the leptonic neutral current, j_Z^μ, and the electromagnetic current, j_{em}^μ, given by

$$j_Z^\mu = 2g_L^v\overline{v'_{\alpha L}}\gamma^\mu v'_{\alpha L} + 2g_L^\ell\overline{\ell'_{\alpha L}}\gamma^\mu\ell'_{\alpha L} + 2g_R^\ell\overline{\ell'_{\alpha R}}\gamma^\mu\ell_{\alpha R}, \qquad (1.36)$$
$$j_{em}^\mu = -\overline{\ell'_\alpha}\gamma^\mu\ell'_\alpha, \qquad (1.37)$$

where we have introduced the left, g_L^f, and right, g_R^f, coupling constants. In addition, we can express the leptonic weak neutral current in terms of the axial and vector coupling constants g_A^f and g_V^f, respectively,

$$j_Z^\mu = \overline{v'_\alpha}\gamma^\mu(g_V^v - g_A^v\gamma^5)v'_\alpha + \overline{\ell'_\alpha}\gamma^\mu(g_V^\ell - g_A^\ell\gamma^5)\ell'_\alpha, \qquad (1.38)$$

where $g_{V,A}^f = g_L^f \pm g_R^f$. A full list of the coupling strengths for the lepton fields is shown in the Table 1.2.

Table 1.2
Values for the Leptonic Field Coupling Constants at Tree Level.

Lepton	g_L^f	g_R^f	g_V^f	g_A^f
ν_e, ν_μ, ν_τ	$+\frac{1}{2}$	0	$+\frac{1}{2}$	$+\frac{1}{2}$
e, μ, τ	$-\frac{1}{2}+\sin^2\theta_W$	$\sin^2\theta_W$	$-\frac{1}{2}+2\sin^2\theta_W$	$-\frac{1}{2}$

Note. The coupling constants are shown in terms of left (gL) and right (gR) couplings and as vector (gV) and axial (gA) terms. f = fermion field

1.3 The Higgs Mechanism

We have seen that, before the symmetry breaking, both fermions and gauge bosons are required to be massless since the presence of mass terms destroys the gauge invariance of the Lagrangian. However, in nature, only the photons are massless. Therefore, it is necessary to introduce the masses by a mechanism that preserves the gauge invariance of the Lagrangian. This will be achieved by the spontaneous symmetry breaking, the so-called Higgs mechanism (Englert & Brout, 1964; Higgs, 1964). To accomplish this task, we introduce a complex scalar field

$$\Phi \equiv \begin{pmatrix} \phi^+ \\ \phi^0 \end{pmatrix} = \frac{1}{\sqrt{2}} \begin{pmatrix} \phi_1 + i\phi_2 \\ \phi_3 + i\phi_4 \end{pmatrix}, \tag{1.39}$$

which is an SU(2) doublet with hypercharge equal to one. The most general Lagrangian for this field, invariant under the gauge symmetry, is given by the expression

$$\mathcal{L}_{Higgs} = (\mathscr{D}_\mu \Phi)^\dagger (\mathscr{D}^\mu \Phi) - V(\Phi^\dagger \Phi). \quad \text{(1.40)}$$

The Higgs potential, $V(\Phi^\dagger \Phi)$, is defined in Equation (1.19). The two possible potential forms are shown in Figure 1.1. The dashed line corresponds to the case $\mu^2 > 0$, where the ground state occurs at $|\Phi| = 0$. The solid line shows $\mu^2 < 0$. In this case, the potential in Equation (1.19) has its minimum at a finite value of $|\Phi|$, where

$$\Phi^\dagger \Phi \equiv \frac{1}{2}(\phi_1^2 + \phi_2^2 + \phi_3^2 + \phi_4^2) = -\frac{\mu^2}{2\lambda}. \quad \text{(1.41)}$$

We must expand Φ about a certain minimum. We can choose without loss of generality,

$$\phi_1 = \phi_2 = \phi_4 = 0, \qquad \phi_3^2 = -\frac{\mu^2}{\lambda} \equiv v^2, \quad \text{(1.42)}$$

where we have defined the vacuum expectation value (VEV) as v. This VEV spontaneously breaks the electroweak gauge symmetry to U(1)em, the symmetry group of electromagnetic interactions

$$SU(2)_L \times U(1)_Y \rightarrow U(1)_{em}. \quad \text{(1.43)}$$

To show the physical particle content of the electroweak theory, the VEV is parametrized in the unitary gauge

$$\Phi = \frac{1}{\sqrt{2}} \begin{pmatrix} 0 \\ v+H \end{pmatrix}, \quad \text{(1.44)}$$

where H is the physical Higgs field. Substituting Equation (1.44) into Equation (1.40), and considering the rotation of the gauge bosons that is given by Equation (1.30), one obtains

$$
\begin{aligned}
\mathscr{L}_{Higgs} = {} & \frac{1}{2}(\partial H)^2 - \lambda v^2 H^2 - \lambda v H^3 - \frac{\lambda}{4} H^4 \\
& + \frac{g^2 v^2}{4} W_\mu^\dagger W^\mu + \frac{g^2 v^2}{8 \cos \theta_W^2} Z_\mu Z^\mu \\
& + \frac{g^2 v}{2} W_\mu^\dagger W^\mu H + \frac{g^2 v}{4 C_W^2} Z_\mu Z^\mu H + \frac{g^2}{4} W_\mu^\dagger W^\mu H^2 + \frac{g^2}{8 C_W^2} Z_\mu Z^\mu H^2.
\end{aligned}
$$

$$(1.45)$$

We shall discuss each term in Equation (1.45): the first two terms correspond to the kinetic energy and the mass of the Higgs boson, respectively; the following two terms describe trilinear and quadrilinear self-coupling of the Higgs field. The second line represents mass terms for the W and

Figure 1.1
The Higgs Potential
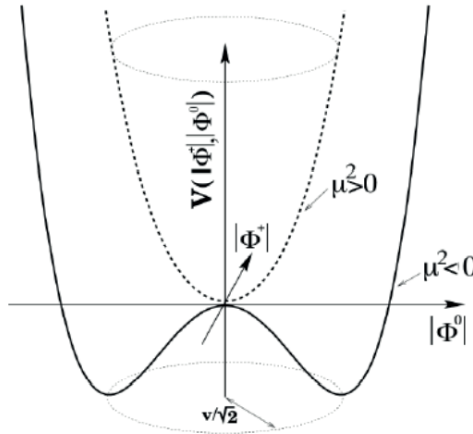
Note. The Higgs potential is $V(\Phi^\dagger \Phi) = \mu^2 \Phi^\dagger \Phi + \lambda (\Phi^\dagger \Phi)^2$.

Z bosons, respectively, and the third line describes interactions among the W, Z, and Higgs bosons. Consequently, the masses of the Higgs and gauge bosons are predicted to be

$$m_H = \sqrt{2\lambda \upsilon^2}, \qquad m_W = \frac{g\upsilon}{2}, \qquad m_Z = \frac{g\upsilon}{2\cos\theta_W}, \qquad m_\gamma = 0. \qquad (1.46)$$

According to the particle data group (Zyla & et al., 2020), their values are the following

$$m_H = (125.09 \pm 0.21(\text{stat}) \pm 0.11\text{syst})\,\text{GeV}, \qquad (1.47)$$

$$m_W = (80.385 \pm 0.015)\,\text{GeV}, \quad m_Z = (91.1876 \pm 0.0021)\,\text{GeV}. \qquad (1.48)$$

Therefore, the electroweak symmetry has been spontaneously broken with the Higgs mechanism, resulting in massive gauge bosons, W±, Z, and a massless photon.

On July 4, 2012, the ATLAS (Aad & et al., 2012) and CMS (Chatrchyan & et al., 2012)

Figure 1.2

Observation of the Higgs Boson with the ATLAS Detector at the LHC.
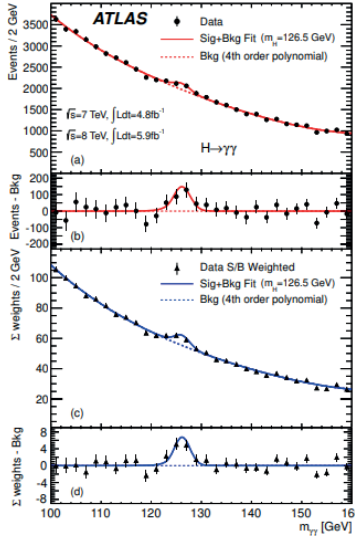
Note. Mass distribution for the two-photon channel. Th

collaborations announced the discovery of resonance at 125GeV, with 5σ signal significance. Figure (1.2) shows the results of the ATLAS collaboration. The new particle appeared as an excess around 126.5GeV with respect to the background. The complete analysis concluded that the probability that the observed signal was due to a background fluctuation is about 1 to 3.3 millions.

1.4 Fermion Masses and Mixing

We reviewed the Higgs mechanism to generate the W± and Z masses in the previous section. In this section, we will see that the same Higgs doublet is sufficient to give masses to the fermions. Here, we also restrict our discussion to the leptonic sector. For a detailed study of the Yukawa quark sector, we refer the reader to the references (Giunti & Kim, 2007; Langacker, 2017;Valle & Romao, 2015).

After spontaneous symmetry breaking, and considering the Higgs doublet in the unitary gauge in Equation (1.44), the Lagrangian of the Yukawa interaction of leptons and the Higgs boson giving by Equation (1.21) can be rewritten in the matrix form

$$\mathcal{L}_{Yukawa}^{leptons} = -\left(\frac{v+H}{\sqrt{2}}\right)[\overline{\ell'}_L Y'^{\ell} \ell'_R + h.c], \qquad \text{(1.49)}$$

$$\ell'_L \equiv \begin{pmatrix} e' \\ \mu' \\ \tau' \end{pmatrix}_L, \qquad \ell'_R = \begin{pmatrix} e' \\ \mu' \\ \tau' \end{pmatrix}_R. \qquad \text{(1.50)}$$

Note that the matrix Y′ℓ is generally non-diagonal. Hence, to identify the mass term for the charged lepton, it is necessary to diagonalize Y′ℓ. To do that, we separate the unitary transformations on the left and right-handed fermion fields, i.e.,

$$\ell_L = V_L^{\ell\dagger}\ell_L', \qquad \ell_R = V_R^{\ell\dagger}\ell_R', \quad \text{(1.51)}$$

where ℓL and ℓR denote the mass eigenstate fields, such that

$$V_L^{\ell\dagger}Y'^{\ell}V_R^{\ell} = Y^{\ell} = \begin{pmatrix} y_e & 0 & 0 \\ 0 & y_\mu & 0 \\ 0 & 0 & y_\tau \end{pmatrix}. \quad \text{(1.52)}$$

Substituting Equation (1.51) and Equation (1.52) into Equation (1.49) one obtains

$$\mathcal{L}_{leptons} = -\sum_\alpha \frac{1}{\sqrt{2}} y_\alpha^\ell \, v \overline{\ell_\alpha} \ell_\alpha - \sum_\alpha \frac{1}{\sqrt{2}} y_\alpha^\ell \overline{\ell_\alpha} \ell_\alpha H. \quad \text{(1.53)}$$

Finally, we can determine the mass term for the charged leptons

$$\boxed{m_\alpha^\ell = \frac{1}{\sqrt{2}} y_\alpha^\ell v.} \qquad \text{(1.54)}$$

However, since y_α^ℓ is a free parameter, the actual masses of charged leptons are not predicted by the SM. Therefore, they must be obtained from experimental measurements. In addition, since the neutrino fields have left-handed components only, it is impossible to generate neutrino masses. The second term on the right-hand side of Equation (1.53) accounts for trilinear couplings between the charged leptons and the Higgs boson.

Let us finally remark that we have reviewed the unified electroweak theory, which is based on the local gauge SU(2)$_L$ ×U(1)$_Y$ invariance. Masses and mixing of the charged fermions appear due to the spontaneous symmetry breaking. Also, the masses of the bosons W$^\pm$ and Z bosons. Summarizing the content of the previous sections, one has

$$
\begin{aligned}
\mathscr{L} \; = \quad & \underbrace{-\frac{1}{4}W^i_{\mu\nu}W^{\mu\nu i} - \frac{1}{4}B_{\mu\nu}B^{\mu\nu}}_{W^\pm, Z, \gamma \text{ kinetic energies and self-interactions}} \\
+ \quad & \underbrace{i\bar{L}\gamma^\mu(\partial_\mu + ig\frac{\tau_i}{2}W^i_\mu + ig'B_\mu\frac{Y}{2})L + i\bar{R}\gamma^\mu(\partial_\mu + ig'B_\mu\frac{Y}{2})R}_{W^\pm, Z, \gamma \text{ lepton and quark kinetic energies and their interactions with } W^\pm, Z, \gamma} \\
+ \quad & \underbrace{|(\partial_\mu + ig\frac{\tau_i}{2}W^i_\mu + ig'B_\mu\frac{Y}{2})\Phi|^2 - V(\Phi^\dagger\Phi)}_{W^\pm, Z, \gamma \text{ and Higgs masses and couplings}} \\
- \quad & \underbrace{(Y^\ell\bar{L}\Phi R + Y^U\overline{Q_L}\tilde{\Phi}q_R + Y^D\overline{Q_L}\Phi q_R + \text{ hermitian conjugate})}_{\text{lepton and quark masses, mixing and couplings to Higgs}}. \quad \textbf{(1.55)}
\end{aligned}
$$

As we have seen in the electroweak theory, neutrinos are massless particles. However, we know through the neutrino oscillation that this is not true. In Chapter 3, we will show that the Higgs mechanism can generate neutrino masses, as discussed before, similar to charged lepton and quark fields. However, it is unlikely that the same Higgs particle is responsible for the neutrino masses due to the small couplings. Therefore, new mechanisms must be searched to explain the neutrino mass.

2. Electroweak Physics with Neutrino Electron Scattering

2 Electroweak Physics with Neutrino Electron Scattering

2.1 Motivation

Neutrino physics has played a significant role in confirming the structure of Glashow-Weinberg-Salam theory (Glashow, 1961; Salam, 1968; Weinberg, 1967). In particular, the first experimental observation of one of the most important predictions of the electroweak theory, the existence of weak neutral currents given by Equation (1.36), was carried out at CERN in 1973 (Hasert & et al., 1973a, 1973b). By 1975, the evidence of weak neutral currents had been fully confirmed with the aid of the following processes (Barish et al., 1975; A. Benvenuti & et al., 1974):

$$\nu_\mu + e^- \rightarrow \nu_\mu + e^- \quad \text{(neutrino-electron elastic scattering)}, \qquad \textbf{(2.1)}$$

$$\overset{(-)}{\nu_\mu} + N \rightarrow \overset{(-)}{\nu_\mu} + X \quad \text{(deep inelastic scattering - DIS)}, \qquad \textbf{(2.2)}$$

where N = p,n and X denotes any set of final hadrons. The next step was to determine the space-time nature of the weak neutral current coupling. The results reported by the HPWF experiment in 1976 showed a mixture of V −A interactions in measurements of neutral-current and charged-current inelastic neutrino and antineutrino scattering, implying parity nonconservation (A. C. Benvenuti & et al., 1976). By 1978, other experiments such as the ones at SLAC (Prescott & et al., 1978) had confirmed that the

weak neutral currents had components of V and A interactions and agreed with the electroweak theory.

One fundamental parameter of the Glashow-Weinberg-Salam theory is the weak-mixing angle, θ_W ; through the years, its value was measured in various experimental setups. One of the earliest determinations of θ_W was carried out by the CDHS group in 1977 (Holder & et al., 1977). This group determined the value of the weak-mixing angle from the ratio of neutral (NC) to charged current (CC) neutrino and antineutrino DIS cross sections given by

$$R^\nu = \frac{\sigma_{NC}(\nu_\mu + N \to \nu_\mu + X)}{\sigma_{CC}(\nu_\mu + N \to \mu^- + X)} = \frac{1}{2} - \sin^2\theta_W + \frac{20}{27}\sin^4\theta_W, \qquad (2.3)$$

$$R^{\bar\nu} = \frac{\sigma_{NC}(\bar\nu_\mu + N \to \bar\nu_\mu + X)}{\sigma_{CC}(\bar\nu_\mu + N \to \mu^+ + X)} = \frac{1}{2} - \sin^2\theta_W + \frac{20}{9}\sin^4\theta_W. \qquad (2.4)$$

Currently, the weak mixing angle measurements at high energies have achieved high precision. However, its measurement at low energies has been difficult, especially in the neutrino sector (Zyla & et al., 2020). On the one hand, the interaction of neutrinos with quarks at low energies gave measurements that appeared to disagree with the electroweak theory (Zeller & et al.,2002). However, a later evaluation of the sea quark contributions indicates a coincidence with the standard model (Ball et al., 2009; Bentz, Cloet, Londergan, & Thomas, 2010). On the other hand, antineutrino-electron scattering reported results with a relatively large value of the weak-mixing angle (Barranco, Miranda, & Rashba, 2008; Deniz & et al., 2010), although without a strong statistical significance. The importance of a new measurement of this fundamental parameter in the low energy region has been noticed in different works and several proposals have been discussed in this direction (Agarwalla & Huber, 2011; Conrad, Link, & Shaevitz, 2005; Garces, Miranda, Tortola, & Valle, 2012).

In 2011, a new calculation of the reactor antineutrino energy spectrum (Huber, 2011; Mueller & et al., 2011) has raised the question of the possibility of an additional sterile neutrino (Mention et al., 2011), which we will investigate in Chapter 4. We want to note that the earlier evaluations of the weak-mixing angle should also be corrected due to the new reactor antineutrino energy spectrum.

In this chapter, we review neutrino-electron scattering using reactor and accelerator neutrino data to present a new value of the weak-mixing angle, considering the effect of electroweak radiative corrections (Bahcall, Kamionkowski, & Sirlin, 1995; Sarantakos, Sirlin, & Marciano, 1983) and improved measurement of the reactor antineutrino energy spectrum (Huber, 2011; Mueller & et al., 2011). With that goal in mind, we organize this chapter in the following manner. In Section 2.2, we define the weak-mixing angle in the modified minimal subtraction scheme. The neutrino-electron scattering at low energies is considered in Section 2.3, wherein we give the theoretical differential cross-section at the tree level as well as including radiative corrections. The description of the statistical analysis from the available neutrino-electron scattering data is presented in Section 2.4. Reactor and accelerator experiments will be considered, such as the Kuo-Sheng (TEXONO) (Deniz & et al., 2010), Bugey (MUNU) (Amsler & et al., 1997; Daraktchieva & et al., 2005), Rovno (Derbin et al., 1993), Krasnoyarsk (Vidyakin et al., 1992), LAMPF (Allen & et al., 1993) and LSND (Auerbach & et al., 2001). In Section 2.5, we show the results for the weak-mixing angle, considering both reactor and accelerator neutrino data. Besides, we discuss the impact of the Daya Bay spectrum, which apparently is not entirely consistent with the updated theoretical predictions

for the antineutrino spectrum at reactors. This chapter is a revised and updated version of the reference (Canas, Garces, Miranda, Tortola, & Valle, 2016).

2.2 The Weak-Mixing Angle

As we have seen in the previous chapter, the weak-mixing angle θW accounts for the mixing between the SU(2) and U(1) sectors, namely, the mixing between the gauge fields, $W3\mu$ and $B\mu$ and the mass eigenstates, $Z\mu$ and $A\mu$. From Equation (1.32), it is defined through the coupling constant of the SU(2) and U(1) gauge groups, g and g', respectively, as

$$\sin^2 \theta_W = \frac{g'^2}{g^2 + g'^2}. \tag{2.5}$$

This expression is valid at the tree level. However, at higher order, one must define a renormalized angle. Hence, we must choose a renormalization scheme to obtain a precise value. One of them is the modified minimal subtraction ($\overline{\text{MS}}$) (Sarantakos et al., 1983; Zyla & et al., 2020):

$$\sin^2 \theta_W(\mu) = \frac{\widehat{g}'^2(\mu)}{\widehat{g}^2(\mu) + \widehat{g}'^2(\mu)}, \tag{2.6}$$

Figure 2.1

Running of the Weak-Mixing Angle Defined in the $\overline{MS}$ Scheme
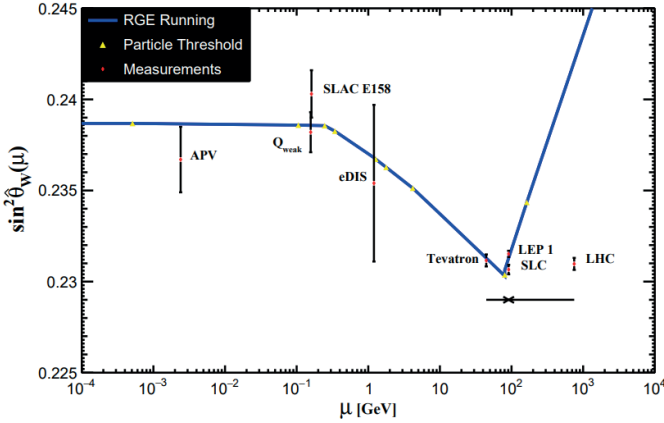
Note. The global fit is sin2 θW (MZ) = 0.23121(4) (Zyla & et al., 2020).

where $g(\mu)$ and $g'(\mu)$ are coupling defined by MS. The scale μ dependence corresponds to an arbitrary sliding mass scale.

  The previous definition of the weak-mixing angle in the Equation (2.6) can be rewritten as (Czarnecki & Marciano, 1996, 1998)

$$\sin^2 \theta_W(\mu) = \widehat{\kappa}(\mu) \sin^2 \theta_W(M_Z), \quad \text{(2.7)}$$

where the factor $\kappa(\mu)$ incorporates the corrections at higher orders; here $\mu = \langle Q \rangle$, being $\langle Q \rangle$ the average momentum transfer. The renormalized weak-mixing angle measured at different scales is shown in Figure 2.1. Besides, we present in Table 2.1 a summary of sin²θw measurements at the Z-pole and low Q_2.

  Another possibility is regarding the W and Z masses after the spontaneous breaking of the

Table 2.1

Summary of sin²θW Measurements at Z-pole and Low Q²

Measure	Experiment	$\sin^2\theta_W(M_Z)$
Z-pole	A_{RL}	0.23070 ± 0.00026
	A_{FB}	0.23193 ± 0.00029
	Average	$0.23125(16)$
Low-Q^2	Atomic parity violation (APV)	0.2283 ± 0.0020
	Moller E158	0.2329 ± 0.0013
	NuTeV	0.2356 ± 0.0016
	Average	0.2328 ± 0.0009

Note. The values of low Q² are extrapolated, for comparison, to the $\overline{\text{MS}}$ scale $\mu = m_Z$. The references of the experiments are the following: A_{RL} (Abe & et al., 2000),AFB (ALEPH & et al., 2010), APV (Bennett & Wieman, 1999), Moller E158 (Anthony & et al., 2005), NuTeV (Zeller & et al.,2002).

gauge symmetry, the so-called on-shell scheme (Sirlin, 1980),

$$\sin^2\theta_W = 1 - \frac{M_W^2}{M_Z^2}. \qquad (2.8)$$

In this case, the tree level Equation (2.8) is promoted to a definition of the renormalized sin²θW to all orders in perturbation theory. The masses of the W and Z bosons in Equation (2.8) are given by

$$M_W = \frac{A_0}{\sin\theta_W(1 - \Delta r)^{1/2}}, \qquad M_Z = \frac{M_W}{\cos\theta_W}, \qquad (2.9)$$

where A_0 = 37.28038 (1) GeV, and Δr = 0.03652 $\mp$ 0.00021±0.00007 (Zyla & et al., 2020).

In addition to the two previous definitions, there are other popular schemes, for instance, the effective angle $s_f^2 = \sin\theta_{\text{eff}}^f$, defined by the effective axial and vector couplings of the Z to fermion f.[1]

Each of the definitions of the weak-mixing angle has advantages and disadvantages; in particular, the $\overline{\text{MS}}$ prescription is more convenient for computational purposes and will be considered in this work.

As we discussed previously, within the $\overline{\text{MS}}$ renormalization scheme, the $\sin^2\theta W$ (μ) is a scale-dependent quantity, Equation (2.7). For low-energy experiments, we can find the effective weak-mixing angle using the Equation (2.7) and considering low average momentum transfer $\langle Q \rangle = 0$ as

$$\sin^2\theta_W(0) = \widehat{\kappa}(0)\sin^2\theta_W(M_Z) \quad \text{(2.10)}$$

where $\widehat{\kappa}(0) = 1.03232(29)$ and $\sin^2\theta_W$ (M_Z) $= 0.23121(4)$ (Kumar et al., 2013). Notice that at low Q^2, $\sin^2\theta_W$ (0) is approximated to 0.23868.

In the following, we will analyze the weak-mixing angle at low energies. We will consider radiative correction effects in the neutrino-electron scattering, considering the $\overline{\text{MS}}$ renormalization scheme.

---

[1]For a detailed discussion, we refer the reader to Reference (Zyla & et al., 2020).

2.3 Neutrino Electron Scattering at Low Energies

As pointed out in Chapter [1], the interactions at the tree level between the leptons and the physical gauge bosons within the electroweak theory are represented by the leptonic charged current Lagrangian in Equation (1.28)

$$\mathcal{L}_{lep}^{CC} = \frac{-g}{2\sqrt{2}} \sum_\alpha \overline{\nu_\alpha}\gamma^\mu(1-\gamma^5)\ell_\alpha W_\mu^+ + \text{h.c.}$$

$$\equiv -\frac{g}{2\sqrt{2}} j_W^\mu W_\mu^+ + \text{h.c.}, \qquad (2.11)$$

and by the leptonic neutral current Lagrangian in Equation (1.35)

$$\mathcal{L}_{lep}^{NC} = -\frac{g}{2\cos\theta_W} \sum_\alpha [\overline{\nu_\alpha}\gamma^\mu(g_V^\nu - g_A^\nu\gamma^5)\nu_\alpha + \overline{\ell_\alpha}\gamma^\mu(g_V^\ell - g_A^\ell\gamma^5)\ell_\alpha]Z_\mu + e\sum_\alpha \overline{\ell_\alpha}\gamma^\mu\ell_\alpha A_\mu$$

$$\equiv -\frac{g}{2\cos\theta_W} j_Z^\mu Z_\mu - e j_{em}^\mu A_\mu, \qquad (2.12)$$

where W± and Z are the intermediate charged and neutral vector bosons, respectively, while $g_V^{\nu,\ell}$ and $g_V^{\nu,\ell}$ stand for the vector and axial coupling constants, which are given in Table 1.2.

Figure 2.2

Tree-Level Diagrams of Electron Neutrino-Electron Scattering
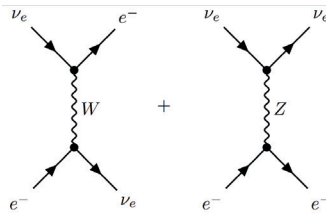
Note. The left panel is charged-current interaction, and the right panel is neutral-current interaction. Figure from (Giunti & Kim, [2007]).

In electroweak theory, many neutrino interactions cover different energy ranges, from the very lowest energies (a few eV) to the highest values (order of TeV). This part of the book discusses neutrino-electron elastic scattering at low energies,

$$\nu_e + e^- \rightarrow \nu_e + e^-, \qquad (2.13)$$

which occurs through a combination of charged and neutral current interactions as is displayed in Figure 2.2. The corresponding Feynman amplitude is given by

$$\mathcal{M} = -\frac{G_F}{\sqrt{2}} [\bar{\nu}_e \gamma^\nu (1 - \gamma_5) \nu_e][\bar{e}\gamma_\nu ((1 + g_V^e) - (1 + g_A^e)\gamma_5)e)]. \quad 2.14)$$

Notice that we assume the momentum transfer is small compared to the W and Z boson masses so that propagator effects can be ignored. In this limit, the coupling strength has been identified as the Fermi constant, GF (Zyla & et al., 2020)

$$\frac{G_F}{\sqrt{2}} = \frac{g^2}{8m_W^2} \quad \Rightarrow \quad G_F = 1.1663787(6) \times 10^{-5} \text{GeV}^{-2}. \quad (2.15)$$

To obtain the prediction for the differential cross section ('t Hooft, 1971a) of neutrino-electron elastic scattering at low energies, one square of the tree level amplitude in Equation (2.14), integrates over the final neutrino momentum, sums over the final electron polarization, and averages over the initial electron polarization. In the laboratory frame, one finds,

$$\frac{d\sigma}{dT} = \frac{2G_F^2 m_e}{\pi} \left[(1 + g_L^e)^2 + (g_R^e)^2 \left(1 - \frac{T}{E_\nu}\right)^2 - g_R^e (1 + g_L^e) \frac{m_e T}{E_\nu^2} \right], \qquad (2.16)$$

where me = 0.51099895000(15) MeV is the electron mass (Zyla & et al., 2020), T is the electron recoil energy and Ev is the incident neutrino energy and we have considered $g_{V,A}^f = g_L^f \pm g_R^f$.

2.3.1 Electroweak Radiative Corrections

Now, we incorporate electroweak radiative corrections of $\mathcal{O}(\alpha)$ to the neutrino-electron scattering (Sarantakos et al., 1983). For this purpose, we employ the modified minimal subtraction $\overline{MS}$ scheme (Marciano & Sirlin, 1981). Two types of corrections will be considered in the following: (1) electroweak corrections, which involve virtual exchanges of heavy particles such as W, Z in vertex and box diagrams, contributions to the $Z - Z$ and $\gamma - Z$ self-energies and neutrino charge radius diagrams (Bahcall et al., 1995; Sarantakos et al., 1983), and (2) QED corrections which include virtual photonic corrections and inner bremsstrahlung, which have been studied by many authors (Bahcall et al., 1995; Passera, 2001; Sarantakos et al., 1983). The corresponding Feynman diagrams for these corrections are found in Figure A.1 and Figure A.2. Therefore, including these two types of corrections and using the $\overline{MS}$ renormalization scheme, one obtains the differential cross section (Bahcall et al., 1995; Sarantakos et al., 1983)

$$
\begin{aligned}
\frac{d\sigma}{dT} = \frac{2G_F^2 m_e}{\pi} & \left\{ g_L^2(T) \left[1 + \frac{\alpha}{\pi} f_-(z) \right] + g_R^2(T)(1-z)^2 \left[1 + \frac{\alpha}{\pi} f_+(z) \right] \right. \\
& \left. - g_R(T)g_L(T)\frac{m_e}{E_\nu}z \left[1 + \frac{\alpha}{\pi} f_{+-}(z) \right] \right\},
\end{aligned}
\tag{2.17}
$$

where $z = T/E\nu$, and the coupling constants are given by

$$
\begin{aligned}
g_L^{(\nu_e,e)}(T) &= \rho_{NC}^{(\nu,l)} \left[\frac{1}{2} - \hat{\kappa}^{(\nu_e,e)}(T) \sin^2 \theta_W(m_Z) \right] - 1, \\
g_R^{(\nu_e,e)}(T) &= -\rho_{NC}^{(\nu,l)} \hat{\kappa}^{(\nu_e,e)}(T) \sin^2 \theta_W(m_Z).
\end{aligned}
\tag{2.18}
$$

Rewording, the functions $f-(z)$, $f+(z)$, and $f+-(z)$ encode the QED corrections, and the coupling constants consider electroweak corrections. Their complete analytical expressions are given in Appendix A.

2.4 Neutrino Data Analysis

We will investigate the impact of $\mathcal{O}(\alpha)$ radiative corrections to neutrino and antineutrino electron scattering to obtain a current limit on the weak-mixing angle from low energy measurements. To reach this goal, we perform a combined analysis of the available data from reactor experiments, namely, TEXONO (Deniz & et al., 2010), MUNU (Daraktchieva & et al., 2005), Rovno (Derbin et al., 1993) and Krasnoyarsk (Vidyakin et al., 1992), as well as accelerator experiments, particularly LAMPF (Allen & et al.,1993) and LSND (Auerbach & et al., 2001). In addition, for the case of reactor antineutrino experiments, we will also consider the role of the systematic uncertainties coming from the antineutrino spectrum in the analysis. The main experimental results reported by each experiment are summarized in Table 2.2. In the following, we describe the statistical analysis.

Table 2.2

Summary of Measured ve −e Scattering Cross Section and
sin²θW

Experiment	E_ν(MeV)	T(MeV)	Published cross-section	$\sin^2\theta_W$
Reactor $\bar{\nu}_e$:				
Krasnoyarsk	$3.2-8.0$	$3.3-5.2$	$[4.5\pm2.4]\times10^{-46}\text{cm}^2/\text{fission}$	$0.22^{+0.7}_{-0.8}$
Rovno	$0.6-8.0$	$0.6-2.0$	$[1.26\pm0.62]\times10^{-44}\text{cm}^2/\text{fission}$	$\ldots$
MUNU	$0.7-8.0$	$0.7-2.0$	$[1.07\pm0.34]\text{events/day}$	$\ldots$
Texono	$3.0-8.0$	$3.0-8.0$	$[1.08\pm0.21\pm0.16]\cdot\sigma_{SM}]$	$0.251\pm0.031\pm0.024$
Accelerator ν_e:				
LAMPF	$7-50$	$7-50$	$[10.0\pm1.5\pm0.9].\,10^{-45}\text{cm}^2$	0.249 ± 0.063
LSND	$20-50$	$20-50$	$[10.1\pm1.1\pm1.0].\,10^{-45}\text{cm}^2$	0.248 ± 0.051

Note. The measurements are from accelerator and reactor experiments at low energies. The references of the experiments are the following: Krasnoyarsk (Vidyakin et al., 1992); Rovno (Derbin et al., 1993); MUNU (Amsler & et al., 1997); Texono (Deniz & et al., 2010); LAMPF (Allen & et al., 1993); LSND (Auerbach & et al., 2001).

2.4.1 Reactor Data

We proceed to describe the reactor antineutrino experiments. In this case, the theoretical number of antineutrino-electron scattering events in each energy bin is given by

$$N_i^{\text{theo}}(\sin^2\theta_W) = \kappa \int \int \int_{T_i'}^{T_{i+1}'} \lambda(E_v) \frac{d\sigma(E_v, T, \sin^2\theta_W)}{dT} R(T, T') dT' dT dE_v, \quad \textbf{(2.19)}$$

where $\kappa = n_e t_{tot}\Phi$; n_e stands for the total number of targets, t_{tot} corresponds to the total exposure time of the experimental run, and Φ is the total antineutrino flux. Here T′ and T are, respectively, the detected electron recoil energy and the real recoil energy, T_i' and $T_i'+1$ are the minimum and maximum energy of the *i*-th bin, and Ev is the neutrino energy. The function $\lambda(E_v)$ is the antineutrino energy spectrum. Here, we have considered a new evaluation of this spectrum reported by Mueller, et al., (Mueller & et al., 2011), which is parametrized by an order five polynomial given by

$$\lambda(E_v) = \sum_{\ell} f_\ell \lambda_\ell(E_v) = \sum_{\ell} f_\ell \exp\left[\sum_{k=1}^{6} \alpha_{k\ell} E_v^{k-1}\right]; \quad E_v \geqslant 2\text{MeV}.$$

There are mainly four fission fragments in a reactor that contribute to its energy spectrum. In Equation 2.20, fℓ is the fission fraction for each isotope, where $\ell \equiv$ ^{235}U, ^{239}Pu, ^{241}Pu and ^{238}U. Their values depend on the experiment under study. The values for the coefficients $\alpha_{k\ell}$ are shown in Table B.1 and Table B.2 (Mueller & et al., 2011). In the case Ev < 2 MeV, we have used the spectrum from Ref. (Kopeikin, Mikaelyan, & Sinev, 1997).

Regarding the resolution function R(T,T′) [2], some of the experiments under study, such as TEXONO and MUNU reported their value, which was considered in the analysis. R(T,T′) is given by

$$R(T,T') = \frac{1}{\sqrt{2\pi}\sigma} \exp\left\{ -\frac{(T-T')^2}{2\sigma^2} \right\},$$ (2.21)

with $\sigma = \sigma(T) = \sigma_0\sqrt{T/MeV}$ [3]. If the experiment does not include this information, we will assume the ideal case of a perfect energy resolution parameterized by $R(T,T') = \delta(T - T')$.

Finally, at order $O(\alpha)$, the differential weak cross section for $\bar{\nu}_e - e^-$ scattering is given by Equation (2.17) after exchange $(1+g_L)$ by g_R.

With all this information, we perform the statistical analysis considering the following χ^2 function

$$\chi^2_{\text{reactor}}(\sin^2\theta_W) = \sum_{ij}(N_i^{\text{theo}}(\sin^2\theta_W) - N_i^{\text{exp}})\sigma_{ij}^{-2}(N_j^{\text{theo}}(\sin^2\theta_W) - N_j^{\text{exp}}),$$ (2.22)

where N_i^{theo} ($\sin^2\theta_W$) and N_i^{exp} are the expected number of events in Equation (2.19), including radiative corrections as given by Equation (2.17), and the observed number of events at the i-th bin, respectively. Included in the analysis of the inverse of the covariance matrix σ_{ij}^{-2}, one considers the statistical uncertainty reported by each experiment and the systematic error associated with the reactor antineutrino spectrum. The systematic uncertainties associated with the energy spectrum of the antineutrinos coming from the reactors are presented in Appendix B.

---

[2] This function accounts for possible differences between the observed electron recoil energy T′ and its true value T in the detector.
[3] σ stands from the error in the kinetic energy determination.

2.4.2 Accelerator Data

We now turn to the case of accelerator neutrinos. We focus on the average cross-section in these experiments to obtain a current limit on the weak-mixing angle. This observable is given by

$$\sigma^{theo}(\sin^2\theta_W) = \int\int \lambda(E_v)\frac{d\sigma(E_v,T,\sin^2\theta_W)}{dT}dTdE_v, \qquad (2.23)$$

where $\lambda(E_v)$ represents the flux of electron neutrinos from pion decay (Allen & et al., 1993; Auerbach & et al., 2001) and $d\sigma/dT$ is given by Equation (2.17).

The statistical analysis is like the one for reactor antineutrinos described in the previous subsection. However, by considering the electron-neutrino flux from (Allen & et al., 1993; Auerbach & et al., 2001), the $\chi2$ function is defined as

$$\chi^2_{accel}(\sin^2\theta_W) = \sum_{i=1}^{2}\frac{(\sigma_i^{theo}(\sin^2\theta_W)-\sigma_i^{exp})^2}{(\Delta_i)^2}, \qquad (2.24)$$

where the subscript i = 1,2 denote the LAMPF and LSND experiment, respectively. For the uncertainties, we have included the statistical and systematical errors on the reported cross-section, added in quadrature, as an uncorrelated error, Δi.

We have calibrated our numerical analysis to reproduce the actual results reported by each experiment. The first row in Table 2.3 shows the results obtained in the reactor case, while the results for accelerator experiments are reported in the first row of Table 2.4. Afterward, we included the new reactor spectrum and the radiative corrections. The results are presented in the following section.

Table 2.3

Limits on the Weak-Mixing Angle Obtained from Reactor Data Using Different Assumptions.

Assumption	MS	RC	TEXONO	MUNU	Rovno	Krasnoyarsk
a)	-	-	$0.256^{+0.032}_{-0.036}$	$0.241^{+0.069}_{-0.088}$	$0.220^{+0.102}_{-0.158}$	$0.220^{+0.068}_{-0.1}$
b)	-	✓	$0.261^{+0.032}_{-0.036}$	$0.248^{+0.069}_{-0.088}$	$0.226^{+0.102}_{-0.156}$	$0.224^{+0.069}_{-0.1}$
c)	✓	-	$0.253^{+0.032}_{-0.036}$	$0.237^{+0.069}_{-0.088}$	$0.228^{+0.102}_{-0.157}$	$0.231^{+0.069}_{-0.1}$
d)	✓	✓	$0.258^{+0.032}_{-0.036}$	$0.244^{+0.068}_{-0.088}$	$0.235^{+0.102}_{-0.157}$	$0.235^{+0.069}_{-0.1}$

Note. For a detailed discussion, see the text. (MS) and (RC) stands for the new reactor antineutrino spectrum and radiative corrections, respectively.

2.5 Limits on the Weak-Mixing Angle

2.5.1 From Reactor Experiments

As mentioned before, we want to know the radiative corrections' impact and the reactor spectrum's updated role in evaluating the weak-mixing angle. To reach this goal, we carry out the statistical analysis considering:

a) the original antineutrino spectrum considered in the original analysis of the experimental collaboration without radiative corrections,
b) the original spectrum, including radiative corrections (RC),
c) the new reactor antineutrino spectrum (MS) without radiative corrections, and
d) the new reactor antineutrino spectrum, including radiative corrections.

Taking into account the χ^2 function given by Equation (2.22), we present the results of this analysis in Table 2.3. Note that each row shows the central value of the weak-mixing angle under the corresponding assumption and the allowed region at 1σ. In addition, considering (d), we plot in Figure 2.3 the allowed region at 1σ that arises from the combined analysis for the weak-mixing angle. In the same figure, the contribution of each experiment is also shown. Here one can see the

Figure 2.3

Allowed Regions for the Weak-Mixing Angle from a Global Analysis.
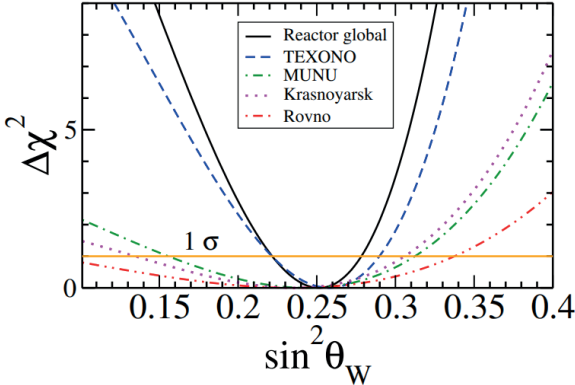
Note. The solid black curve is allowed values for the weak-mixing angle from the global analysis as reported in (Canas et al., 2016). The horizontal orange line shows values at 1σ. The dashed curves show the restrictions from the individual experiments. TEXONO dominates the result.

dominant role played by TEXONO data. However, the global analysis shifts the preferred value of $\sin^2\theta_W$ towards a slightly smaller central value in agreement with the prediction at low energies in the $\overline{MS}$ scheme: $\sin^2\theta_W = 0.23867$. The bound from the combined analysis of reactor data, at 1σ, is

$$\sin^2 \theta_W = 0.252 \pm 0.030. \qquad \text{(2.25)}$$

Figure 2.4

Impact of the Daya Bay Antineutrino Spectrum Measurement on the TEXONO Data.
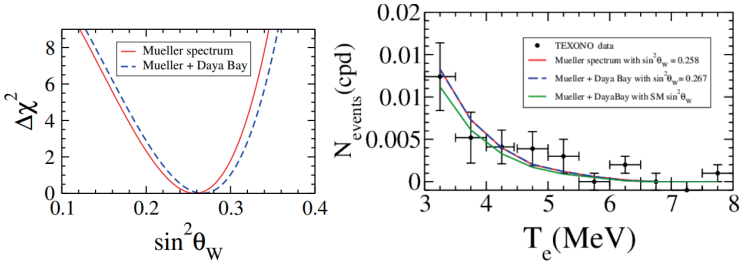
Note. Impact of the Daya Bay antineutrino spectrum measurement on the TEXONO data as reported in (Canas et al., 2016). In the left panel, the determination of $\sin^2\theta_W$ from TEXONO data using the original Mueller spectrum (solid red line) and the Mueller spectrum was corrected by the Daya Bay measurement of the total reactor antineutrino flux (dashed blue line). In the right panel, expected event numbers in TEXONO using the Mueller spectrum for the TEXONO $\sin^2\theta_W$ bestfit value (solid red line). The blue dashed line corresponds to the best fit analysis obtained using the Mueller spectrum modified by the Daya Bay flux measurement. The solid green line shows the prediction for the electroweak (SM) weak-mixing angle, $\sin^2\theta_W = 0.23867$.

Measurements of the Antineutrino Spectrum Reported by the Daya Bay Experiment

Up to now, we have considered the prediction of the antineutrino spectrum reported by Mueller, et al.(Mueller & et al., 2011). However, results reported by the Daya Bay collaboration suggest a deviation concerning Mueller's prediction (5.4%) (Leitner, 2017). Further theoretical

developments and accurate experimental measurements are needed to find the correct answer. It is interesting to consider the impact of the Daya Bay reactor flux measurement upon the statistical analysis carried out on TEXONO data.

On the one hand, we correct the theoretical spectrum predicted by Mueller et al. (Mueller & et al., 2011) with the overall normalization factor 0.946, which is the central value for the ratio of measured to predicted flux, as reported by the Daya Bay collaboration (Leitner, 2017). The left part of Figure 2.4 shows this result. From this plot, we can conclude that if the Daya Bay result is confirmed, the resulting value of the weak-mixing angle will shift towards higher values compared with the prediction at low energies in the $\overline{\text{MS}}$ scheme. In this case, we obtain

$$\sin^2 \theta_W = 0.267 \pm 0.033 \quad \text{(Mueller + DayaBay spectrum)}. \tag{2.26}$$

On the other hand, the right part of Figure 2.4 shows the expected number of counts per day versus the kinetic energy of the recoil electron from TEXONO. The red and blue lines correspond to Mueller spectrum (Mueller & et al., 2011) with the best-fit value of the weak-mixing angle obtained from the TEXONO data analysis, $\sin^2\theta_W = 0.258$ (see Table 2.3); and the reactor antineutrino spectrum predicted by Mueller including both the correction factor indicated by the Daya Bay measurements and the obtained best-fit value for $\sin^2\theta_W = 0.267$ in Figure 2.4 (left panel: dashed blue line). The solid green line shows the Mueller reactor antineutrino spectrum corrected by the Daya Bay result for the electroweak prediction of the weak-mixing angle at low energies in the $\overline{\text{MS}}$ scheme: $\sin^2\theta_W = 0.23867$. From these plots, we can conclude that TEXONO data slightly favors higher values for $\sin^2\theta_W$.

We should stress that further antineutrino electron scattering measurements will be necessary to better understand the neutrino reaction and the reactor spectrum. In addition, they could measure the weak-mixing angle with better sensitivities of ±1%. Unfortunately, achieving this goal implies challenging efforts; nevertheless, overcoming these difficulties could unveil interesting phenomena of new physics (Agarwalla & Huber, 2011; de Gouvea & Jenkins, 2006).

2.5.2 From Accelerator Experiments

It is possible to go one step further and combine the previous reactor analysis with accelerator experiments.

Firstly, in Table 2.4, we only summarize the results from accelerator data analysis. As we

Table 2.4

Limits on the Weak-Mixing Angle at 1σ Derivate From the LAMPF and LSND Data Analysis.

RC	LAMPF	LSND
-	$0.249^{+0.061}_{-0.067}$	$0.248^{+0.054}_{-0.058}$
✓	$0.261^{+0.061}_{-0.068}$	$0.261^{+0.056}_{-0.058}$

Note. (RC) stands for radiative corrections.

can see from these results, the central value of the weak-mixing angle, including radiative corrections, shifts toward higher values compared with the electroweak prediction but with more significant uncertainties. Performing the combined analysis from accelerator experiments, one finds the following constraint on the weak-mixing angle

$$\boxed{\sin^2 \theta_W = 0.261 \pm 0.042.}$$

<div align="right">(2.27)</div>

Secondly, for comparison purposes, we show in Figure 2.5 the results obtained from reactor and accelerator experiments. Note that we present our results with (continuous error bars) or without (dashed error bars) radiative corrections. Additionally, for reactor experiments, the impact of the Mueller spectrum is shown, concluding that - with the current statistical uncertainties - the inclusion of the new spectrum has a mild effect on the determination of $\sin^2\theta_W$. On the other hand, the inclusion of radiative corrections increases the value of the weak-mixing angle concerning the theoretical prediction in the $\overline{MS}$ scheme: $\sin^2\theta_W = 0.23867$.

Combining all the experiments at low energies considered up to now, we obtain a global determination of the weak-mixing angle equal to

$$\boxed{\sin^2 \theta_W = 0.254 \pm 0.024.}$$

<div align="right">(2.28)</div>

Let us finally emphasize that we have performed a phenomenological study of neutrino-electron scattering at low energies, including radiative corrections, to get a new

Figure 2.5
Values of the Weak-Mixing Angle for the Combined Analysis of Reactor and Accelerator Experiments.
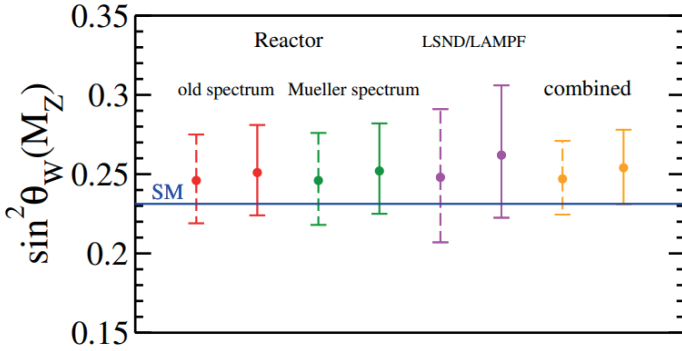
Note. In the reactor experiments, we have considered the old or the Mueller reactor spectrum and with (continuous error bars) or without (dashed error bars) radiative corrections. For accelerator experiments, we show the results with and without radiative corrections. It is a result from (Canas et al., 2016).

evaluation of the weak-mixing angle parameter. In the particular case of reactor antineutrino data, we have also shown the impact of the new predicted reactor spectrum (Mueller & et al., 2011).

For comparison purposes, we display in Figure 2.6 the results (blue and green lines) along with other much more precise determinations at different energy ranges.

We want to stress the importance of further, more refined, experiments in (anti)neutrino-electron scattering to improve the low energy determination of the weak mixing angle from neutrino experiments.

Figure 2.6

Values of the Weak-Mixing Angle from Various Experimental Determinations.
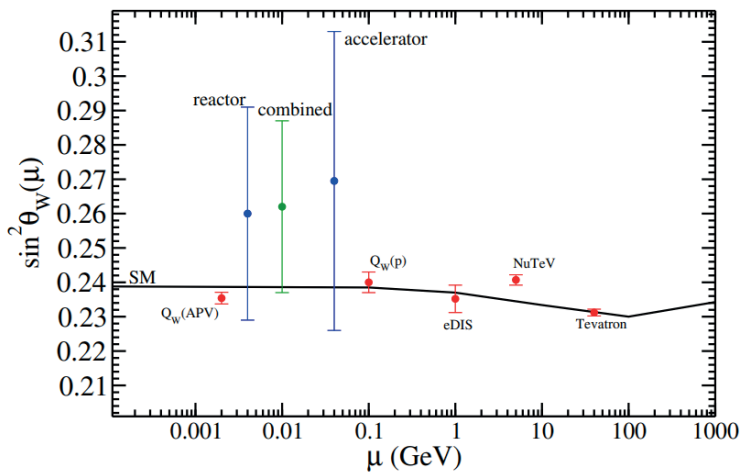
Note. Values of the weak-mixing angle, in the $\overline{\text{MS}}$ scheme, from various experimental determinations, according to Ref. (Zyla & et al., 2020). For comparison, we extrapolate our results to the low-energy limit, as discussed in the text. A result from (Canas et al., 2016).

Capítulo 3

Neutrino Mass, Mixing and Oscillations

3 Neutrino Mass, Mixing and Oscillations

When Pauli postulated the existence of the "neutrino" in 1930, he proposed that this new particle might have a mass of the same order as the electron mass or not larger than 0.01 proton mass, page 27 on (Brown, 1978). Later, in 1934, Fermi (Fermi, 1934) and Perrin (Perrin, 1933) proposed a method for measuring the neutrino mass through the beta spectrum near the endpoint, in which the neutrino has a small energy. This investigation was carried out by Hanna and Pontecorvo in 1949, obtaining the upper bound $m_v \lesssim 500\text{eV}$ (Hanna & Pontecorvo, 1949). At the beginning of 1957, two groups led by Wu (Wu, Ambler, Hayward, Hoppes, & Hudson, 1957) and Lederman (Garwin, Lederman, & Weinrich, 1957) obtained the first evidence of parity violation in beta decay. Soon after and following experimental data, Landau (Landau, 1957), Lee and Yang (Lee & Yang, 1957) and, Salam (Salam, 1957) developed the two-component theory of the neutrino, wherein they assumed that it does not have mass and that the neutrino field is either v_L or v_R.

In 1958, Goldhaber et al. (Goldhaber, Grodzins, & Sunyar, 1958) showed that neutrinos are left-handed particles. Such a particle can only be massless since otherwise, with an appropriate Lorentz transformation, the neutrino might spin in the wrong sense. Only with the success of the unified electroweak theory did it become clear that this argument was misleading. The handedness was not a

property of neutrinos but was intrinsic to the interaction that created them. In particular, in 1978, Prescott et al. (Prescott & et al., 1978) observed parity non-conservation in the inelastic scattering of longitudinally polarized electrons from a target of unpolarized deuterium, which means a process where neutrinos play no role. Within the Glashow-Weinberg-Salam theory, the neutrinos were not provided with right-handed field components; hence, they were assumed to be massless particles.

Currently, it is a well-established experimental fact that neutrinos are massive and mixed particles (see Section 3.3) (de Salas et al., 2021; Zyla & et al., 2020), and hence the electroweak theory must be extended to explain their small value and large mixing. More detailed discussions may be found in a number of books (Giunti & Kim, 2007; Langacker, 2017; Valle & Romao, 2015) and review articles (Gonzalez-Garcia & Maltoni, 2008; Mohapatra & Smirnov, 2006; Strumia & Vissani, 2006).

In this chapter, we study the underlying issues related to the neutrino masses and mixings and the neutrino oscillation mechanism. We start in Section 3.1 with a brief review of massive neutrinos beyond the electroweak theory. In Section 3.2, we discuss the mathematical formulation of neutrino oscillation in a vacuum. In Section 3.3, we overview the indications in favor of neutrino oscillations. Finally, in Section 3.4, we present the current status of the global analysis of neutrino oscillation data.

3.1 Massive Neutrinos

In the electroweak theory studied in Chapter 1, charged fermions and neutrinos are described respectively by massive and massless Dirac fields (Dirac, 1928). On the one hand, the massive fields are represented by a four-

component Dirac spinor (left- and right-handed particles and left- and right-handed antiparticles). On the other hand, the massless fields, the neutrinos, are described by a single chiral field (left-handed neutrino or right-handed antineutrino). Particles and antiparticles are different and can be distinguished by the law of the lepton number.

Let us briefly discuss this experimental result. The neutral particle emitted in the positive (negative) pion decay, $\pi^+ \to \mu^+ + \nu_\mu$ ($\pi^- \to \mu^- + \bar{\nu}_\mu$), interacts with a detector, N, producing a muon (antimuon), μ^- (μ^+):

$$\nu_\mu N \longrightarrow \mu^- X; \qquad \bar{\nu}_\mu N \longrightarrow \mu^+ X \qquad (\checkmark). \tag{3.1}$$

Moreover, the following processes are not observed experimentally

$$\nu_\mu N \longrightarrow \mu^+ X; \qquad \bar{\nu}_\mu N \longrightarrow \mu^- X \qquad (\text{X}). \tag{3.2}$$

Therefore, the neutral particle emitted in the positive (negative) pion decay is defined as *muon neutrino (muon antineutrino)*. The following statements support the previous experimental facts:

1. ν_μ and $\bar{\nu}_\mu$ are different particles.

2. Conservation of the leptonic number. Each lepton is defined with lepton number $L_\ell = +1$, while, each antilepton with $L_{\bar{\ell}} = -1$. Hence, μ^- and ν_μ have $L_\mu = +1$, and $\mu+$ and $\bar{\nu}_\mu$ have $L_{\bar{\mu}} = -1$.

On the other hand, considering the well-established experimental fact of neutrino oscillations - the change of the flavor of neutrinos during their propagation - it can be concluded that the flavor lepton numbers are not conserved. Nevertheless, then, how can we distinguish a particle

from its antiparticle? The answer might be in the theory developed by Majorana in 1937 (Majorana, 1937) wherein particles are their own antiparticles. Let us see how. In the Majorana formulation, we can associate the different behavior observed in the processes (3.1) with different helicity states, namely, the neutral particle emitted in the positive pion decay $\pi^+ \rightarrow \mu^+ + \nu_\mu$ has a left-handed helicity, while the one emitted in negative pion decay $\pi^- \rightarrow \mu^- + \bar{\nu}_\mu$ has a right-handed helicity. Considering the Majorana approach, left and right helicity states belong to one single particle known as Majorana particle, and these helicity states agree with the experimental observation. Within the matter content of the electroweak theory, elementary fermions are not known to be their own antiparticle, except possibly for neutrinos. Therefore, in the following, we review how to generate both Dirac and Majorana mass terms beyond the electroweak theory.

3.1.1 Dirac Mass

As we saw in Chapter 1, in the electroweak theory, lepton masses arise from the Yukawa couplings that is given by Equation (1.53) between the Higgs doublet and both left- and right-handed components of the lepton fields. Note that due to the lack of a right-handed neutrino component, this remains massless after the spontaneous breaking of the gauge symmetry. Nevertheless, if it includes three right-handed neutrino fields $\nu'_{\alpha R}$, Dirac neutrino mass terms will be generated by the same Higgs mechanism, which is responsible for the fermion masses. This extension is known as the *minimally extended electroweak theory*. In this case, the Yukawa Lagrangian term will have the form

$$\mathscr{L}^D = -\sum_{\alpha,\beta} Y'^\nu_{\alpha\beta} \overline{L'}_{\alpha L} \widetilde{\Phi} \nu'_{\beta R} + h.c, \tag{3.3}$$

where we have written explicitly only the terms containing the neutrino fields. In the unitary gauge, the Yukawa Lagrangian in Equation (3.3) is given by

$$\mathcal{L}^D = -\left(\frac{\upsilon+H}{\sqrt{2}}\right)\overline{v'_L}Y'^v v'_R + h.c, \tag{3.4}$$

where we have defined the left- and right-handed neutrino fields as

$$v'_L \equiv \begin{pmatrix} v'_e \\ v'_\mu \\ v'_\tau \end{pmatrix}_L, \quad v'_R = \begin{pmatrix} v'_e \\ v'_\mu \\ v'_\tau \end{pmatrix}_R. \tag{3.5}$$

Following the ideas developed in Section 1.4, we diagonalize the matrix $Y'v$ through biunitary transformations to obtain the mass eigenstates fields. As a result, one has

$$\begin{aligned} \mathcal{L}^D &= -\left(\frac{\upsilon+H}{\sqrt{2}}\right)\sum_k y^v_k \overline{v_{kL}} v_{kR} + h.c, \\ &= -\sum_k \frac{y^v_k}{\sqrt{2}} \upsilon \overline{v_k} v_k - \sum_k \frac{y^v_k}{\sqrt{2}} \overline{v_k} v_k H. \end{aligned} \tag{3.6}$$

Notice that the first term in Equation (3.6) has generated a mass term for the neutrino with the same Higgs mechanism that gives masses to fermions in the electroweak theory.

$$\boxed{\mathcal{L}^D = -\frac{1}{\sqrt{2}}\sum_k y^v_k \upsilon \overline{v_k} v_k.} \tag{3.7}$$

This is known as a *Dirac mass term*.

3.1.2 Majorana Mass

In the previous subsection, we have seen that the Dirac mass term for the neutrino requires the existence of its right-handed field. Nevertheless, in the early '30s, Majorana asked if he could describe a massive neutrino using only the left-handed neutrino field. The answer was yes. If right-handed fields are defined as

$$\nu_{\alpha R} = \mathscr{C}\overline{\nu_{\alpha L}}^T, \tag{3.8}$$

where $\mathscr{C}$ is the charge conjugation operator, it is possible to write a Majorana mass term with the same structure as a Dirac one. As a result, one obtains

$$\mathscr{L}^M = \frac{1}{2}\sum_{\alpha\beta} \nu_{\alpha L}^T \mathscr{C}^\dagger M_{\alpha\beta}\nu_{\beta L} + \text{h.c.}, \tag{3.9}$$

with M being a complex symmetric matrix. As in the Dirac neutrino case, we must diagonalize this matrix to obtain the mass eigenstate fields, after which one obtains

$$\mathscr{L}^M = \frac{1}{2}\sum_k m_k \nu_{kL}^T \mathscr{C}^\dagger \nu_{kL} + \text{h.c.}, \tag{3.10}$$

This is known as a Majorana mass term. In the same way, as we express a Dirac field in terms of its right- and left-handed components, let us write the Majorana field as follows

$$\nu_\alpha = \nu_{\alpha L} + \nu_{\alpha R} = \nu_{\alpha L} + \mathscr{C}\overline{\nu_{\alpha L}}^T, \tag{3.11}$$

and now, if we take the charge conjugate of the Majorana field

$$\nu_\alpha^C = (\nu_{\alpha L} + \mathscr{C}\overline{\nu_{\alpha L}}^T)^C = \nu_{\alpha L}^C + \nu_{\alpha L} = \nu_\alpha. \tag{3.12}$$

That is, the charge conjugate of the field is the same field. This relation implies that particles and antiparticles are equal. As we mentioned before, among the elementary matter content in the electroweak theory, only the neutrinos are neutral particles and might satisfy this condition.

Figure 3.1

Schematic Point of View of Neutrino Oscillation Phenomena
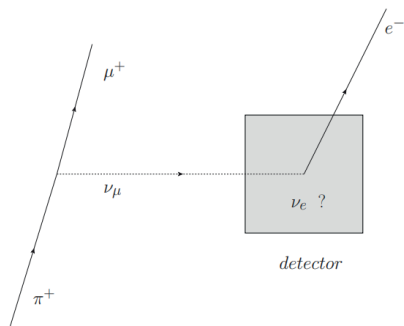
Note. Figure adapted from (Kayser, Gibrat-Debu, & Perrier, 1989).

3.2 Neutrinos Oscillations

Now, let us describe the neutrino oscillation phenomenon in vacuum. As an example, let us take the previously discussed pion decay. The neutral particle emitted in this decay interacts with matter producing a muon. However, what would happen if, in the final state, another charged lepton will be detected, for instance, an electron? (see Figure 3.1). The explanation for this phenomenon was discovered by the pioneering experiment Kamiokande (Fukuda & et al., 1994) and confirmed by Super-Kamiokande (Fukuda & et al., 1998a), SNO (Ahmad & et al., 2002), KamLAND (Eguchi & et al., 2003), and many others.

Thanks to the results obtained with all these experiments, it is known that the flavor neutrino fields (ν_e,ν_μ,ν_τ) are mixtures of the massive neutrino fields (ν_1,ν_2,ν_3), that is

$$\nu_{\alpha L} = \sum_{i=1}^{3} U_{\alpha i}\nu_{iL}, \qquad (\alpha = e, \mu, \tau), \qquad (3.13)$$

where $U_{\alpha i}$ are the matrix elements of the 3×3 unitary mixing matrix, U, which is known as the Pontecorvo-Maki-Nakagawa-Sataka (PMNS) matrix (Maki, Nakagawa, & Sakata, 1962). It has six independent parameters: three mixing angles ($\theta_{12},\theta_{23}, \theta_{13}$) and three phases ($\delta_{CP},\alpha,\beta$).

However, the only phase significant for the oscillation probabilities is δ_{CP} (CP-violating phase). The PMNS matrix can be written as

$$U = \begin{pmatrix} c_{12}c_{13} & s_{12}c_{13} & s_{13}e^{-i\delta_{CP}} \\ -s_{12}c_{23}-c_{12}s_{13}s_{23}e^{i\delta_{CP}} & c_{12}c_{23}-s_{12}s_{13}s_{23}e^{i\delta_{CP}} & c_{13}s_{23} \\ s_{12}s_{23}-c_{12}s_{13}c_{23}e^{i\delta_{CP}} & -c_{12}s_{23}-s_{12}s_{13}c_{23}e^{i\delta_{CP}} & c_{13}c_{23} \end{pmatrix} \qquad (3.14)$$

where $s_{ij} \equiv \sin\theta_{ij}$, and $c_{ij} \equiv \cos\theta_{ij}$. The allowed values for the mixing angles and CP-violating phase are $\theta_{ij}\in[0,\pi/2]$ and $\delta_{CP} \in[0,2\pi]$ (Workman & et al., 2022). Now, we will calculate the vacuum oscillation probability that a neutrino produced with flavor α is detected with flavor β. Let us suppose that at time $t=0$, it is produced a neutrino ν_α, with momentum p_ν such that

$$|\nu_\alpha(t = 0)\rangle = \sum_{k=1}^{3} U_{\alpha k}^*|\nu_k\rangle. \qquad (3.15)$$

where $|\nu_\alpha(t = 0)\rangle = |\nu_\alpha\rangle$. After a time t, the evolution of this state will be given by

$$|\nu_\alpha(t)\rangle = \sum_{\beta=e,\mu,\tau} \left(\sum_{k=1}^{3} U_{\alpha k}^* e^{-iE_k t} U_{\beta k} \right) |\nu_\beta\rangle, \qquad (3.16)$$

where we are describing the neutrino states as plane waves, and we are going to assume that the three states of mass have the same momentum $\vec{p}_\nu$ and are ultra-relativistic, $L = ct$ with $c = 1$: $E_k = \sqrt{\vec{p}_\nu{}^2 + m_k^2}$ and $m_k \ll p_\nu$, one has $E_k \simeq E + m_k^2/2E$ where $E = |\vec{p}_\nu|$.

This standard theory of neutrino oscillations is based on the following assumptions: The neutrino flavor state, Equation (3.1), depends on the interaction process, neither the production nor the detention of neutrinos; Massive neutrinos have the same momentum despite having different masses; Describing neutrinos as plane waves. Although these assumptions greatly simplify the treatment of neutrino oscillations, these assumptions lead to the correct oscillation probability for neutrino oscillations experiments that are not sensitive to the physical details of this phenomenon. Readers can find a discussion of these assumptions and the proper approach to the phenomenon of neutrino oscillations at the end of Section 7.1 and Chapter 8 in (Giunti & Kim, 2007) and the reference (Akhmedov, 2019).

The probability of finding the neutrino with flavor ν_β at a distance L from its source, if originally it had flavor ν_α is given by

$$P_{\nu_\alpha \to \nu_\beta}(L) = |\langle \nu_\beta | \nu_\alpha(L) \rangle|^2, \tag{3.17}$$

$$P_{\nu_\alpha \to \nu_\beta}(L) = \delta_{\alpha\beta} - 4 \sum_{i>j} \mathrm{Re}(U^*_{\alpha i} U_{\alpha j} U_{\beta i} U^*_{\beta j}) \sin^2\left(\frac{\Delta m_{ij}^2 L}{4E}\right)$$

$$+ 2 \sum_{i>j} \mathrm{Im}(U^*_{\alpha i} U_{\alpha j} U_{\beta i} U^*_{\beta j}) \sin\left(\frac{\Delta m_{ij}^2 L}{2E}\right), \tag{3.18}$$

where $\Delta m_{ij}^2 \equiv m_i^2 - m_i^2$.

The Equation (3.16) indicates that a neutrino flavor state evolves over time as a linear combination of flavor states. To do it, the neutrinos must have mass and be mixed.

This phenomenon is called neutrino oscillations, meaning that the flavor lepton number is not conserved during neutrino propagation. This can be seen in Equation (3.18) since there is a non-zero probability that a neutrino of another flavor will be detected.

The neutrino oscillation experiments are classified as appearance and disappearance experiments. The former look for $\nu\alpha \to \nu\beta$, where $\alpha = \beta$, that is, they measure the transition probability between differents flavors. The latter look for deficits in the original flux ($\nu\alpha \to \nu\alpha$), that is, they measure the survival probability and in this case, the probability, Equation (3.18), can be rewritten as:

$$P_{\nu_\alpha \to \nu_\alpha}(L) = 1 - 4\sum_{i>j} |U_{\alpha i}|^2 |U_{\alpha j}|^2 \sin^2\left(\frac{\Delta m_{ij}^2 L}{4E}\right). \qquad (3.19)$$

To calculate the oscillation probability for the antineutrino case, we follow basically the same steps as above but exchange $U \to U^*$ in the mixing matrix. The antineutrino oscillation probability will be:

$$P_{\bar{\nu}_\alpha \to \bar{\nu}_\beta}(L) = \delta_{\alpha\beta} - 4\sum_{i>j} \mathrm{Re}(U_{\alpha i}^* U_{\alpha j} U_{\beta i} U_{\beta j}^*) \sin^2\left(\frac{\Delta m_{ij}^2 L}{4E}\right)$$

$$- 2\sum_{i>j} \mathrm{Im}(U_{\alpha i}^* U_{\alpha j} U_{\beta i} U_{\beta j}^*) \sin\left(\frac{\Delta m_{ij}^2 L}{2E}\right). \qquad (3.20)$$

Regarding the discrete CP symmetry, comparing the oscillation probabilities for neutrinos and antineutrinos, Equation (3.18) and Equation (3.20) respectively, we can say that the term containing the real part preserves the CP symmetry and the violation of the CP symmetry in the lepton sector is present in the imaginary part.

The concept of oscillation length L_{ij}^{osc} indicates the sensitivity of a neutrino oscillation experiment to the oscillation parameter $\Delta m_{ij}^2 \equiv m_i^2 - m_j^2$,

$$L_{ij}^{\text{osc}} = \frac{4\pi E}{\Delta m_{ij}^2} = 2.479 \frac{E/1\text{MeV}}{\Delta m_{ij}^2/\text{eV}^2} m. \tag{3.21}$$

If $E/L \gg \Delta m_{ij}^2$ $(L \ll L_{ij}^{\text{osc}})$, the oscillations due to the oscillation phase have not been generated, and there is no pattern of oscillations in the experiment. In the other extreme case, if $E/L \ll \Delta m_{ij}^2$ $(L \gg L_{ij}^{\text{osc}})$, the oscillation phase generates many oscillations leading to the oscillation probability to be averaged. Finally, an oscillation experiment is sensitive to Δm_{ij}^2 when $L_{ij}^{\text{osc}} \sim 1$.

3.3 Indications of Neutrinos Oscillations

3.3.1 Solar Neutrino Experiments

Solar neutrinos (νe) arise from thermonuclear reactions inside the sun, where the two leading fluxes are given by the pp chain and the CNO (carbon-nitrogen-oxygen) cycle. The sources of solar neutrinos are listed in Table 3.1. The first five lines correspond to the pp cycle, while the last three belong to the CNO cycle.

The first indication of neutrino oscillations' flavor was obtained in 1968 by the radiochemical experiment Homestake (Davis, Harmer, & Hoffman, 1968). The solar neutrino flux

Table 3.1
Sources of Solar Neutrinos

Source	Reaction	Average neutrino energy (MeV)	Maximum neutrino energy (MeV)
pp	$p + p \to d + e^+ + \nu_e$	0.2668	0.423 ± 0.03
pep	$p + e^- + p \to d + \nu_e$	1.445	1.445
hep	$^3\text{He} + p \to {}^4\text{He} + e^+ + \nu_e$	9.628	18.778
^7Be	$e^- + {}^7\text{Be} \to {}^7\text{Li} + \nu_e$	0.3855	0.3855
		0.8631	0.8631
^8B	$^8\text{B} \to {}^8\text{Be}^* + e^+ + \nu_e$	6.735 ± 0.036	~ 15
^{13}N	$^{13}\text{N} \to {}^{13}\text{C} + e^+ + \nu_e$	0.7063	1.1982 ± 0.0003
^{15}O	$^{15}\text{O} \to {}^{15}\text{N} + e^+ + \nu_e$	0.9964	1.7317 ± 0.0005
^{17}F	$^{17}\text{F} \to {}^{17}\text{O} + e^+ + \nu_e$	0.9977	1.7364 ± 0.0003

Note. Data taken from (Giunti & Kim, 2007)

measured by this experiment was about three times smaller than the predicted by the standard solar model (Bahcall, Bahcall, & Shaviv, 1968; Bahcall & Pena-Garay, 2004; Bahcall & Pinsonneault, 2004). This discrepancy was so-called as The Solar Neutrino Problem, and it was confirmed by subsequent solar neutrino experiments such as Homestake (Cleveland et al., 1998), Kamiokande (Fukuda & et al., 1996), GALLEX (Hampel & et al., 1996), SAGE (D. N. Abdurashitov & et al., 1996), and Super-Kamiokande (Fukuda & et al., 1998b). All of these experiments were predominantly sensitive to electron neutrinos.

The hypothesis of neutrino flavor change was confirmed by the Sudbury Neutrino Observatory (SNO) after a combined analysis in which they concluded that over two-thirds of the electron neutrinos change into other flavors before reaching the SNO detector (Aharmim & et al., 2013). By this discovery, the SNO research group, led by Arthur B. McDonald and the Super-Kamiokande experiment conducted by Takaaki Kajita were awarded the Nobel Prize in Physics in 2015. The latter experiment reported evidence of neutrino oscillations in atmospheric neutrinos.

Figure 3.2

Data/Prediction as a Function of the Reconstructed L/E from Super-Kamiokande Experiment
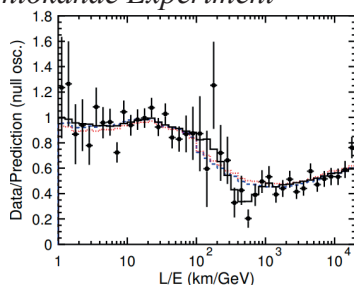
Note. Figure taken from the results of Super-Kamiokande experiment (Ashie & et al., 2004).

3.3.2 Atmospheric Neutrino Experiments

Atmospheric neutrinos ($\overset{(-)}{\nu}_\mu$ and $\overset{(-)}{\nu}_e$) are generated as decay products in hadronic showers resulting from interactions of cosmic rays with nuclei in the upper atmosphere. These neutrinos are mainly produced by the process

$$\pi^+ \rightarrow \mu^+ + \nu_\mu \tag{3.22}$$

$$\downarrow$$

$$e^+ + \nu_e + \overline{\nu}_\mu$$
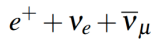
and their charge conjugates. These neutrinos are produced with approximately the same energy and, hence, when it is calculated the ratio of μ-type to e-type, the result is around two. The first evidence for atmospheric neutrino oscillations was reported by the Super-Kamiokande experiment in 1998 (Fukuda & et al., 1998a). At that time, two other experiments, MACRO (Ambrosio & et al., 1998) and Soudan-2 (Allison & et al., 1999), confirmed the zenith angle distribution for

Figure 3.3

Ratio of Measured to Expected Electron Antineutrino Flux from KamLAND Experiment
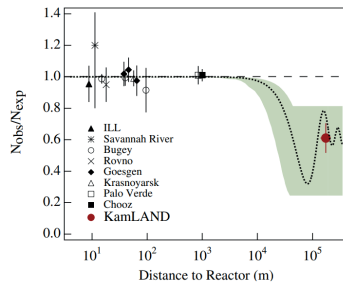
Note. Figure taken from the results of KamLAND experiment (Eguchi & et al., 2003).

atmospheric neutrino announced by the Super-Kamiokan-de collaboration. In Figure 3.2 is displayed the observed L/E distribution in Super-Kamiokande, assuming νμ ↔ ντ oscillations (solid line). It represented the first direct evidence that the neutrino survival probability has a sinusoidal behavior as neutrino flavor oscillations predict it.

3.3.3 Reactor Neutrinos Experiments

Reactor antineutrinos ($\overline{V}e$) are produced in the core of a nuclear reactor as beta decay products of fission fragments. Among the pioneer reactor experiments, we find the KamLAND experiment, which was carried out to check the oscillation solution of the solar neutrino problem. In 2002 (Eguchi & et al., 2003), KamLAND demonstrated, for the first time, both the deficit of electron antineutrinos from reactors and that the large mixing angle was the correct solution to the solar neutrino problem. We can see in Figure 3.3 one of the results reported by the KamLAND collabora-tion (Eguchi & et al., 2003). There, it is shown the ratio of measured to expected flux for several reactor experiments. In particular, we can see that short baseline reactor experi-ments (L = 10−100 m) did not observe any $\overline{V}e$ disappearan-ce. In 2011, Mueller et al. (Mueller & et al., 2011) recalcu-lated the reactor antineutrino spectrum, and the new flux estimate has increased about 3%. This re-evaluation affects all the reactor neutrino experiments. In particular, they conducted a reanalysis with the SBL experiments, showing that the ratio of observed to expected events rates decrea-sed. This deficit is known as rector antineutrino anomaly (Mention et al., 2011). This topic will be studied in more detail in Chapter 4. In addition, previous reactor experi-ments such as CHOOZ (Apollonio & et al., 1999) and Palo

Verde (Boehm & et al., 2001) did not report any neutrino oscillation.

3.4 Global Fit Results for Neutrino Oscillation Parameters

Currently, several groups (de Salas et al., 2021; Esteban, Gonzalez-Garcia, Maltoni, Schwetz, & Zhou, 2020) report global analysis of the existing neutrino oscillation data. In Table 3.2, we present the results of the global analysis of neutrino oscillation data. These results are obtained within the standard three neutrino framework.

In Figure 3.4, we represent the two possibilities of organizing the mass spectrum of the neutrino mass states: On the left, we describe the Normal Ordering (NO) - the order of mass states is $m_1 < m_2 < m_3$; On the right, we represent the Inverted Ordering (IO) -the order of mass states is $m_3 < m_1 < m_2$. The numerical values of a squared mass difference (Δm_{ij}^2) are given in Table 3.2. With the colors green, blue, and red, we are representing the content percentage of the states of flavor, $\nu e, \nu \mu, \nu \tau$, respectively, in the mass states. This percentage is obtained from the values of the mixing angles given in Table 3.2, and we can indicate that if the ordering of the masses is NO, the lightest mass state is constituted mainly by the flavor state νe but, if the order is inverted, the lightest mass state almost does not contain the state of flavor νe. As neutrino oscillations are governed by the squared mass difference of the mass states, Δm^2, and not by the mass of the mass states, we can not be determined the absolute neutrino mass from neutrino oscillation experiments, as indicated in Figure 3.4 for the question mark. Experiments like KATRIN (Osipowicz & et al.,

Table 3.2
Neutrino Oscillation Parameter Overview

Parameter	Best fit ±1σ	2σ range	3σ range
$\Delta m^2_{21}[10^{-5}eV^2]$	$7.50^{+0.22}_{-0.20}$	$7.12 - 7.93$	$6.94 - 8.14$
$|\Delta m^2_{31}|[10^{-3}eV^2](NO)$	$2.55^{+0.02}_{-0.03}$	$2.49 - 2.60$	$2.47 - 2.63$
$|\Delta m^2_{31}|[10^{-3}eV^2](IO)$	$2.45^{+0.02}_{-0.03}$	$2.39 - 2.50$	$2.37 - 2.53$
$\sin^2\theta_{12}/10^{-1}$	3.18 ± 0.16	$2.86 - 3.52$	$2.71 - 3.69$
$\theta_{12}/°$	34.3 ± 1.0	$32.3 - 36.4$	$31.4 - 37.4$
$\sin^2\theta_{23}/10^{-1}(NO)$	5.74 ± 0.14	$5.41 - 5.99$	$4.34 - 6.10$
$\theta_{23}/°(NO)$	49.26 ± 0.79	$47.37 - 50.71$	$41.20 - 51.33$
$\sin^2\theta_{23}/10^{-1}(IO)$	$5.78^{+0.10}_{-0.17}$	$5.41 - 5.98$	$4.33 - 6.08$
$\theta_{23}/°(IO)$	$49.46^{+0.60}_{-0.97}$	$47.35 - 50.67$	$41.16 - 51.25$
$\sin^2\theta_{13}/10^{-2}(NO)$	$2.200^{+0.069}_{-0.062}$	$2.069 - 2.337$	$2.000 - 2.405$
$\theta_{13}/°(NO)$	$8.53^{+0.13}_{-0.12}$	$8.27 - 8.79$	$8.13 - 8.92$
$\sin^2\theta_{13}/10^{-2}(IO)$	$2.225^{0.064}_{-0.070}$	$2.086 - 2.356$	$2.018 - 2.424$
$\theta_{13}/°(IO)$	$8.58^{0.12}_{-0.14}$	$8.30 - 8.83$	$8.17 - 8.96$
$\delta_{CP}/\pi(NO)$	$1.08^{+0.13}_{-0.12}$	$0.84 - 1.42$	$0.71 - 1.99$
$\delta_{CP}/°(NO)$	194^{+24}_{-22}	$152 - 255$	$128 - 359$
$\delta_{CP}/\pi(IO)$	$1.58^{+0.15}_{-0.16}$	$1.26 - 1.85$	$1.11 - 1.96$
$\delta_{CP}/°(IO)$	284^{+26}_{-28}	$226 - 332$	$200 - 353$

Note. Data taken from (de Salas et al., 2021).

2001) and the upcoming Project 8 (Ashtari Esfahani & et al., 2017) are designed to make measurements of the mass of neutrinos. In 2022, KATRIN reported that combining the first (Aker & et al., 2019, 2021) and second physics campaigns, the upper neutrino mass limit is less than 0.8 eV ($m_{\bar{\nu}e}^{eff} < 0.8$ eV) with a 90% CL (Aker & et al., 2022).

Figure 3.4

The Mass Spectra of the Neutrinos are Organized in Normal Ordering and Inverted Ordering
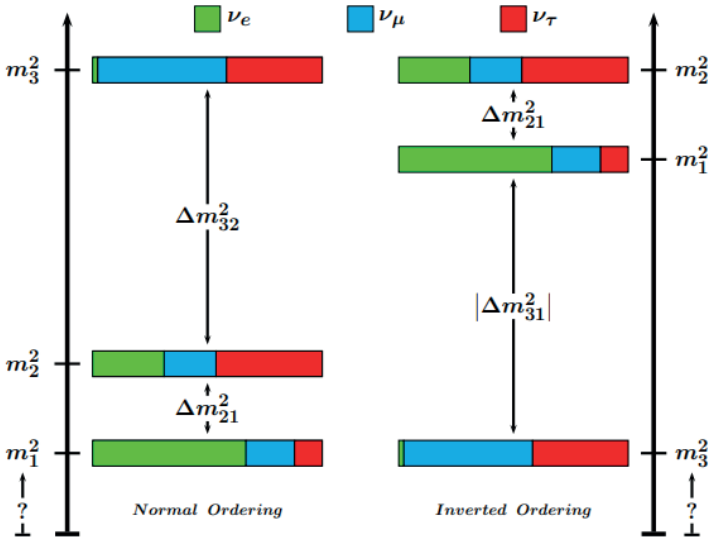
Note. The mass spectra of the neutrinos are organized in a Normal Ordering (NO), blocks on the left, or in an Inverted Ordering (IO), blocks on the right. The percentage of flavor in each mass is represented in color. The question mark means that we do not know the value of the mass of the lightest state.

Capítulo 4

Beyond the three neutrino framework

4 Beyond the three neutrino framework

4.1 Motivation

In Chapter 3, we discussed the current status of the neutrino oscillation phenomenon in the framework of three neutrino mixing. In this scheme, there are two mass-squared differences: $\Delta m_{21}^2 = (7.50^{+0.22}_{-0.20}) \times 10^{-5} \text{eV}^2$ and $|\Delta m_{31}^2| = (2.55^{+0.02}_{-0.03}) \times 10^{-3} \text{eV}^2$ (for NO) at 1σ (see Table 3.2). However, currently, there are four anomalies that cannot be explained within this scenario (Acero & et al., 2022): the Gallium anomaly (J. N. Abdurashitov & et al., 2009; Anselmann & et al., 1995), the reactor antineutrino anomaly (Mention et al., 2011), the LSND anomaly (A. Aguilar-Arevalo & et al., 2001) and MiniBooNE low-energy excess (A. A. Aguilar-Arevalo & et al., 2007). These anomalies could be explained if new light sterile neutrinos with a mass of O(eV) exist. We must keep in mind that constraint from the invisible decay width of the Z boson established that the effective number of light active neutrino states should be three (ALEPH & et al., 2010; Zyla & et al., 2020). Therefore, additional neutrinos states must be sterile (Pontecorvo, 1967), i.e., they do not have standard weak interactions.

In this chapter, we will investigate the possible $\nu e \rightarrow \nu e$ oscillations of $\Delta m^2 \sim 1 e\text{V}^2$ scale sterile neutrinos, by incorporating data from Gallium and reactor short baseline experiments. Moreover, for the first time in this kind of analysis, we will include reactor antineutrino-electron

scattering data. We will also briefly present the LSND anomaly and MiniBooNE low-energy excess that arise when looking for evidence of $\nu\mu \to \nu e$ ($\overline{\nu}\mu \to \overline{\nu}e$) oscillations from $\Delta m^2 \sim 1 eV^2$.

This chapter is organized as follows. In Section 4.2, we will present the framework of 3+1 sterile neutrinos. In Sections 4.3- 4.5, we will describe the statistical analysis of the Gallium anomaly and the reactor antineutrino anomaly. In Section 4.6 we will discuss the LSND anomaly and Mini-BooNE low-energy excess. This chapter is a revised and updated version of Reference (Cañas, Garcés, Miranda, & Parada, 2018)

4.2 The 3+1 Mixing Scheme

As we discussed in the previous section, the existence of three different scales of Δm^2 implies that at least four light massive neutrinos must exist in nature. Here we consider the so-called 3+1 mixing scheme in which, besides the three standard massive neutrinos, there is a new *non-standard massive neutrino.*

In this scheme, in the flavor basis, the three active neutrinos $\nu e, \nu\mu$, $\nu\tau$ are connected with one sterile neutrino ν_s that does not participate in standard weak interactions.

The mass eigenstates ν_1, ν_2, ν_3, and ν_4 are labeled such that ν_1, ν_2, ν_3 contribute mainly to the three active flavor eigenstates; $\nu e, \nu\mu, \nu\tau$, and provide the squared-mass differences required for standard three-flavor oscillation: the solar and atmospheric mass-squared differences (de Salas et al., 2021). The mass state $\nu 4$ is mostly sterile and provides the new squared-mass difference at the eV^2 scale. These conditions are summarized in

$$\Delta m_{21}^2 \ll |\Delta m_{31}^2| \ll \Delta m_{41}^2, \qquad \textbf{(4.1)}$$

where $\Delta m^2_{kj} \equiv m^2_k - m^2_j$. In Figure 4.1, we schematically represent the flavor content of each mass state in this 3+1 framework.

The connection between flavor basis, ν_α, and mass basis, ν_k, is through the relation

$$\nu_\alpha = \sum_{k=1}^{4} U_{\alpha k} \nu_k \qquad (\alpha = e, \mu, \tau, s), \qquad (4.2)$$

where U, in this case, is a 4×4 unitary mixing matrix that is characterized by nine physical parameters: six mixing angles, $\theta_{12}, \theta_{13}, \theta_{23}$ (the three active mixing angles), $\theta_{14}, \theta_{24}, \theta_{34}$ (three new active-sterile mixing angles) and three CP violating phases, δ_{CP} (CP-violation on active neutrinos), δ_{14}, δ_{24} (Acero & et al., 2022; Giunti & Kim, 2007). Since the non-standard massive neutrino must be mostly sterile, we have an additional condition

$$|U_{\alpha 4}|^2 \ll 1 \qquad (\alpha = e, \mu, \tau), \qquad (4.3)$$

Figure 4.1
Schematic Representation of the Mass Spectrum of Neutrinos in the Framework of 3+1
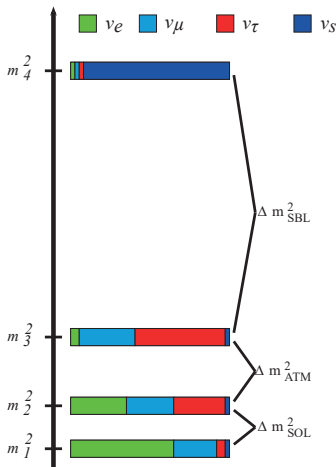
Note. Three neutrinos are active in the framework of 3+1 mixing neutrinos, and one neutrino is sterile. In this scheme, we assume the normal ordering of the masses for the states ν_1, ν_2, ν_3. SBL stands for short baseline.

to preserve the solar, atmospheric and long-baseline neutrino oscillation data.

$$U_{3+1} = \begin{bmatrix} U_{e1} & U_{e2} & U_{e3} & U_{e4} \\ \vdots & & \vdots & U_{\mu 4} \\ \vdots & & \vdots & U_{\tau 4} \\ U_{s1} & U_{s2} & U_{s3} & U_{s4} \end{bmatrix}. \tag{4.4}$$

In particular, $|U_{e4}|^2$ describes the mixing of the electron neutrino flavor with the eV-scale neutrino mass state $\nu 4$. In 3+1 neutrino mixing, the transition and survival probabilities at short baseline can be written as

$$P_{\nu_\alpha \to \nu_\beta}^{\text{SBL}} = 4|U_{\alpha 4}|^2 |U_{\beta 4}|^2 \sin^2\left(\frac{\Delta m_{41}^2 L}{4E}\right), \qquad \alpha \neq \beta, \tag{4.5}$$

$$P_{\nu_\alpha \to \nu_\alpha}^{\text{SBL}} = 1 - 4|U_{\alpha 4}|^2 (1 - |U_{\alpha 4}|^2) \sin^2\left(\frac{\Delta m_{41}^2 L}{4E}\right), \tag{4.6}$$

where, we have taken into account the Equation (4.1). The transition and survival probabilities are often defined in terms of the following effective mixing angles,

$$\sin^2 2\theta_{\alpha\beta} = 4|U_{\alpha 4}|^2 |U_{\beta 4}|^2 \qquad (\alpha \neq \beta), \tag{4.7}$$

$$\sin^2 2\theta_{\alpha\alpha} = 4|U_{\alpha 4}|^2 (1 - |U_{\alpha 4}|^2). \tag{4.8}$$

From now on, we consider $\nu e(\bar{\nu}e)$ disappearance experiments, which means we will use the Equation (4.6) to perform both the individual and the combined analysis related to the SBL anomalies discussed in this chapter.

4.3 The Gallium Anomaly

In this section, we study two primary solar neutrino experiments, which measured for the first time the low energy neutrinos (E < 0.42 MeV) produced in the pp-chain: The GALLEX (Gallium Experiment) (Anselmann & et al., 1995) and the SAGE (Sovietic American Gallium Experiment) (J. N. Abdurashitov & et al., 2009). These two experiments detected a deficit of the solar neutrino flux, which did not agree with the Standard Solar Model predictions. Hence, to test their solar neutrino detectors, GALLEX and SAGE conducted investigations with intense neutrino sources placed inside the detectors. The main characteristics of each experiment and their results are summarized in Table 4.1.

The average ratio from these experiments was R = 0.86±0.05, indicating a deficit in the number of measured events. This effect was known as *the Gallium Anomaly*, and it could explain the disappearance of νe due to transitions of νe into another neutrino state (Giunti & Laveder, 2011).

Table 4.1

The Ratio of the Measured Rate of 71Ge to Predicted at SAGE and GALLEX Experiments

Ratio	GALLEX		SAGE	
	G1	G2	S1	S2
R_B	$0.95^{+0.11}_{-0.11}$	$0.81^{+0.10}_{-0.11}$	$0.95^{+0.12}_{-0.12}$	$0.79^{+0.08}_{-0.08}$
radius[m]	1.9		0.7	
height[m]	5.0		1.47	
source height[m]	2.7	2.38	0.72	

Note. Row 1: RB stand for the measured to predicted ratio ^{71}Ge production rates in the two GALLEX ^{51}Cr radioactive source experiments, G1 (Hampel & et al., 1998) and G2 (Kaether, Hampel, Heusser, Kiko, & Kirsten, 2010), and the SAGE 51Cr and 37Ar radioactive source experiments, S1 (J. N. Abdurashitov & et al., 1999) and S2 (J. N. Abdurashitov & et al., 2006), respectively. The subscript B stress that the theoretical event was calculated with the best-fit values of the Bahcall cross sections. For a detailed discussion, see the text.

Rows 2 and 3: we present the radii and heights of the GALLEX and SAGE detectors.

Row 4: the height of the source measured from the base of the detector and on the detector axis.

Adapted from (Acero, Giunti, & Laveder, 2008).

4.3.1 Statistical Analysis of the Gallium Anomaly

In this subsection, we describe the statistical analysis used to obtain the allowed regions in the $\sin^2 2\theta_{ee} - \Delta m^2_{41}$ plane under the hypothesis of one sterile neutrino as a possible solution to the Gallium Anomaly.

As mentioned above, GALLEX and SAGE experiments were tested with intense artificial ^{51}Cr and ^{37}Ar neutrino sources placed inside the detectors. The chromium and argon sources decay through electron capture

$$e^- + {}^{51}\mathrm{Cr} \to {}^{51}\mathrm{V} + \nu_e, \qquad e^- + {}^{37}\mathrm{Ar} \to {}^{37}\mathrm{Cl} + \nu_e, \qquad \textbf{(4.9)}$$
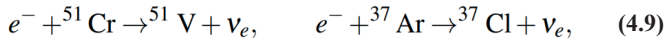
Figure 4.2

Nuclear Levels for the ^{51}Cr and ^{37}Ar Radioactive Sources Decay

^{51}Cr (27.7 days)

427 keV v (9.0%)
432 keV v (0.9%)

747 keV v (81.6%)
752 keV v (8.5%)

^{37}Ar (35.04 days)

320 keV γ

813 keV v (9.8%)
811 keV v (90.2%)

^{37}Cl (stable)

^{51}V
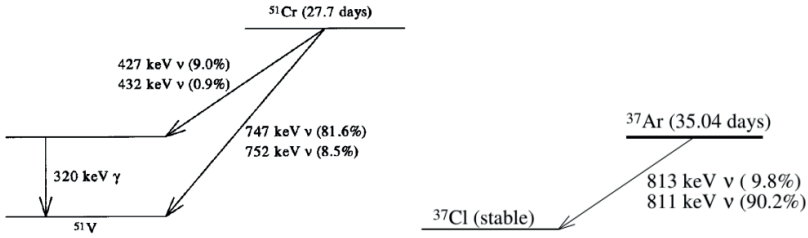
Note. Nuclear levels for the ^{51}Cr and ^{37}Ar radioactive sources decay, corresponding to the process (4.9). Figures from (J. N. Abdurashitov & et al., 1999, 2006)

emitting mono-energetic electron neutrinos, as shown in Figure 4.2. These neutrinos' energies, branching ratios, and cross-sections are shown in Table. 4.2. In both experiments, the electron neutrino detection is through the same reaction employed for the detection of solar neutrinos given by

$$\nu_e +^{71} \text{Ga} \rightarrow^{71} \text{Ge} + e^-, \quad (4.10)$$
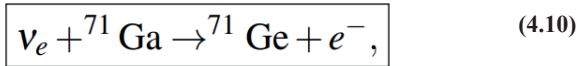
which has a threshold energy of $E\nu^{th} = 0.233$ MeV (233 keV).

The predicted ^{71}Ge event rates in Table 4.1 were calculated considering the best-fit values of the Bahcall cross-sections (without considering their uncertainties) given by (Bahcall, 1997)

$$\sigma_B^{bf}(^{51}\text{Cr}) = (58.1^{+2.1}_{-1.6}) \times 10^{-46}\text{cm}^2, \quad (4.11)$$

$$\sigma_B^{bf}(^{37}\text{Ar}) = (70.0^{+4.9}_{-2.1}) \times 10^{-46}\text{cm}^2. \quad (4.12)$$

These predictions took into account transitions from the ground state of ^{71}Ga to the ground state of ^{71}Ge as well as transitions from the ground state of ^{71}Ga to the two excited states of ^{71}Ge at 175 and 500 KeV. The former has been computed accurately by Bahcall (Bahcall, 1997), and the latter is inferred using nuclear models, as we shall discuss later. As we can see from the Figure

Table 4.2

Summary of the Neutrino Energies, Branching ratios, and Cross Sections for the Production of ^{71}Ge

Features	^{51}Cr				^{37}Ar	
E_v[keV]	747	752	427	432	811	813
B.R.	0.8163	0.0849	0.0895	0.0093	0.902	0.098
$\sigma[10^{-46}\text{cm}^2]$	60.8	61.5	26.7	27.1	70.1	70.3

Note. Ev are the neutrino energies, B.R. are the branching ratios, and σ are the cross sections for the process in Equation (4.10). The cross sections are interpolated from Tab. II of Ref. (Bahcall, 1997).

4.3, neutrinos stemming from ^{51}Cr and ^{37}Ar can excite the lowest three energy levels in ^{71}Ge. Before continuing with the statistical analysis, let us see how to obtain the average ratio (R = 0.86±0.05) of the four radioactive source experiments (Table 4.1):

→ For each of the ratios reported in Table 4.1, we assume Gaussian probability distribution defined as

$$p_{R_B^k}(r) = \frac{1}{\sqrt{2\pi}\Delta R_B^k} \exp\left[-\frac{1}{2}\left(\frac{r - R_B^k}{\Delta R_B^k}\right)^2\right], \qquad (4.13)$$

where the index k = (G1,G2,S1,S2), R_B^k and ΔR_B^k correspond to the central value of the ratio and its uncertainty, respectively.

$\rightarrow$ To obtain the combined probability distribution, we calculate

$$P_{R_B^{Ga}} = \prod_k P_{R_B^k}.$$

(4.14)

According to the analysis, the combined result of the four radioactive source experiments gives

$$\boxed{R_B^{Ga} = 0.86 \pm 0.05.}$$

(4.15)

This value indicates a deficit of ve with a statistical significance of 2.7σ, the so-called Gallium Anomaly. This deficit can be interpreted as the disappearance of electron neutrinos in short distances, Equation (4.6).

Figure 4.3
Nuclear Transitions from the Ground State of ^{71}Ga to ^{71}Ge Induced by ^{51}Cr and ^{37}Ar Neutrinos
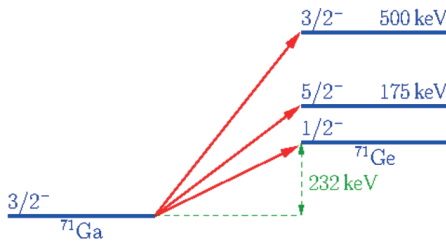
Note. Figure taken from (Giunti, Laveder, Li, Liu, & Long, 2012).

As we have already mentioned, the original analysis only took into account the central values of Equation (4.11) and Equation (4.12) without considering their corresponding uncertainties. However, as we can see from Equation (4.11) and Equation (4.12), these errors are significant.

Therefore, to carry out a correct estimation of the statistical weight of the Gallium Anomaly, we need to consider all the contributions to the cross-sections and include their uncertainties in the analysis. Let us see how to do that:

→ The cross section for the reaction in Equation (4.10) can be written as (Giunti et al., 2012)

$$\sigma = \sigma_{gs} \left(1 + \xi_{175} \frac{BGT_{175}}{BGT_{gs}} + \xi_{500} \frac{BGT_{500}}{BGT_{gs}} \right), \quad (4.16)$$

where σ_{gs} and BGT_{gs} correspond to the cross-section and its corresponding Gamow-Teller strengths for the transition from the ground state of ^{71}Ga to the ground state of ^{71}Ge, BGT_{175} and BGT_{500} are the Gamow-Teller strengths of the transitions from the ground state of ^{71}Ga to the two excited states of ^{71}Ge at 175 and 500 keV. The ground-state to

Table 4.3
Coefficients ξ_{175} and ξ_{500} from Constraint on Excited State Transitions

	σ_{gs}	ξ_{175}	ξ_{500}
^{51}Cr	$55.3 \times 10^{-46} cm^2$	0.669	0.220
^{37}Ar	$66.2 \times 10^{-46} cm^2$	0.695	0.263

Note. Data taken from (Bahcall, 1997).

ground-state transition for each source and the coefficients ξ_{175} and ξ_{500} have been calculated accurately by Bahcall (Bahcall, 1997) (see Table 4.3)

And finally, BGT_{175} and BGT_{500} have been measured by several groups. We consider three differents measurements to calculate the cross section in Equation (4.16) : the (p,n) experiment of Krofcheck (Krofcheck & et al., 1985), the shell model of Haxton (Haxton, 1998) and the $(^3He,^3H)$ of Frekers (Frekers & et al., 2011). The measurements are listed in Table 4.4.

→ We follow closely the procedure described by Giunti et al. (Acero et al., 2008; Giunti & Laveder, 2011; Giunti et al., 2012). They considered in the analysis the following three approaches: the HK approach, where they used Haxton BGT_{175} value and Krofcheck et al. BGT_{500} value; the FF approach, with Frekers et al. values of both BGT_{175} and BGT_{500}; and the HF approach, with Haxton BGT_{175} value and Frekers et al. BGT_{500} value. In particular, we choose the HK approach to outline the statistical procedure. The others approach follow the same procedure.

→ The Haxton cross section for a ^{51}Cr source is given by [1] (Haxton, 1998)

$$\sigma_H(^{51}Cr) = (63.9 \pm 6.8) \times 10^{-46} cm^2. \qquad (4.17)$$

Table 4.4
BGT Values Determined by Krofcheck, Haxton and Frekers

Reference	Method	BGT_{175}	$\frac{BGT_{175}}{BGT_{gs}}$	BGT_{175}	$\frac{BGT_{500}}{BGT_{gs}}$
Krofcheck	$^{71}Ga(p,n)^{71}Ge$	< 0.005	< 0.057	0.011 ± 0.002	0.126 ± 0.023
Haxton	shell Model	0.017 ± 0.015	$0.84^{+0.13}_{-0.12}$		
Frekers	$^{71}Ga(^3He,^3H)^{71}Ge$	0.039 ± 0.030	$0.83^{+0.13}_{-0.12}$	0.0176 ± 0.0014	0.202 ± 0.016

Note. Data taken from: Krofcheck (Krofcheck & et al., 1985), Haxton (Haxton, 1998) and Frekers (Frekers & et al., 2011).

---

[1] Note that although the central value is bigger than the Bahcall one, its error is also bigger.

If we compare the Haxton cross-section with respect to Bahcall cross-section, we obtain

$$R_B^H(^{51}Cr) = \frac{\sigma_H(^{51}Cr)}{\sigma_B^{bf}(^{51}Cr)} = 1.10 \pm 0.12. \tag{4.18}$$

It means that the previous ratios reported by the original experiments (Table 4.1) must be rescaled to consider the particular HK approach. In the same way, for a ^{37}Ar source, we obtain the ratio

$$R_B^H(^{37}Ar) = \frac{\sigma_H(^{37}Ar)}{\sigma_B^{bf}(^{37}Ar)} = 1.10 \pm 0.12, \tag{4.19}$$

therefore, the original ratios must be rescaled to account for the uncertainties in the analysis. With all this information, we calculate the probability distribution of the ratio, $R^{Ga} = R_B^{Ga}/R_B^H$, using

$$p_{R^{Ga}}(r) = \int_{R_B^{gs}}^{\infty} p_{R_B^{Ga}}(rs) p_{R_B^H}(s) s \, ds. \tag{4.20}$$

where we have considered the uncertainty of R_B^H given in Equation (4.18) and Equation (4.19), through

$$p_{R_B^H} \propto \begin{cases} \exp\left[-\frac{1}{2}\left(\frac{r - \langle R \rangle_B^H}{\Delta R_B^H}\right)^2\right], & r \geq R_B^{gs}, \\ 0, & r < R_B^{gs}, \end{cases}$$

with $R_B^H = 1.10$, $\Delta R_B^H = 0.12$ and $R_B^{gs} = \sigma^{gs}/\sigma^{gs}$ B $= 0.95$ (Bahcall, 1997). Integrating Equation (4.20), we obtain the average ratio at 68.27% C.L. for the HK approach.

$$R_{HK} = 0.77 \pm 0.08. \tag{4.22}$$

From this result, we can conclude that the Gallium anomaly persists after including the uncertainties in the statistical analysis. Following the same procedure, we obtain different ratios according to the approach under study. The results are shown in Table 4.5.

To investigate the hypothesis of one sterile neutrino as a possible solution to the Gallium Anomaly, we perform a statistical analysis, where the oscillation parameters $\sin^2 2\theta_{ee}$ and Δm^2_{41} are determined from

$$\mathcal{L}(\sin^2 2\theta, \Delta m^2) = p_{\vec{R}}(\vec{R}(\sin^2 2\theta, \Delta m^2)). \quad (4.23)$$

Thus,

$$\mathcal{L}(\sin^2 2\theta, \Delta m^2) = \int_{R_B^{gs}}^{\infty} p_{\bar{R}_B^{G1}}[R^{G1}(\sin^2 2\theta, \Delta m^2)s] \dots p_{\bar{R}_B^{S2}}[R^{S2}(\sin^2 2\theta, \Delta m^2)s] p_{R_B^{H}}(s) s^4 \, ds \quad (4.24)$$

where each $p_{\bar{R}_B^k}[R^k(\sin^2 2\theta, \Delta m^2)s]$ is given by

$$p_{\bar{R}_B^k}[R^k(\sin^2 2\theta, \Delta m^2)s] = \frac{1}{\sqrt{2\pi}\Delta R^k} \exp\left[-\frac{1}{2}\left(\frac{R^k(\sin^2 2\theta, \Delta m^2)s - \langle R^k\rangle}{\Delta R^k}\right)^2\right], \quad (4.25)$$

and the theoretical expression of the ratio R^k for every experiment (k = G1,G2,S1,S2), taking into consideration neutrino oscillations, is given by

$$R^k(\sin^2 2\theta, \Delta m^2) = \frac{\int_k dV L^{-2} \sum_i (B.R.)_i^k \sigma_i^k P_{\nu_e \to \nu_e}^{SBL}(L, E_{\nu,i})}{\sum_i (B.R.)_i^k \sigma_i^k \int_k dV L^{-2}}. \quad (4.26)$$

Here the sum over i takes into account the respective contribution of each neutrino line emitted in ^{51}Cr and ^{37}Ar decay, see Table 4.2, and L is the distance between the source and the detection point. In the integration over the volume, $\int_k dV$, we assume that each detector has a cylindrical

Table 4.5
Ratio for the Measured to the Predicted Event Rate of ^{71}Ge at GALLEX and SAGE Radioactive Source Experiments

Model	GALLEX		SAGE		
	G1	G2	S1	S2	AVE
R_B	$0.95^{+0.11}_{-0.11}$	$0.81^{+0.10}_{-0.11}$	$0.95^{+0.12}_{-0.12}$	$0.79^{+0.08}_{-0.08}$	$0.86^{+0.05}_{-0.05}$
R_{HK}	$0.85^{+0.12}_{-0.12}$	$0.71^{+0.11}_{-0.11}$	$0.84^{+0.13}_{-0.12}$	$0.71^{+0.09}_{-0.09}$	$0.77^{+0.08}_{-0.08}$
R_{FF}	$0.93^{+0.11}_{-0.11}$	$0.79^{+0.10}_{-0.11}$	$0.93^{+0.11}_{-0.12}$	$0.77^{+0.09}_{-0.07}$	$0.84^{+0.05}_{-0.05}$
R_{HF}	$0.83^{+0.13}_{-0.11}$	$0.71^{+0.11}_{-0.11}$	$0.83^{+0.13}_{-0.12}$	$0.69^{+0.10}_{-0.09}$	$0.75^{+0.09}_{-0.07}$

Note. R stand for the measured to the predicted ratio of ^{71}Ge event rate in the two GALLEX ^{51}Cr radioactive source experiments, G1 and G2, and the SAGE ^{51}Cr and ^{37}Ar radioactive source experiments, S1 and S2, respectively.

geometry, see Table 4.1.

The dependence in the parameter oscillations, $\sin^2 2\theta$ and Δm^2_{41}, is in the effective electron neutrino survival probability

$$P_{\nu_e \to \nu_e} = 1 - \sin^2 2\theta \sin^2 \left(\frac{\Delta m^2_{41} L}{4E} \right). \tag{4.27}$$

4.3.2 Statistical Analysis of the Antineutrino-Electron Scattering Measurements

In this section, we will consider the measurements of antineutrino-electron scattering from short-distance reactor experiments. This interaction was studied in Chapter 2 to obtain an improved determination for the weak mixing angle. Here, we investigate the potential of this process to explore the sterile allowed parameter space.

The effective survival probability for short baseline (bellow 100m) antineutrino experiments in the so-called 3+1 mixing scheme is given by Equation (4.27). We will use the following expression to estimate the expected number of events in the detector, considering a

Table 4.6
Summary of Measured $\bar{\nu}_e - e$ Scattering Cross Section at Reactor Experiments

Experiment	^{235}U	^{239}Pu	^{238}U	^{241}Pu	T_{thres} (MeV)	Published cross-section
Krasno	$\simeq 1$	–	–	–	$3.15 - 5.175$	$[4.5\pm2.4]\times10^{-46}$cm^2/fision
Rovno	$\simeq 1$	–	–	–	$0.6 - 2$	$[1.26\pm0.62]\times10^{-44}$cm^2/fision
MUNU	0.54	0.33	0.07	0.06	$0.7 - 2$	$[1.07\pm0.34]$events/day
Texono	0.55	0.32	0.07	0.06	$3 - 8$	$[1.08\pm0.21\pm0.16]\cdot\sigma_{SM}$

Note. The fuel proportions and the electron recoil energy are shown for each experiment. Ta□ble adapted from (Cañas et al., 2018). The references to the experiments:Krasno (Vidyakin et al., 1992); Rovno (Derbin et al., 1993); MUNU (Amsler & et al., 1997); Texono (Deniz & et al., 2010).

fourth sterile neutrino state

$$N_i = n_e\Delta t \int \int_{T_i}^{T_{i+1}} \int \lambda(E_v) P_{v_\alpha \to v_\alpha}^{SBL} \frac{d\sigma}{dT} R(T,T') dT' dT dE_v, \quad \textbf{(4.28)}$$

where $\lambda(E_v)$ is the antineutrino energy spectrum given by Equation (2.20)(Mueller & et al., 2011). $R(T,T')$ is the resolution function for the given experiment, and $\frac{d\sigma}{dT}$ is the differential cross section for the antineutrino-electron scattering as shown in Equation (2.17) after the exchange $(1+g_L)$ by g_R. The experiments considered for this analysis are Krasnoyarsk, Rovno, Texono, and MUNU. We have computed the expected number of events regarding the experimental details of each experiment, presented in Table (4.6).

4.3.3 Gallium Anomaly and Antineutrino-Electron Scattering Data

Now, we present in Figure 4.4 a superposition of the 90% C.L. allowed regions in the (sin^2 $2\theta_{ee}$,Δm_{41}^2) plane obtained from the fit of the Gallium anomaly and the exclusion curve obtained from the fit of antineutrino-electron scattering data. Figure 4.4 indicates that these oscillations of electron neutrinos are due to $\Delta m_{41}^2 \gtrsim 0.4$ eV^2.

Figure 4.4

Confidence Intervals at 90% C.L., for the 3+1 Mixing Scheme Obtained from a Combined Analysis of Neutrino Electron Scattering from Reactor Experiments
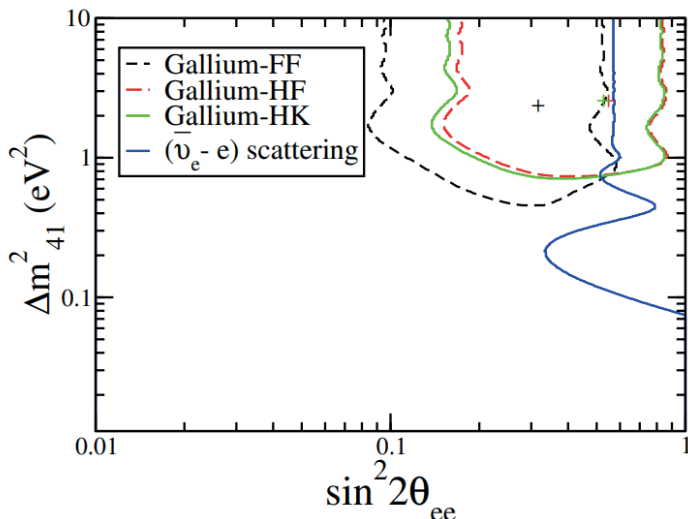
Note. Confidence intervals at 90% C.L. for the 3+1 mixing scheme were obtained from a combined analysis of neutrino electron scattering from reactor experiments. The results for the Gallium data (Giunti et al., 2012) are also shown. The region to the right of the blue curve is excluded at 90% C.L. A cross indicates the best-fit values. Figure presented in (Cañas et al., 2018).

In Table 4.7, we present the best-fit analysis of the Gallium anomaly, considering that it is due to the disappearance of electron neutrinos when mixed with a sterile state in the 3 + 1 scenario.

In 2022 the BEST experiment, an experiment proposed to analyze the Gallium anomaly, reported that the ratio of predicted and observed events rates continues to be significantly distant from the unit, 4σ, confirming the Gallium anomaly. Analysis of this electron neutrino deficit in terms of sterile neutrino oscillations by the BEST collaboration

locates the best fit at $\Delta m^2 = 3.3\,^{+\infty}_{-2.3}eV^2$ and $\sin^2 2\theta = 0.42\,^{+0.15}_{-0.17}$ (Barinov & et al., 2022).

Table 4.7
Best-Fit Values of the 3 + 1 oscillation parameters obtained from the three fits of Gallium Anomaly

Best-Fit	HK	FF	HF
Δm^2_{41}	2.17	2.03	2.17
$\sin^2 2\theta_{ee}$	0.52	0.29	0.55

4.4 The Reactor Antineutrino Anomaly

For the studies of the reactor antineutrino anomaly (Mention et al., 2011), we will include in the statistical analysis the following short baseline neutrino experiments: ILL (Hoummada et al., 1995; Kwon et al., 1981), Gosgen (Zacek & et al., 1986), Rovno91 (Kuvshinnikov, Mikaelyan, Nikolaev, Skorokhvatov, & Etenko, 1990) and Bugey4 (Declais & et al., 1994). We show in Table 4.8 a summary with the main details of the reactor experiments under study. We will perform a fit to these data within the 3+1 sterile neutrino framework.

Table 4.8
Summary of Short Baseline Reactor Experiments and Best-Fits

Experiment	L(m)	τ_n(s)	$R = \sigma^{obs}/\sigma^{the}$	$\sin^2 \theta$	Δm^2
Bugey4	15	888.7	0.987 ± 0.030	< 0.086	$> 2eV^2$
Rovno91	18	888.6	0.985 ± 0.038	$-$	$-$
Gosgen-I	38	897	1.018	< 0.21	$> 5eV^2$
Gosgen-II	45	897	1.045	< 0.21	$> 5eV^2$
Gosgen-III	65	897	0.975	< 0.21	$> 5eV^2$
ILL	9	926	0.955 ± 0.035	< 0.32	$-$
ILL-Reanalysis	9	889	0.832 ± 0.035	< 0.32	$-$

Note. The references of the experiments are the following: Bugey4(Declais & et al., 1994), Rovno91(Kuvshinnikov et al., 1990), Gosgen-I(Zacek & et al., 1986), Gosgen-II(Zacek & et al., 1986), Gosgen-III(Zacek & et al., 1986), ILL (Kwon et al., 1981), ILL-Reanalysis (Hoummada et al., 1995) .

4.4.1 Statistical Analysis of Reactor Neutrino Data

In this part, we discuss the statistical analysis used to restrict the neutrino oscillation parameters under the scheme 3+1 with short-baseline reactor data. Usually, for studying reactor neutrino oscillations, we choose the inverse beta decay

$$\bar{\nu}_e + p \rightarrow e^+ + n, \qquad (4.29)$$

because it has a larger cross-section compared with neutrino-electron scattering. Also, the good signature at the detector is generated by the delayed coincidence between gamma rays produced by the annihilation of the positron and the neutron capture. For an electron-antineutrino process, the threshold energy E_ν^{thr} is

$$E_\nu^{thr} = \frac{(M_n + m_e)^2 - M_p^2}{2M_p} \simeq 1.806 \text{ MeV}, \qquad (4.30)$$

where M_n and M_p are the neutron and proton mass, respectively. The cross-section is given by

$$\sigma(E_\nu) = \frac{2\pi^2}{m_e^5 f^R \tau_n}[E_\nu - (M_n - M_p)]\{[E_\nu - (M_n - M_p)]^2 - m_e^2\}^{1/2}, \qquad (4.31)$$

where $\tau_n = 880.2 \pm 1.0$ s and $f^R = 1.71517 \pm 0.00009$ (Zyla & et al., 2020) are the measured neutron lifetime and the phase space factor [2], respectively.

$$Y_i^{\text{pred}}(L, \Delta m_{41}^2, \theta_{ee}) = \frac{\kappa}{4\pi L^2} \int_{E_\nu^{thr}}^{E_\nu^{max}} \int_{E'_{e^+,i}}^{E'_{e^+,i+1}} \sigma(E_\nu)\lambda(E_\nu)R(E_{e^+}, E'_{e^+})P(E_\nu, \Delta m_{41}^2, \theta_{ee})dE'_{e^+}dE_\nu$$

$$(4.32)$$

where κ stands for the product of the number of target protons with the neutron detection efficiency, L is the distance between the detector and the source, and the resolution function is

---

[2] The phase space factors account for Coulomb, recoil, weak magnetism, and outer radioactive corrections.

given by

$$R(E_{e+}, E'_{e+}) = \frac{1}{\sqrt{2\pi\sigma_0}} \exp\left[-\frac{(E'_{e+} - E_{e+})^2}{2\sigma_0^2}\right]. \qquad (4.32)$$

The effective electron antineutrino survival probability, which depends on the oscillation parameters for the case of a sterile neutrino, is

$$P_{\bar{\nu}_e \to \bar{\nu}_e} = 1 - \sin^2 2\theta_{ee} \sin^2\left(\frac{\Delta m_{41}^2 L}{4E_\nu}\right). \qquad (4.33)$$

To test the hypothesis of one sterile neutrino, we define the following χ^2 function

$$\chi^2(\Delta m_{41}^2, \theta_{ee}) = \sum_i \left[\frac{Y_i^{\text{exp}} - Y_i^{\text{pred}}(L, \Delta m_{41}^2, \theta_{ee})}{\sigma_i}\right]^2, \qquad (4.34)$$

where Y_i^{pred} and Y_i^{exp} are the predicted positron rate that is given by Equation (4.32) including a fourth sterile neutrino and the experimental observation at the i−th bin, respectively. Here σi is the statistical error at each bin reported by each experiment.

4.5 Limits on the Oscillation Parameter for Reactor Anomaly

The fit is obtained by minimizing the χ^2 function defined in Equation (4.34). In Figure 4.5, we show the allowed regions in the ($\sin^2 2\theta_{ee}, \Delta m_{41}^2$) plane, at 68% and 90% C.L.

The best fit values of Δm_{41}^2 and $\sin^2 2\theta_{ee}$ from reactor antineutrino short baseline experiments are: $|\Delta m_{41}^2| = 0.89$ eV^2 y $\sin^2 2\theta_{ee} = 0.1$.

Comparing the results of the Gallium anomaly Figure 4.4 and the Reactor antineutrino anomaly Figure 4.5, we see that there is a tension between these two results. For $\Delta m_{41}^2 \lesssim$ 2 eV², the allowed values of sin²2θee for Gallium anomaly are between 0.15 and 0.8, for Gallium-HF and Gallium-HK models, while for the Reactor antineutrino anomaly the allowed values for sin² 2θee is between 0.07 and 0.15. This tension may suggest that new physics needs to be considered to explain these anomalies.

Figure 4.5

Exclusion Contours at 68% and 90% C.L., for the 3+1 Mixing Scheme Using Appearance Data in Short Baseline Experiments
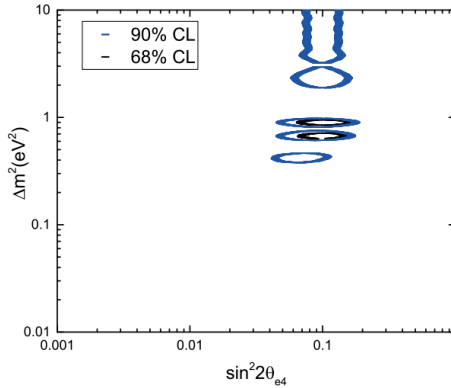
The STEREO (Allemandou & et al., 2018; Almazán & et al., 2018, 2020) experiment aims to investigate if Reactor Antineutrino Anomalies are due to oscillations of electron antineutrino to sterile neutrino and performer an accurate measurement of the antineutrino energy spectrum of the fission of ²³⁵U. A possible explanation of the Reactor Antineutrino Anomalies is the mis-modeled reactor electron antineutrino fluxes. Daya Bay (An & et al., 2017) and RENO (Bak & et al., 2019) *e*xperiments performed

measurements of ^{235}U and a combined fit (Giunti, Li, Little-john, & Surukuchi, 2019) show a discrepancy more significant than 3σ with the model of Huber-Mueller.

Searching for sterile neutrinos in the STEREO experiment for induced spectral variations at six different segments in the detector was performed. The baseline range is within 9 to 11 m. The results of the STEREO experiment exclude oscillations from antineutrinos to sterile neutrinos as the cause of Reactor Antineutrino Anomalies (Almazán & et al., 2023). This experiment also found a significant deviation in both the shape and normalization relative to the antineutrino spectrum for ^{235}U predicted by the Huber-Mueller model.

4.6 Electron Neutrino Appearance Anomalies

Now we will describe two anomalies that arise in experiments carried out in accelerators, the LSND Anomaly and the excess at low energies in MiniBooNE. These anomalies are an excess of electron neutrinos relative to the expected background.

4.6.1 The LSND Anomaly

The Liquid Scintillator Neutrino Detector (LSND) (Athanassopoulos & et al., 1997) was an experiment that produced a nearly pure beam of $\bar{\nu}\mu$ muon antineutrinos with the higher energy of about 50 MeV and a baseline approximately of 30 m through the resting decay of electrically charged pions: $\pi^+ \rightarrow \mu^+ + \nu\mu$, $\mu^+ \rightarrow e^+ + \nu e + \bar{\nu}\mu$. In the LSND detector, positrons were identified from inverse beta decay $\bar{\nu}e + p \rightarrow e^+ + n$, indicating oscillations of $\bar{\nu}\mu \rightarrow \bar{\nu}e$; this is called the LSND anomaly. The excess of this signal is much more significant than the events due to the background of

this experiment. The explanation of this excess is given through the 3 + 1 model of mixing between active and sterile states of neutrinos. LSND reported a best fit with an amplitude of the oscillation of $\sin^2 2\theta_{\mu e} = 0.003$ and an oscillation phase of $\Delta m^2 = 1.2 \ eV^2$ (A. Aguilar-Arevalo & et al., 2001). A less sensitive experiment, KArlsruhe Rutherford Medium Energy Neutrino (KARMEN), also sought to identify $\overline{\nu}\mu \rightarrow \overline{\nu}e$ oscillations without success for a value of L/E similar to that of LSND (Armbruster & et al., 2002). For more details on the LSND Anomaly, go to the reference (Acero & et al., 2022) and references therein.

4.6.2 MiniBooNE Low-Energy Excess (LEE)

To independently examine the LSND results preserving the same sensitivity and same L/E fraction, it was performed the MiniBooNE experiment at Fermilab (A. A. Aguilar-Arevalo & et al., 2009a, 2009b) that searched for the appearance of $\nu e(\overline{\nu}e)$ in a beam of $\nu\mu(\overline{\nu}\mu)$. This experiment could operate both in the almost pure channel of a neutrino beam ($\nu\mu$) and in the nearly pure channel of an antineutrino beam ($\overline{\nu}\mu$). The decay of pions produced these neutrinos in flight, and these channels were obtained by focusing in the direction of the detector $\pi+$ or $\pi-$. The baseline of this experiment was approximately 540 m, and the average energy of the neutrinos was around 600 MeV.

The first result published by MiniBooNE in the neutrino channel did not report the appearance of νe for the neutrino energy greater than 475 MeV for quasi-elastic energy reconstruction. For a neutrino energy less than 475 MeV, MiniBooNE observed an excess of events relative to the background. This excess of events is known as MiniBooNE Low-Energy Excess (LEE). The final results of MiniBooNE published in 2020 for both the neutrino and the antineutrino channels (A. A. Aguilar-Arevalo & et al.,2021)

continue to present this excess of $\overline{v}e$ and $\overline{v}e$ events. The best fit for the combined analysis of neutrinos and antineutrinos in the range of energies reconstructed from 200 MeV to 1250 MeV is $\Delta m^2 = 0.043$ eV² and $\sin^2 2\theta = 0.807$. For more details on the LEE anomaly, go to the reference (Acero & et al., 2022) and references there. Finally, in the study about short baseline anomalies, we have presented a statistical analysis for both Gallium experiments and reactor antineutrino experiments at baselines less than 100 m. For Gallium experiments, we have obtained confidence levels in the $(\Delta m^2_{41}, \sin^2 2\theta e4)$ plane, following the works of Giunti et al. (Giunti & Laveder, 2011; Giunti et al., 2012) closely. Moreover, we have included the reactor antineutrino-electron scattering data for the first time to investigate the restrictions on the oscillation parameter space. We have also presented a summary of the LSND anomaly and the Mini-BooNE Low-Energy Excess.

A. Radiative Corrections to Neutrino-Electron Scatterin

We outline in this appendix the $\mathcal{O}(\alpha)$ radiative corrections to neutrino-electron scattering, which has been investigated by several authors such as W.J. Marciano and A. Sirlin (Marciano & Sirlin, 1980), S. Sarantakos et al., (Sarantakos et al., 1983), J. Bahcall et al., (Bahcall et al., 1995) among others. Here we employ the MS renormalization scheme (Marciano & Sirlin, 1981). The differential cross section for $vl + e \rightarrow vl + e$ ($l = e, \mu$) is given by (Bahcall et al., 1995; Sarantakos et al., 1983)

$$
\begin{aligned}
\frac{d\sigma}{dT} = \frac{2G_F^2 m_e}{\pi} & \left\{ g_L^2(q^2) \left[1 + \frac{\alpha}{\pi} f_-(z) \right] + g_R^2(q^2)(1-z)^2 \left[1 + \frac{\alpha}{\pi} f_+(z) \right] \right. \\
& \left. - g_R(q^2) g_L(q^2) \frac{m}{q} z \left[1 + \frac{\alpha}{\pi} f_{+-}(z) \right] \right\},
\end{aligned}
$$

(A.1)

where $T = E - m$ is the kinetic energy of recoil of the electron, E_V is the incident neutrino energy, and $z = T/E_V$. The functions $f_-(z)$, $f_+(z)$, and $f_{+-}(z)$ represent the QED corrections, and the coupling constants g_L, g_R include electroweak corrections.

The differential cross section for $\bar{v}l + e \to \bar{v}l + e$ is simply obtained by interchanging $g_L \leftrightarrow g_R$ (Sarantakos et al., 1983).

For $v_e - e$ scattering,

$$g_L^{(v_e,e)}(q^2) = \rho_{NC}^{(v,l)}\left[\frac{1}{2} - \hat{\kappa}^{(v_e,e)}(q^2)\sin^2\theta_W(m_Z)\right] - 1 \quad \text{(A.2)}$$

$$g_R^{(v_e,e)}(q^2) = -\rho_{NC}^{(v,l)}\hat{\kappa}^{(v_e,e)}(q^2)\sin^2\theta_W(m_Z),$$

where $\hat{\kappa}$ (v_e,e) (q^2) is

$$\hat{\kappa}^{(v_e,e)}(q^2) = 1 - \frac{\hat{\alpha}}{2\pi\hat{s}^2}\left[\sum_i (C_{3i}Q_i - 4\hat{s}^2 Q_i^2)J_i(q^2) - 2J_e(q^2) + \frac{\hat{c}^2}{3} + \frac{1}{2} + \frac{\hat{c}_\gamma}{\hat{c}^2}\right], \text{(A.3)}$$

with $\hat{c}_\gamma = \frac{19}{8} - \frac{17}{4}\hat{s}^2 + 3\hat{s}^4$, $\hat{s}^2 = \sin^2\theta_W$ and $\hat{\alpha} = \hat{\alpha}(m_Z) \simeq 1/127.9$.

Figure A.1
Feynman Diagrams for Electroweak Corrections to $v_e - e$ Scattering

Note. These corrections are calculated in (Bahcall et al., 1995).

For $\nu\mu - e$ scattering,

$$g_L^{(\nu_\mu,e)}(q^2) = \rho_{NC}^{(v,l)}\left[\frac{1}{2} - \hat{\kappa}^{(\nu_\mu,e)}(q^2)\sin^2\theta_W(m_Z)\right] - 1 \quad \text{(A.4)}$$

$$g_R^{(\nu_\mu,e)}(q^2) = -\rho_{NC}^{(v,l)}\hat{\kappa}^{(\nu_\mu,e)}(q^2)\sin^2\theta_W(m_Z),$$

where $\hat{\kappa}^{(\nu_\mu,e)}(q^2)$ is obtained from $\hat{\kappa}^{(\nu_e,e)}(q^2)$ by replacing $-2J_e(q^2)$ by $-2J_\mu(q^2)$ in Equation A.3.

The renormalization factor $\rho_{NC}^{(v,l)}$ is given by

$$\rho_{NC}^{v;\ell} = 1 + \frac{\hat{\alpha}}{4\pi\hat{s}^2}\left\{\frac{3}{4\hat{s}^2}\ln c^2 - \frac{7}{4} + \frac{2\hat{c}_Z}{\hat{c}^2} + \frac{3}{4}\hat{\xi}\left[\frac{\ln(\hat{c}^2/\xi)}{\hat{c}^2 - \xi} + \frac{1}{\hat{c}^2}\frac{\ln\xi}{1-\xi}\right] + \frac{3}{4}\frac{m_t^2}{m_W^2}\right\}, \quad \text{(A.5)}$$
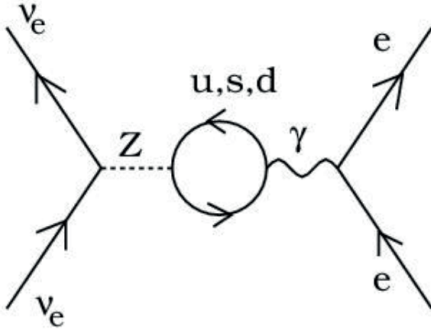
where

$$\hat{c}_Z = \frac{19}{8} - \frac{7}{2}\hat{s}^2 + 3\hat{s}^4, \quad \text{(A.6)}$$

and $\xi = m_H^2/m_Z^2$.

Figure A.2
Feynman Diagrams for QCD Corrections to $\nu_e - e$ Scattering

Note. These corrections are calculated in (Bahcall et al., 1995).

QED Effects

The functions $f-(z)$, $f+(z)$, and $f+-(z)$ in Equation A.1 describe QED effects. These functions, in the nonrelativistic regime, are given by (Bahcall et al., 1995).

$f-$:

$$
\begin{aligned}
f_-(z) = & \left[\frac{E}{l}\ln\left(\frac{E+l}{m}\right)-1\right]\left[2\ln\left(1-z-\frac{m}{E+l}\right)-\ln(1-z)-\frac{1}{2}\ln(z)-\frac{5}{12}\right] \\
& +\frac{1}{2}[L(z)-L(\beta)]-\frac{1}{2}\ln^2(1-z)-\left(\frac{11}{12}+\frac{z}{2}\right)\ln(1-z) \\
& +z\left[\ln(z)+\frac{1}{2}\ln\left(\frac{2q}{m}\right)\right]-\left(\frac{31}{18}+\frac{1}{12}\ln(z)\right)\beta-\frac{11}{12}z+\frac{z^2}{24},
\end{aligned} \tag{A.7}
$$

where $L(x) = -Li_2(x) = l\int_0^x \ln|1-t|(dt/t)$ is the Spence function, $Li_2(x)$[1] is the dilogarithm function, and $\beta = l/E$.

$f+$:

$$
\begin{aligned}
(1-z)^2 f_+(z) = & \left[\frac{E}{l}\ln\left(\frac{E+l}{m}\right)-1\right]* \\
& \left\{(1-z)^2\left[2\ln\left(1-z-\frac{m}{E+l}\right)-\ln(1-z)-\frac{1}{2}\ln(z)-\frac{2}{3}\right]-\frac{z^2\ln(z)+1-z}{2}\right\} \\
& -\frac{(1-z)^2}{2}\{\ln^2(1-z)+\beta[L(1-z)-\ln(z)\ln(1-z)]\} \\
& +\ln(1-z)\left[\frac{z^2}{2}\ln(z)+\frac{1-z}{3}\left(2z-\frac{1}{2}\right)\right]-\frac{z^2}{2}L(1-z)-\frac{z(1-2z)}{3}\ln(z) \\
& -\frac{z(1-z)}{6}-\frac{\beta}{12}\left[\ln(z)+(1-z)\left(\frac{115-109z}{6}\right)\right],
\end{aligned} \tag{A.8}
$$

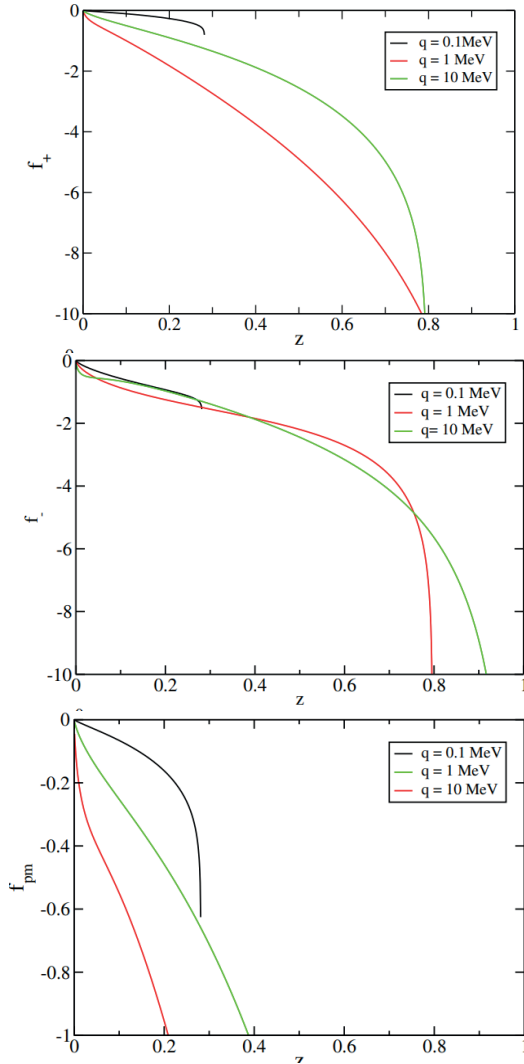$f+-$:

$$
f_{+-}(z) = \left[\frac{E}{l}\ln\left(\frac{E+l}{m}\right)-1\right]2\ln\left(1-z-\frac{m}{E+l}\right). \tag{A.9}
$$

---

[1] http://hep.fi.infn.it/cernlib.pdf

Figure A.3

Functions that Describe QED Effects in the Non-Relativistic Regime

Note. Top panel: $f+$ function. Middle panel: $f-$ function. Bottom panel: $f+-$ function (Bahcall et al., 1995).

B. Statistical Analysis

In this appendix, we review the statistical approach known as the covariance approach, allowing us to compare the expected number of events with the experimental results reported by each experiment.

$$\lambda(E_\nu) = \sum_\ell f_\ell \lambda_\ell(E_\nu) = \sum_\ell f_\ell \exp\left[\sum_{k=1}^{6} \alpha_{k\ell} E_\nu^{k-1}\right] ; \qquad E_\nu \geqslant 2\text{MeV},$$
(B.1)

where $f\ell$ is the fission fraction for the isotope $\ell \equiv {}^{235}\text{U}$, ${}^{239}\text{Pu}$, ${}^{241}\text{Pu}$ and ${}^{238}\text{U}$, at the reactor under study.

The values for the coefficients, $\alpha_{k\ell}$, its errors, $\delta\alpha_{k\ell}$, as well as their corresponding correlation matrix, $\rho_{kk'}^l$, are shown in Table B.1 and Table B.2. We can write the covariance matrix in terms of these quantities as follows

$$V_{kk'}^\ell = \delta\alpha_{k\ell}\,\delta\alpha_{k'\ell}\,\rho_{kk'}^\ell,$$
(B.2)

and compute the different elements of the systematics error matrix, σ_{ij}^2. In this case the systematic error in the number of events associated with the antineutrino flux is given by

$$(\delta N_\ell^\nu)^2 = \sum_{kk'} \frac{\partial N_\ell^\nu}{\partial \alpha_{k\ell}} \frac{\partial N_\ell^\nu}{\partial \alpha_{k'\ell}} V_{kk'}^\ell.$$
(B.3)

Note that for the numerical analysis it is better to work with the diagonal form of the

Table B.1

Coefficients $\alpha_{k\ell}$ of the Polynomial for the Antineutrino for a Flux Fuel Composition of ^{235}U, ^{238}U and, ^{239}Pu

$\ell = {}^{235}U$			Correlation matrix $\rho^\ell_{kk'}$					
k	$\alpha_{k\ell}$	$\delta\alpha_{k\ell}$	1	2	3	4	5	6
1	3.217	4.09(-2)	1.00	-0.86	0.60	0.07	-0.17	-0.14
2	-3.111	2.34(-2)	-0.86	1.00	-0.84	0.12	0.25	0.01
3	1.395	4.88(-3)	0.60	-0.84	1.00	-0.56	-0.19	0.24
4	-3.690(-1)	6.08(-4)	0.07	0.12	-0.56	1.00	-0.42	-0.14
5	4.445(-2)	7.77(-5)	-0.17	0.25	-0.19	-0.42	1.00	-0.77
6	-2.053(-3)	6.79(-6)	-0.14	0.01	0.24	-0.14	-0.77	1.00

$\ell = {}^{238}U$			Correlation matrix $\rho^\ell_{kk'}$					
k	$\alpha_{k\ell}$	$\delta\alpha_{k\ell}$	1	2	3	4	5	6
1	4.033(-1)	1.24(-1)	1.00	-0.86	0.20	0.30	0.08	-0.27
2	1.927(-1)	5.86(-2)	-0.86	1.00	-0.58	-0.21	0.04	0.23
3	-1.283(-1)	1.11(-2)	0.20	-0.58	1.00	-0.48	-0.17	0.20
4	-6.762(-3)	1.92(-3)	0.30	-0.21	-0.48	1.00	-0.36	-0.20
5	2.233(-3)	2.84(-4)	0.08	0.04	-0.17	-0.36	1.00	-0.77
6	-1.536(-4)	2.86(-5)	-0.27	0.23	0.20	-0.20	-0.77	1.00

$\ell = {}^{239}Pu$			Correlation matrix $\rho^\ell_{kk'}$					
k	$\alpha_{k\ell}$	$\delta\alpha_{k\ell}$	1	2	3	4	5	6
1	6.413	4.57(-2)	1.00	-0.86	0.60	0.10	-0.17	-0.13
2	-7.432	2.85(-2)	-0.86	1.00	-0.84	0.08	0.25	-0.01
3	3.535	6.44(-3)	0.60	-0.84	1.00	-0.54	-0.20	0.26
4	-8.820(-1)	9.11(-4)	0.10	0.08	-0.54	1.00	-0.45	-0.08
5	1.025(-1)	1.38(-4)	-0.17	0.25	-0.20	-0.45	1.00	-0.79
6	-4.550(-3)	1.29(-5)	-0.13	-0.01	0.26	-0.08	-0.79	1.00

Note. Coefficients $\alpha_{k\ell}$ are for the antineutrino flux in Equation B.1. In the column $\delta\alpha_{k\ell}$ the 1σ errors on $\alpha_{k\ell}$ are given. Furthermore the correlation matrix of the errors is shown (Mueller & et al., 2011).

Table B.2

Coefficients $\alpha_{k\ell}$ of the Polynomial for the Antineutrino for a Flux Fuel Composition of ^{241}Pu

$\ell = {}^{241}Pu$			Correlation matrix $\rho^\ell_{kk'}$					
k	$\alpha_{k\ell}$	$\delta\alpha_{k\ell}$	1	2	3	4	5	6
1	3.251	4.37(-2)	1.00	0.87	-0.60	-0.08	0.17	0.13
2	-3.204	2.60(-2)	0.87	1.00	-0.84	0.11	0.25	-0.00
3	1.428	5.66(-3)	-0.60	-0.84	1.00	-0.56	-0.19	0.26
4	-3.675(-1)	7.49(-4)	-0.08	0.11	-0.56	1.00	-0.43	-0.11
5	4.254(-2)	1.02(-4)	0.17	0.25	-0.19	-0.43	1.00	-0.78
6	-1.896(-3)	9.03(-6)	0.13	0.00	0.26	-0.11	-0.78	1.00

covariance matrix. In order to perform this rotation we introduce new coefficients, $c_{k\ell}$, such that

$$\alpha_{k\ell} = \sum_{k'} \mathscr{O}^{\ell}_{k'k}\, c_{k'\ell}, \tag{B.4}$$

where the rotation matrix $\mathscr{O}\ell$ is given by

$$\mathscr{O}^{\ell} V^{\ell} (\mathscr{O}^{\ell})^{T} = \mathrm{diag}\left[(\delta c_{k\ell})^2\right]. \tag{B.5}$$

The new phenomenological parametrization of the flux in Equation (2.20) can be rewritten as

$$\lambda_{\ell}(E_v) = \exp\left[\sum_{k=1}^{6} c_{k\ell}\, p^{\ell}_k(E_v)\right], \tag{B.6}$$

where $p^{\ell}_k (E_v)$ is a polynomial of E_v given by

$$p^{\ell}_k(E_v) = \sum_{k'=1}^{6} \mathscr{O}^{\ell}_{kk'} E_v^{k'-1}. \tag{B.7}$$

With all these ingredients we can now define the χ^2 function we will use in our statistical analysis as

$$\chi^2 = \sum_{ij} (N_i^{\mathrm{theo}} - N_i^{\mathrm{exp}})\sigma_{ij}^{-2}(N_j^{\mathrm{theo}} - N_j^{\mathrm{exp}}), \tag{B.8}$$

where the expected number of events N_i^{theo} given by Equation 2.19, takes into account the contributions from each isotope

$$N_i^{theo} = N_i^{235} + N_i^{238} + N_i^{241} + N_i^{239}, \tag{B.9}$$

and σ_{ij}^2 is given as

$$
\sigma_{ij}^2 =
\begin{pmatrix}
\Delta_1^2 + \delta N_1^{235}\,\delta N_1^{235} + \dots & \delta N_1^{235}\,\delta N_2^{235} + \dots & \delta N_1^{235}\,\delta N_3^{235} + \dots & \dots \\
\delta N_2^{235}\,\delta N_1^{235} + \dots & \Delta_2^2 + \delta N_2^{235}\,\delta N_2^{235} + \dots & \dots & \dots \\
\delta N_3^{235}\,\delta N_1^{235} + \dots & \dots & \dots & \dots \\
\dots & \dots & \dots & \dots \\
\dots & \dots & \dots & \dots
\end{pmatrix},
\tag{B.10}
$$

where Δi corresponds to the statistical error for each experimental bin and δN^ℓ is the contribution from each isotope to the systematic error in the number of events. This is calculated as follows.

$$
\delta N_i^\ell = \sum_k \delta c_{k\ell}\,\frac{\partial N_i^\ell}{\partial c_{k\ell}}
\tag{B.11}
$$

$$
= \sum_k \delta c_{k\ell} \int \int \int_{T_i'}^{T_{i+1}'} \lambda_\ell(E_v)\,p_k^\ell(E_v)\,\frac{d\sigma(E_v,T,\sin^2\theta_W)}{dT}\,R(T,T')\,dT'\,dT\,dE_v.
$$

References

Aad, G., & et al. (2012). Observation of a new particle in the search for the Standard Model Higgs boson with the ATLAS detector at the LHC. Phys. Lett. B, 716, 1–29. arXiv:1207.7214. doi: 10.1016/j.physletb.2012.08.020

Aad, G., & et al. (2015). Combined Measurement of the Higgs Boson Mass in pp Collisions at$\sqrt{s}$ = 7 and 8 TeV with the ATLAS and CMS Experiments. Phys. Rev. Lett., 114, 191803. arXiv:1503.07589. doi: 10.1103/PhysRevLett.114.191803

Abdurashitov, D. N., & et al. (1996). The Russian-American gallium experiment (SAGE) Cr neutrino source measurement. Phys. Rev. Lett., 77, 4708–4711. doi: 10.1103/PhysRevLett.77.4708

Abdurashitov, J. N., & et al. (1999). Measurement of the response of the Russian-American gallium experiment to neutrinos from a Cr-51 source. *Phys. Rev. C,* 59, 2246–2263. arXiv:hep-ph/9803418. doi: 10.1103/PhysRevC.59.2246

Abdurashitov, J. N., & et al. (2006). Measurement of the response of a Ga solar neutrinon experiment to neutrinos from an Ar-37 source. P*hys. Rev. C,* 73, 045805. arXiv:nucl-ex/0512041. doi: 10.1103/PhysRevC.73.045805

Abdurashitov, J. N., & et al. (2009). Measurement of the solar neutrino capture rate with gallium metal. III: Results for the 2002–2007 data-taking period. *Phys. Rev. C,* 80, 015807. arXiv:0901.2200. doi: 10.1103/PhysRevC.80.015807

Abe, K., & et al. (2000). A High precision measurement of the left-right Z boson cross-section asymmetry. *Phys. Rev. Lett.,* 84, 5945–5949. arXiv:hep-ex/0004026. doi: 10.1103/PhysRevLett.84.5945

Acero, M. A., & et al. (2022, 3). *White Paper on light sterile Neutrino Searches and Related Phenomenology.* arXiv:2203.07323. (e-print)

Acero, M. A., Giunti, C., & Laveder, M. (2008). Limits on nu(e) and anti-nu(e) disappearance from Gallium and reactor experiments. *Phys. Rev. D,* 78, 073009. arXiv:0711.4222. doi: 10.1103/PhysRevD.78.073009

Agarwalla, S. K., & Huber, P. (2011). Potential measurement of the weak mixing angle with neutrino-electron scattering at low energy. JHEP, 08, 059. arXiv:1005.1254. doi: 10.1007/JHEP08(2011)059

Aguilar-Arevalo, A., & et al. (2001). Evidence for neutrino oscillations from the observation of $\overline{\nu}$e appearance in a $\overline{\nu}\mu$ beam. *Phys. Rev. D,* 64, 112007. arXiv:hep-ex/0104049. doi: 10.1103/PhysRevD.64.112007

Aguilar-Arevalo, A. A., & et al. (2007). A Search for Electron-Neutrino Appearance at the $\Delta m^2 \sim 1eV^2$ Scale. *Phys. Rev. Lett.,* 98, 231801. arXiv:0704.1500. doi: 10.1103/PhysRevLett.98.231801

Aguilar-Arevalo, A. A., & et al. (2009a). The MiniBooNE Detector. *Nucl. Instrum. Meth.* A, 599, 28–46. arXiv:0806.4201. doi: 10.1016/j.nima.2008.10.028

Aguilar-Arevalo, A. A., & et al. (2009b). The Neutrino Flux prediction at MiniBooNE. *Phys. Rev. D,* 79, 072002. arXiv:0806.1449. doi: 10.1103/PhysRevD.79.072002

Aguilar-Arevalo, A. A., & et al. (2021). Updated MiniBooNE neutrino oscillation results with increased data and new background studies. *Phys. Rev. D,* 103(5), 052002. arXiv:2006.16883. doi: 10.1103/PhysRevD.103.052002

Aharmim, B., & et al. (2013). Combined Analysis of all Three Three Phases of Solar Neutrino Data from the Sudbury Neutrino Observatory. *Phys. Rev. C,* 88, 025501. arXiv:1109.0763. doi: 10.1103/PhysRevC.88.025501

Ahmad, Q. R., & et al. (2002). Direct evidence for neutrino flavor transformation from neutral current interactions in the Sudbury Neutrino Observatory. *Phys. Rev. Lett.,* 89, 011301. arXiv:nucl-ex/0204008. doi: 10.1103/PhysRevLett.89.011301

Aker, M., & et al. (2019). Improved Upper Limit on the Neutrino Mass from a Direct Kinematic Method by KATRIN. Phys. Rev. Lett., 123(22), 221802. arXiv:1909.06048. doi: 10.1103/PhysRevLett.123.221802

Aker, M., & et al. (2021). Analysis methods for the first KATRIN neutrino-mass measurement. *Phys. Rev. D,* 104(1), 012005. arXiv:2101.05253. doi: 10.1103/PhysRevD.104.012005

Aker, M., & et al. (2022). Direct neutrino-mass measurement with sub-electronvolt sensitivity. Nature Phys., 18(2), 160–166. arXiv:2105.08533. doi: 10.1038/s41567-021-01463-1

Akhmedov, E. (2019, 1). Quantum mechanics aspects and subtleties of neutrino oscillations. In International Conference on History of the Neutrino: 1930-2018. arXiv:1901.05232.

ALEPH, & et al. (2010, 12). *Precision Electroweak Measurements and Constraints on the Standard Model.* arXiv:1012.2367. (e-print)

Allemandou, N., & et al. (2018). The STEREO Experiment. *JINST, 13(07), P07009. doi: 10.1088/1748-0221/13/07/P07009*

Allen, R. C., & et al. (1993). Study of electron-neutrino electron elastic scattering at LAMPF. Phys. Rev. D, 47, 11–28. doi: 10.1103/PhysRevD.47.11

Allison, W. W. M., & et al. (1999). The Atmospheric neutrino flavor ratio from a 3.9 fiducial kiloton year exposure of Soudan-2. *Phys. Lett. B,* 449, 137–144. arXiv:hep-ex/9901024.
doi: 10.1016/S0370-2693(99)00056-8

Almazán, H., & et al. (2018). Sterile Neutrino Constraints from the STEREO Experiment with 66 Days of Reactor-On Data. *Phys. Rev. Lett.,* 121(16), 161801. doi: 10.1103/PhysRevLett.121.161801

Almazán, H., & et al. (2020). Improved sterile neutrino contraints from the STEREO experiment with 179 days of reactor-on data. *Phys. Rev. D,* 102(5), 052002. doi: 10.1103/PhysRevD.102.052002

Almazán, H., & et al. (2023). STEREO neutrino spectrum of ^{235}U fission rejects sterile neutrino hypothesis. Nature, 613(7943), 257–261. doi: 10.1038/s41586-022-05568-2

Ambrosio, M., & et al. (1998). Measurement of the atmospheric neutrino induced upgoing muon flux using MACRO. Phys. Lett. B, 434, 451–457. arXiv:hep-ex/9807005.
doi: 10.1016/S0370-2693(98)00885-5

Amsler, C., & et al. (1997). The MUNU experiment, general description. *Nucl. Instrum. Meth. A,* 396, 115–129. doi: 10.1016/S0168-9002(97)00724-9

An, F. P., & et al. (2017). Evolution of the Reactor Antineutrino Flux and Spectrum at Daya Bay. *Phys. Rev. Lett.,* 118(25), 251801. doi: 10.1103/PhysRevLett.118.251801

Anselmann, P., & et al. (1995). First results from the Cr-51 neutrino source experiment with the GALLEX detector. Phys. Lett. B, 342, 440–450. doi: 10.1016/0370-2693(94)01586-2

Anthony, P. L., & et al. (2005). Precision measurement of the weak mixing angle in Moller scattering. Phys. Rev. Lett., 95, 081601. arXiv:hep-ex/0504049. doi: 10.1103/PhysRevLett.95.081601

Apollonio, M., & et al. (1999). Limits on neutrino oscillations from the CHOOZ experiment. *Phys. Lett. B,* 466, 415–430. arXiv:hep-ex/9907037. doi: 10.1016/S0370-2693(99)01072-2

Armbruster, B., & et al. (2002). Upper limits for neutrino oscillations muon-anti-neutrino $\longrightarrow$ electron-anti-neutrino from muon decay at rest. Phys. Rev. D, 65, 112001. arXiv:hep-ex/0203021. doi: 10.1103/PhysRevD.65.112001

Ashie, Y., & et al. (2004). Evidence for an oscillatory signature in atmospheric neutrino oscillation. *Phys. Rev. Lett.,* 93, 101801. arXiv:hep-ex/0404034. doi: 10.1103/PhysRevLett.93.101801

Ashtari Esfahani, A., & et al. (2017). Determining the neutrino mass with cyclotron radiation emission spectroscopy—Project 8. J. Phys. G, 44(5), 054004. arXiv:1703.02037.doi: 10.1088/1361-6471/aa5b4f

Athanassopoulos, C., & et al. (1997). The Liquid scintillator neutrino detector and LAMPF neutrino source. Nucl. Instrum. Meth. A, 388, 149–172. arXiv:nucl-ex/9605002.
doi: 10.1016/S0168-9002(96)01155-2

Auerbach, L. B., & et al. (2001). Measurement of electron - neutrino - electron elastic scattering. *Phys. Rev. D,* 63, 112001. arXiv:hep-ex/0101039. doi: 10.1103/PhysRevD.63.112001

Bahcall, J. N. (1997). Gallium solar neutrino experiments: Absorption cross-sections, neutrino spectra, and predicted event rates. *Phys. Rev. C,* 56, 3391–3409. arXiv:hep-ph/9710491. doi: 10.1103/PhysRevC.56.3391

Bahcall, J. N., Bahcall, N. A., & Shaviv, G. (1968). Present status of the theoretical predictions for the Cl-36 solar neutrino experiment. *Phys. Rev. Lett.,* 20, 1209–1212. doi: 10.1103/PhysRevLett.20.1209

Bahcall, J. N., Kamionkowski, M., & Sirlin, A. (1995). Solar neutrinos: Radiative corrections in neutrino - electron scattering experiments. Phys. Rev. D, 51, 6146–6158. (arXiv:astro-ph/9502003) doi: 10.1103/PhysRevD.51.6146

Bahcall, J. N., & Pena-Garay, C. (2004). Solar models and solar neutrino oscillations. New J. Phys., 6, 63. arXiv:hep-ph/0404061.
doi: 10.1088/1367-2630/6/1/063

Bahcall, J. N., & Pinsonneault, M. H. (2004). What do we (not) know theoretically about solar neutrino fluxes? P*hys. Rev. Lett.,* 92, 121301. arXiv:astro-ph/0402114. doi: 10.1103/PhysRevLett.92.121301

Bak, G., & et al. (2019). Fuel-composition dependent reactor antineutrino yield at RENO. *Phys. Rev. Lett.,* 122(23), 232501. doi: 10.1103/PhysRevLett.122.232501

Ball, R. D., Del Debbio, L., Forte, S., Guffanti, A., Latorre, J. I., Piccione, A., . . . Ubiali, M. (2009). Precision determination of electroweak parameters and the strange content of the proton from neutrino deep-inelastic scattering. Nucl. Phys. B, 823, 195–233. arXiv:0906.1958. doi: 10.1016/j.nuclphysb.2009.08.003

Barinov, V. V., & et al. (2022, 1). *A Search for Electron Neutrino Transitions to Sterile States in the BEST Experiment.* arXiv:2201.07364. (e-print)

Barish, B. C., Bartlett, J. F., Brown, K. W., Buchholz, D., Jacquet, F., Merritt, F. S., . . . Krafczyk, G. (1975). Neutral Currents in High-Energy Neutrino Collisions: An Experimental Search. *Phys. Rev. Lett.,* 34, 538. doi: 10.1103/PhysRevLett.34.538

Barranco, J., Miranda, O. G., & Rashba, T. I. (2008). Improved limit on electron neutrino charge radius through a new evaluation of the weak mixing angle. *Phys. Lett. B,* 662, 431–435. arXiv:0707.4319. doi: 10.1016/j.physletb.2008.03.039

Bennett, S. C., & Wieman, C. E. (1999). Measurement of the 6S $\longrightarrow$ 7S transition polarizability in atomic cesium and an improved test of the Standard Model. Phys. Rev. Lett., 82, 2484–2487. arXiv:hep-ex/9903022. ([Erratum: *Phys.Rev.Lett.*

82, 4153 (1999), Erratum: Phys.Rev.Lett. 83, 889 (1999)]) doi: 10.1103/PhysRevLett.82.2484

Bentz, W., Cloet, I. C., Londergan, J. T., & Thomas, A. W. (2010). Reassessment of the NuTeV determination of the weak mixing angle. *Phys. Lett. B,* 693, 462–466. arXiv:0908.3198. doi: 10.1016/j.physletb.2010.09.001

Benvenuti, A., & et al. (1974). Observation of Muonless Neutrino Induced Inelastic Interactions. *Phys. Rev. Lett.,* 32, 800–803. doi: 10.1103/PhysRevLett.32.800

Benvenuti, A. C., & et al. (1976). Evidence for Parity Nonconservation in the Weak Neutral Current. *Phys. Rev. Lett.,* 37, 1039. doi: 10.1103/PhysRevLett.37.1039

Bethe, H., & Peierls, R. (1934). The 'neutrino'. Nature, 133, 532. doi: 10.1038/133532a0

Boehm, F., & et al. (2001). Final results from the Palo Verde neutrino oscillation experiment. *Phys. Rev. D,* 64, 112001. arXiv:hep-ex/0107009. doi: 10.1103/PhysRevD.64.112001

Brown, L. M. (1978). The idea of the neutrino. *Phys. Today,* 31N9, 23–28. doi: 10.1063/1.2995181

Cañas, B. C., Garcés, E. A., Miranda, O. G., & Parada, A. *(2018).* The reactor antineutrino anomaly and low energy threshold neutrino experiments. *Phys. Lett. B,* 776, 451–456. arXiv:1708.09518. doi: 10.1016/j.physletb.2017.11.074

Canas, B. C., Garces, E. A., Miranda, O. G., Tortola, M., & Valle, J. W. F. (2016). The weak mixing angle from low energy neutrino measurements: a global update. *Phys. Lett. B,* 761, 450–455. arXiv:1608.02671. doi: 10.1016/j.physletb.2016.08.047

Chadwick, J. (1914). The intensity distribution in the magnetic spectrum of beta particles from radium (B + C). Verh. Phys. Gesell., 16, 383–391.

Chadwick, J. (1932). Possible Existence of a Neutron. Nature, 129, 312. doi: 10.1038/129312a0

Chatrchyan, S., & et al. (2012). Observation of a New Boson at a Mass of 125 GeV with the CMS Experiment at the LHC. Phys. Lett. B, 716, 30–61. arXiv:1207.7235. doi: 10.1016/j.physletb.2012.08.021

Cleveland, B. T., Daily, T., Davis, R., Jr., Distel, J. R., Lande, K., Lee, C. K., . . . Ullman, J. (1998). Measurement of the solar electron neutrino flux with the Homestake chlorine detector. Astrophys. J., 496, 505–526. doi: 10.1086/305343

Conrad, J. M., Link, J. M., & Shaevitz, M. H. (2005). Precision measurement of sin**2 theta(W) at a reactor. Phys. Rev. D, 71, 073013. arXiv:hep-ex/0403048. doi: 10.1103/PhysRevD.71.073013

Cowan, C. L., Reines, F., Harrison, F. B., Kruse, H. W., & McGuire, A. D. (1956). Detection of the free neutrino: A Confirmation. Science, 124, 103–104. doi: 10.1126/science.124.3212.103

Czarnecki, A., & Marciano, W. J. (1996). Electroweak radiative corrections to polarized Moller scattering asymmetries. *Phys. Rev. D,* 53, 1066–1072. arXiv:hep-ph/9507420. doi: 10.1103/PhysRevD.53.1066

Czarnecki, A., & Marciano, W. J. (1998). Parity violating asymmetries at future lepton colliders. *Int. J. Mod. Phys. A,* 13, 2235–2244. arXiv:hep-ph/9801394. doi: 10.1142/S0217751X98001037

Danby, G., Gaillard, J. M., Goulianos, K. A., Lederman, L. M., Mistry, N. B., Schwartz, M., & Steinberger, J. (1962). Observation of High-Energy Neutrino Reactions and the Existence of Two Kinds of Neutrinos. *Phys. Rev. Lett.,* 9, 36–44. doi: 10.1103/PhysRevLett.9.36

Daraktchieva, Z., & et al. (2005). Final results on the neutrino magnetic moment from the MUNU experiment. *Phys. Lett. B,* 615, 153–159. (arXiv:hep-ex/0502037) doi: 10.1016/j.physletb.2005.04.030

Davis, R., Jr., Harmer, D. S., & Hoffman, K. C. (1968). Search for neutrinos from the sun. *Phys. Rev. Lett.,* 20, 1205–1209. doi: 10.1103/PhysRevLett.20.1205

Declais, Y., & et al. (1994). Study of reactor anti-neutrino interaction with proton at Bugey nuclear power plant. *Phys. Lett. B,* 338, 383–389. doi: 10.1016/0370-2693(94)91394-3

de Gouvea, A., & Jenkins, J. (2006). What can we learn from neutrino electron scattering? *Phys. Rev. D,* 74, 033004. arXiv:hep-ph/0603036. doi: 10.1103/PhysRevD.74.033004

Deniz, M., & et al. (2010). Measurement of Nu(e)-bar - Electron Scattering Cross-Section with a CsI(Tl) Scintillating Crystal Array at the Kuo-Sheng Nuclear Power Reactor. *Phys. Rev. D,* 81, 072001. arXiv:0911.1597. doi: 10.1103/PhysRevD.81.072001

Derbin, A. I., Chernyi, A. V., Popeko, L. A., Muratova,V. N. Shishkina, G. A., & Bakhlanov, S. I. (1993). Experiment on anti-neutrino scattering by electrons at a reactor of the Rovno nuclear power plant. JETP Lett., 57, 768–772.

de Salas, P. F., Forero, D. V., Gariazzo, S., Martínez- Miravé, P., Mena, O., Ternes, C. A., . . .Valle, J. W. F. (2021). 2020 global reassessment of the neutrino oscillation picture. JHEP, 02, 071. arXiv:2006.11237. doi: 10.1007/JHEP02(2021)071

Dirac, P. A. M. (1928). The quantum theory of the electron. *Proc. Roy. Soc. Lond. A,* 117, 610–624. doi: 10.1098/rspa.1928.0023

Eguchi, K., & et al. (2003). First results from KamLAND: Evidence for reactor anti-neutrino disappearance. Phys. Rev. Lett., 90, 021802. arXiv:hep-ex/0212021. doi: 10.1103/PhysRevLett.90.021802

Englert, F., & Brout, R. (1964). Broken Symmetry and the Mass of Gauge Vector Mesons. *Phys. Rev. Lett.,* 13, 321–323. doi: 10.1103/PhysRevLett.13.321

Esteban, I., Gonzalez-Garcia, M. C., Maltoni, M., Schwetz, T., & Zhou, A. (2020). The fate of hints: updated global analysis of three-flavor neutrino oscillations. JHEP, 09, 178. arXiv:2007.14792. doi: 10.1007/JHEP09(2020)178

Fermi, E. (1934). An attempt of a theory of beta radiation. 1. Z. Phys., 88, 161–177. doi: 10.1007/BF01351864

Frekers, D., & et al. (2011). The Ga-71(He-3, t) reaction and the low-energy neutrino response. Phys. Lett. B, 706, 134–138. doi: 10.1016/j.physletb.2011.10.061

Fukuda, Y., & et al. (1994). Atmospheric muon-neutrino / electron-neutrino ratio in the multiGeV energy range. Phys. Lett. B, 335, 237–245. doi: 10.1016/0370-2693(94)91420-6

Fukuda, Y., & et al. (1996). Solar neutrino data covering solar cycle 22. *Phys. Rev. Lett.,* 77, 1683–1686. doi: 10.1103/PhysRevLett.77.1683

Fukuda, Y., & et al. (1998a). Evidence for oscillation of atmospheric neutrinos. *Phys. Rev. Lett., 81, 1562–1567. arXiv:hep-ex/9807003. doi: 10.1103/PhysRevLett.81.1562*

Fukuda, Y., & et al. (1998b). Measurements of the solar neutrino flux from Super-Kamiokande's first 300 days. Phys. Rev. Lett., 81, 1158–1162. arXiv:hep-ex/9805021. ([Erratum: Phys.Rev.Lett. 81, 4279 (1998)]) doi: 10.1103/PhysRevLett.81.1158

Garces, E. A., Miranda, O. G., Tortola, M. A., & Valle, J. W. F. (2012). Low-Energy Neutrino-Electron Scattering as a Standard Model Probe: The Potential of LENA as Case Study. *Phys. Rev. D,* 85, 073006. arXiv:1112.3633. doi: 10.1103/PhysRevD.85.073006

Garwin, R. L., Lederman, L. M., & Weinrich, M. (1957). Observations of the Failure of Conservation of Parity and Charge Conjugation in Meson Decays: The Magnetic Moment of the Free Muon. *Phys. Rev.,* 105, 1415–1417. doi: 10.1103/PhysRev.105.1415

Giunti, C., & Kim, C. W. (2007). *Fundamentals of Neutrino Physics and Astrophysics.* Oxford University Press.

Giunti, C., & Laveder, M. (2011). Statistical Significance of the Gallium Anomaly. *Phys. Rev. C,* 83, 065504. arXiv:1006.3244. doi: 10.1103/PhysRevC.83.065504

Giunti, C., Laveder, M., Li, Y. F., Liu, Q. Y., & Long, H. W. (2012). Update of Short-Baseline Electron Neutrino and Antineutrino Disappearance. *Phys. Rev. D,* 86, 113014. arXiv:1210.5715. doi: 10.1103/PhysRevD.86.113014

Giunti, C., Li, Y. F., Littlejohn, B. R., & Surukuchi, P. T. (2019). Diagnosing the Reactor Antineutrino Anomaly with Global Antineutrino Flux Data. *Phys. Rev. D,* 99(7), 073005. doi: 10.1103/PhysRevD.99.073005

Glashow, S. L. (1961). Partial Symmetries of Weak Interactions. Nucl. Phys., 22, 579–588. doi: 10.1016/0029-5582(61)90469-2

Goldhaber, M., Grodzins, L., & Sunyar, A. W. (1958). Helicity of Neutrinos. *Phys. Rev.,* 109, 1015–1017. doi: 10.1103/PhysRev.109.1015

Gonzalez-Garcia, M. C., & Maltoni, M. (2008). Phenomenology with Massive Neutrinos. *Phys. Rept.,* 460, 1–129. arXiv:0704.1800. doi: 10.1016/j.physrep.2007.12.004

Hampel, W., & et al. (1996). GALLEX solar neutrino observations: Results for GALLEX III. *Phys. Lett. B,* 388, 384–396. doi: 10.1016/S0370-2693(96)01121-5

Hampel, W., & et al. (1998). Final results of the Cr-51 neutrino source experiments in GALLEX. *Phys. Lett. B,* 420, 114–126. doi: 10.1016/S0370-2693(97)01562-1

Hanna, G. C., & Pontecorvo, B. (1949). The β Spectrum of H³. *Phys. Rev.,* 75, 983–984. doi: 10.1103/PhysRev.75.983.3

Hasert, F. J., & et al. (1973a). Observation of Neutrino Like Interactions Without Muon Or Electron in the Gargamelle Neutrino Experiment. *Phys. Lett. B,* 46, 138–140. doi: 10.1016/0370-2693(73)90499-1

Hasert, F. J., & et al. (1973b). Search for Elastic νμ Electron Scattering. *Phys. Lett. B,* 46, 121–124. doi: 10.1016/0370-2693(73)90494-2

Haxton, W. C. (1998). Cross-section uncertainties in the gallium neutrino source experiments. *Phys. Lett. B,* 431, 110–118. arXiv:nucl-th/9804011. doi: 10.1016/S0370-2693(98)00581-4

Higgs, P. W. (1964). Broken symmetries, massless particles and gauge fields. *Phys. Lett.,* 12, 132–133. doi: 10.1016/0031-9163(64)91136-9

Holder, M., & et al. (1977). Measurement of the Neutral to Charged Current Cross-Section Ratio in Neutrino and anti-neutrino Interactions. Phys. Lett. B, 71, 222. doi: 10.1016/0370-2693(77)90783-3

Hoummada, A., Lazrak Mikou, S., Avenier, M., Bagieu, G., Cavaignac, J., & Holm Koang, D. (1995). Neutrino oscillations i.l.l. experiment reanalysis. Applied Radiation and Isotopes, 46(6), 449-450. doi: https://doi.org/10.1016/0969-8043(95)00048-8

Huber, P. (2011). On the determination of anti-neutrino spectra from nuclear reactors. *Phys. Rev. C,* 84, 024617. arXiv:1106.0687. ([Erratum: Phys.Rev.C 85, 029901 (2012)]) doi: 10.1103/PhysRevC.85.029901

Huber, P., & Schwetz, T. (2004). Precision spectroscopy with reactor anti-neutrinos. *Phys. Rev. D,* 70, 053011. arXiv:hep-ph/0407026. doi: 10.1103/PhysRevD.70.053011

Kaether, F., Hampel, W., Heusser, G., Kiko, J., & Kirsten, T. (2010). Reanalysis of the GALLEX solar neutrino flux and source experiments. Phys. Lett. B, 685, 47–54. arXiv:1001.2731. doi: 10.1016/j.physletb.2010.01.030

Kayser, B., Gibrat-Debu, F., & Perrier, F. (1989). *The Physics of massive neutrinos* (Vol. 25).

Kodama, K., & et al. (2001). Observation of tau neutrino interactions. *Phys. Lett. B,* 504, 218–224. arXiv:hep-ex/0012035.
doi: 10.1016/S0370-2693(01)00307-0

Kopeikin, V. I., Mikaelyan, L. A., & Sinev, V. V. (1997). Spectrum of electronic reactor anti-neutrinos. Phys. Atom. Nucl., 60, 172–176.

Krofcheck, D., & et al. (1985). Gamow-Teller Strength Function in Ge-71 via the (p, n) Reaction at Medium-Energies. *Phys. Rev. Lett.,* 55, 1051–1054. doi: 10.1103/PhysRevLett.55.1051

Kumar, K. S., Mantry, S., Marciano, W. J., & Souder, P. A. (2013). Low Energy Measurements of the Weak Mixing Angle. *Ann. Rev. Nucl. Part. Sci.,* 63, 237–267. arXiv:1302.6263. doi: 10.1146/annurev-nucl-102212-170556

Kuvshinnikov, A. A., Mikaelyan, L. A., Nikolaev, S. V., Skorokhvatov, M. D., & Etenko, A. V. (1990). Measuring the anti-electron-neutrino + p —> n + e+ cross-section and beta decay axial constant in a

new experiment at Rovno NPP reactor. (In Russian). Yad. Fiz., 52, 472–479.

Kwon, H., Boehm, F., Hahn, A. A., Henrikson, H. E., Vuilleumier, J. L., Cavaignac, J. F., . . . Mossbauer, R. L. (1981). Search for Neutrino Oscillations at a Fission Reactor. *Phys. Rev. D,* 24, 1097–1111. doi: 10.1103/PhysRevD.24.1097

Landau, L. D. (1957). On the conservation laws for weak interactions. *Nucl. Phys., 3,* 127–131. doi: 10.1016/0029-5582(57)90061-5

Langacker, P. (2017). *The Standard Model and Beyond.* Taylor & Francis. doi: 10.1201/b22175

Lee, T. D., & Yang, C.-N. (1957). Parity Nonconservation and a Two Component Theory of the Neutrino. Phys. Rev., 105, 1671–1675. doi: 10.1103/PhysRev.105.1671

Leitner, R. (2017). Recent results of Daya Bay reactor neutrino experiment. Nucl. *Part. Phys. Proc.,* 285-286, 32–37. doi: 10.1016/j.nuclphysbps.2017.03.007

Lindley, D. (2007). Landmarks: Detecting the Elusive Neutrino *Phys. Rev. Focus,* 19, 13. doi: 10.1103/PhysRevFocus.19.13

Majorana, E. (1937). Teoria simmetrica dell'elettrone del positrone. Nuovo Cim., 14, 171–184. doi: 10.1007/BF02961314

Maki, Z., Nakagawa, M., & Sakata, S. (1962). Remarks on the unified model of elementary particles. Prog. Theor. Phys., 28, 870–880. doi: 10.1143/PTP.28.870

Marciano, W. J., & Sirlin, A. (1980). Radiative Corrections to Neutrino Induced Neutral Current Phenomena in the SU(2)-L x U(1) Theory. *Phys. Rev. D,* 22, 2695. ([Erratum: Phys.Rev.D 31, 213 (1985)]) doi: 10.1103/PhysRevD.22.2695

Marciano, W. J., & Sirlin, A. (1981). Precise SU(5) Predictions for sin**2-Theta(W), m(W) and m(Z). *Phys. Rev. Lett.,* 46, 163. doi: 10.1103/PhysRevLett.46.163

Mention, G., Fechner, M., Lasserre, T., Mueller, T. A., Lhuillier, D., Cribier, M., & Letourneau, A. (2011). The Reactor Antineutrino Anomaly. *Phys. Rev. D,* 83, 073006. (arXiv:1101.2755) doi: 10.1103/PhysRevD.83.073006

Mohapatra, R. N., & Smirnov, A. Y. (2006). Neutrino Mass and New Physics. Ann. *Rev. Nucl. Part. Sci.,* 56, 569–628. arXiv:hep-ph/0603118. doi: 10.1146/annurev.nucl.56.080805.140534

Mueller, T. A., & et al. (2011). Improved Predictions of Reactor Antineutrino Spectra. *Phys. Rev. C,* 83, 054615. arXiv:1101.2663. doi: 10.1103/PhysRevC.83.054615

Osipowicz, A., & et al. (2001, 9). *KATRIN: A Next generation tritium beta decay experiment with sub-eV sensitivity for the electron neutrino mass. Letter of intent.* arXiv:hep-ex/0109033. (e-print)

Passera, M. (2001). QED corrections to neutrino electron scattering. *Phys. Rev. D,* 64, 113002. arXiv:hep-ph/0011190. doi: 10.1103/PhysRevD.64.113002

Perrin, F. (1933). Possibilité d'émission de particules neutres de masse intrinsèque nulle dans les radioactivités beta. Comptes-Rendus, 197, 1625.

Pontecorvo, B. (1967). Neutrino Experiments and the Problem of Conservation of Leptonic Charge. Zh. Eksp. Teor. Fiz., 53, 1717–1725.

Prescott, C. Y., & et al. (1978). Parity Nonconservation in Inelastic Electron Scattering. *Phys. Lett. B,* 77, 347–352. doi: 10.1016/0370-2693(78)90722-0

Reines, F., & Cowan, C. L. (1959). Free anti-neutrino absorption cross-section. 1: Measurement of the free anti-neutrino absorption cross-section by protons. Phys. Rev., 113, 273–279. doi: 10.1103/PhysRev.113.273

Salam, A. (1957). On parity conservation and neutrino mass. *Nuovo Cim.,* 5, 299–301. doi: 10.1007/-BF02812841

Salam, A. (1968). Weak and Electromagnetic Interactions. *Conf. Proc. C,* 680519, 367–377. doi: 10.1142/9789812795915_0034

Sarantakos, S., Sirlin, A., & Marciano, W. J. (1983). Radiative Corrections to Neutrino-Lepton Scattering in the SU(2)-L x U(1) Theory. *Nucl. Phys*. B, 217, 84–116. doi: 10.1016/0550-3213(83)90079-2

Schwinger, J. S. (1957). A Theory of the Fundamental Interactions. Annals Phys., 2, 407–434. doi: 10.1016/0003-4916(57)90015-5

Sirlin, A. (1980). Radiative Corrections in the SU(2)-L x U(1) Theory: A Simple Renormalization Framework. Phys. Rev. D, 22, 971–981. doi: 10.1103/PhysRevD.22.971

Strumia, A., & Vissani, F. (2006, 6). *Neutrino masses and mixings and...* arXiv:hep-ph/0606054. (e-print)

't Hooft, G. (1971a). Predictions for neutrino - electron cross-sections in Weinberg's model of weak interactions. *Phys. Lett. B,* 37, 195–196. doi: 10.1016/0370-2693(71)90050-5

't Hooft, G. (1971b). Renormalization of Massless Yang-Mills Fields. Nucl. Phys. B, 33, 173–199. doi: 10.1016/0550-3213(71)90395-6

't Hooft, G., & Veltman, M. J. G. (1972). Regularization and Renormalization of Gauge Fields. Nucl. Phys. B, 44, 189–213. doi: 10.1016/0550-3213(72)90279-9

Valle, J. W. F., & Romao, J. C. (2015). *Neutrinos in high energy and astroparticle physics.* Weinheim: Wiley-VCH.

Vidyakin, G. S., Vyrodov, V. N., Gurevich, I. I., Kozlov, Y. V., Martemyanov, V. P., Sukhotin, S. V., . . . Khakhimov, S. K. (1992). Limitations on the magnetic moment and charge radius of the electron-anti-neutrino. JETP Lett., 55, 206–210.

Weinberg, S. (1967). A Model of Leptons. *Phys. Rev. Lett.,* 19, 1264–1266. doi: 10.1103/PhysRevLett.19.1264

Workman, R. L., & et al. (2022). Review of Particle Physics. *PTEP,* 2022, 083C01. doi: 10.1093/ptep/ptac097

Wu, C. S., Ambler, E., Hayward, R. W., Hoppes, D. D., & Hudson, R. P. (1957). Experimental Test of Parity Conservation in β Decay. Phys. Rev., 105, 1413–1414. doi: 10.1103/PhysRev.105.1413

Yang, C.-N., & Mills, R. L. (1954). Conservation of Isotopic Spin and Isotopic Gauge Invariance. Phys. Rev., 96, 191–195. doi: 10.1103/PhysRev.96.191

Zacek, G., & et al. (1986). Neutrino Oscillation Experiments at the Gosgen Nuclear Power Reactor. Phys. Rev. D, 34, 2621–2636. doi: 10.1103/PhysRevD.34.2621

Zeller, G. P., & et al. (2002). A Precise Determination of Electroweak Parameters in Neutrino Nucleon Scattering. *Phys. Rev. Lett.,* 88, 091802. arXiv:hep-ex/0110059. ([Erratum: Phys.Rev.Lett. 90, 239902 (2003)]) doi: 10.1103/PhysRevLett.88.091802

Zyla, P. A., & et al. (2020). Review of Particle Physics. *PTEP,* 2020(8), 083C01. doi:10.1093/ptep/ptaa104

UNIPAMPLONA